

**Design and Synthesis
of Analogs of Oleic Acid**

by

Kexin Xu

MS Pharmaceutical Sciences, University of Pittsburgh, 2021

Submitted to the Graduate Faculty of
University of Pittsburgh in partial fulfillment
of the requirements for the degree of
Master of Science

University of Pittsburgh

2021

UNIVERSITY OF PITTSBURGH
Faculty of Pharmaceutical Sciences

This thesis was presented

by

Kexin Xu

It was defended on

July 29th, 2021

Paul A. Johnston, PhD, Associate Professor

Zhiwei Feng, PhD, Assistant Professor

Vinayak Sant, PhD, Associate Professor

Thesis Advisor/Dissertation Director: Donna Huryn, Ph.D, Professor

Copyright © by Kexin Xu

2021

TABLE OF CONTENTS

1.0	Introduction.....	1
1.1	Friedreich Ataxia.....	1
1.2	Friedreich's Ataxia (FRDA) cell models.....	2
1.3	Ferroptosis.....	4
1.4	Effects of oleic acid on FRDA cell models.....	7
2.0	Synthesis and Follow-up of Trifluoromethyl Isosteres of Oleic acid.....	10
2.1	Background information.....	10
2.1.1	Trifluoromethyl group in drug design.....	10
2.1.2	Original Synthesis of 1, 2-R, 2-S and 2-rac.....	11
2.2	Scale-up synthesis of 1, 2-R, 2-S and 2-rac.....	13
2.3	Synthesis of Methyl Ethers of 2-R, 2-S and 2-rac.....	19
2.4	Bioevaluation of Methyl Ethers of 2-R, 2-S and 2-rac.....	21
2.5	Future plans of trifluoromethyl alcohols.....	23
2.5.1	Other Analogs of 2-R.....	23
2.5.2	Long-chain unsaturated fatty acids other than oleic acid.....	24
3.0	Design and synthesis of other isosteres of oleic acid.....	25
3.1	Synthesis of N-(2-aminophenyl)oleamide (4).....	27
3.2	Synthesis of (Z)-2-(octadec-9-en-1-ylthio)phenol (5).....	29

3.3	Synthesis of (9Z)-octadec-9-enyl(methylsulfonyl)amine (6) and {[(9Z)-octadec-9-enylamino]sulfonyl}dimethylamine (7)	30
3.4	Synthesis of (15Z)-2-oxo-3,5-diazatricos-14-enamide (8).....	32
3.5	Bioevaluation of 4, 5, 6, 7 and 8.....	33
3.5.1	Bioevaluation of Compound 4, 5, 6, 7 and 8.....	33
3.5.2	Studies towards additional novel isosteres.....	37
4.0	Conclusion.....	42
5.0	Experimental Section.....	45
	References.....	83

LIST OF TABLES

- Table 1. Chemical shift (ppm) of the α -H in oleic acid, α -H in compound 1, and α -H and β -H in compound 2-R, 2-S and 2-rac.....16
- Table 2. ^1H -NMR spectra from $\sim 3\text{ppm}$ to 4.2ppm of 2-R, 2-S and 2-rac18
- Table 3. Prediction of the value of $\text{pKa}(298\text{K})$, numbers of H-bond donor (HBD) and H-bond acceptor (HBA), $\log P$ and $\log D_{7.4}$ of compounds 1, 2-rac, 3-rac, 4, 5, 6, 7, 8 and oleic acid using

LIST OF FIGURES

Figure 1. Mechanisms of ferroptosis.....	5
Figure 2. Structure of erastin.....	5
Figure 3. Structure of H-linoleate.....	7
Figure 4. Structure of oleic acid.....	8
Figure 5. Structure of 2-R and 2-S.....	9
Figure 6. Structure of trifluoromethyl ketone group and trifluoro- methyl alcohol group.....	10
Figure 7. Trifluoromethyl ketone isostere of oleic acid (1) inhibits oleamide hydrolase.....	11
Figure 8. Synthesis scheme of compound 1, 2-R, 2-S, and 2-rac.....	12
Figure 9. Mechanism of synthesis from oleic acid to compound 1.....	13
Figure 10. Mosher's method.....	17
Figure 11. Synthesis scheme of compound 3-R, 3-S, and 3-rac.....	21
Figure 12. Efficacy of compound 3-rac and 2-R in protecting FRDA cells treated with erastin.....	22
Figure 13. Efficacy of compound 3-S and 3-R in protecting FRDA cells treated with erastin.....	23
Figure 14. Structure of Cis-Vaccenic Acid, Petroselinic Acid, Petroselinic Acid, Erucic acid, Heptadecenoic acid and Palmitoleic	

Acid.....	24
Figure 15. Structure of compounds 4, 5, 6, 7 and 8.....	26
Figure 16. Prediction of the value of pKa and ionization state of compound 4 using MarvinSketch at 298K.....	28
Figure 17. Synthesis scheme of compound 4.....	28
Figure 18. Synthesis scheme of compound 5.....	30
Figure 19. Synthesis scheme of compound 6 and 7.....	32
Figure 20. Synthesis scheme of compound 8.....	33
Figure 21. Efficacy of compound 2-R, 3-rac, 4, 5, 6, 7 and 8 in protecting FRDA cells treated with erastin at 20 μ m.....	34
Figure 22. Efficacy of compound 4 in protecting FRDA cells treated with erastin.....	35
Figure 23. Efficacy of compound 4, 2-R, 2-S and oleic acid in protecting FRDA cells treated with erastin.....	36
Figure 24. Mechanism of hydrolysis of compound 4 into oleic acid when exposed to nitric oxide and oxygen.....	36
Figure 25. Modification of compound 4 by replacing the nitrogen atom in the amide bond with a carbon atom.....	38
Figure 26. Synthesis plan of the a new isostere of oleic acid by Grignard reaction.....	39
Figure 27. Synthesis scheme of oleylnitrile.....	40
Figure 28. Failed synthesis scheme of a Grignard reagent.....	41

Figure 29. Structure of compound 1, 2-rac, 2-R, 2-S, 3-rac, 3-R, 3-S, 4, 5, 6, 7 and 8.....43

Figure 30. Structure-Activity Relationships (SAR) model based on the bioassay of 1, 2-rac, 2-R, 2-S, 3-rac, 3-R, 3-S, 4, 5, 6, 7 and 8.....44

ACKNOWLEDGEMENTS

I would like to thank my advisor, Professor Donna M. Hury, for her valuable guidance and patience during this project here. I also thank Professors Lee Apostle McDermott, Paul A Johnston, Zhiwei Feng and Vinayak Sant for serving as members of my committee.

I would also like to thank the Hury lab members, both past and present. I would like to thank Dr. Sipak Joyasawal, Dr. Sangeetha Subramani, Zoe Vaughn and Keith Long for their help.

I would also like to thank our collaborators, Dr. M. Grazia Cotticelli, Dr. Shujuan Xia and Dr. Taehee Lee from Dr. Robert B Wilson Lab (CHOP) and Dr. Roberto Forestieri from Dr. Amos B Smith, III Lab (UPenn).

Design and Synthesis of Analogs of Oleic Acid

Abstract:

Friedreich's ataxia (FRDA) is an autosomal recessive genetic disease causing disability and early death and there is no effective treatment. Previous studies suggested that ferroptosis, a cell death mechanism caused by iron-dependent accumulation of lipid hydroperoxides, may be a potential target for the treatment of FRDA. In previous studies, oleic acid was identified as a ferroptosis inhibitor and it was also shown to be effective in protecting FRDA cell models from death. In order to improve the efficacy of oleic acid, we designed and synthesized a series of analogs of oleic acid in which the carboxylic acid was replaced with an isostere. We tested these isosteres in FRDA models, and some proved to be effective. These compounds may be a potential starting point of the treatment for FRDA, and a valuable probe molecule for studying this disorder.

1.0 Introduction

1.1 Friedreich Ataxia

Friedreich's Ataxia (FRDA) is an autosomal recessive genetic disease characterized by a loss of vibratory and position sense, motor speech disorders, loss of response to stimuli in muscles, progressive gait and limb ataxia, and progressive motor weakness. Cardiomyopathy and diabetes are also common in FRDA patients. [2] Onset usually appears during adolescence, and most patients suffer from a shortened life expectancy. [3] As reported, 1 in 50,000 people suffer from FRDA in the world. [3]

FRDA is caused by a triplet repeat expansion in the first intron of both alleles of the FXN gene, a protein-coding gene that provides genetic information for making a mitochondrial protein called frataxin. This mutation leads to severely reduced levels of frataxin, resulting in iron accumulation and lipid peroxidation in mitochondria, respiratory chain dysfunction, and eventually leading to cell death. [4] Typical symptoms include loss of sight, hearing and the ability to walk, all of which worsens over time. Other symptoms also include cardiomyopathy, scoliosis, diabetes, etc. As a consequence, most patients suffer from an early death. [2]

While there are no approved therapeutics, several approaches to FRDA drug discovery have been reported. These include HDAC inhibitors as a potential treatment for the deficiency of frataxin[5] and ferroptosis as a novel therapeutic target for FRDA. [6] To support these drug discovery efforts, several cellular models that reflect the FRDA phenotype have been developed.

1.2 Friedreich's Ataxia (FRDA) cell models

In 2009, Calmels, N., et al. created the first murine cellular models based on frataxin missense mutations, in which the endogenous frataxin was depleted and missense-mutated human frataxin was expressed. [7] This cell model demonstrated an FRDA-like phenotype, including abnormal mitochondrial morphology and iron accumulation in mitochondria. They attempted to insert either G130V or I154F missense mutations (expressed in heterozygous FRDA patients) into the cell models, and found that I154F missense mutations caused a more severe phenotype, including mitochondria dysfunction and increased sensitivity to oxidative stress. Compared with cell lines from FRDA patients which suffer from high variability, this humanized murine FRDA cell model created in the lab is more stable and is widely used to study potential treatment for FRDA.

Our collaborators, Robert Wilson and M. Grazia Coticelli from the Children's Hospital of Philadelphia designed a screening assay for Friedreich Ataxia based on the Calmels murine cellular model[8]. In this assay, murine fibroblasts harboring human frataxin with the disease-associated I154F point mutation are treated with iron, as ferric ammonium citrate (FAC) and L-buthionine (S,R)-sulfoximine (BSO).

As iron overload is a hallmark of FRDA, this assay reflects that phenotype. Besides, BSO inhibits the rate-limiting step of glutathione synthesis, while glutathione is critical to the metabolization of the potentially toxic hydroperoxides in cells.[1] Furthermore, the FRDA cells show significant sensitivity to FAC+BSO treatment compared to normal cells. [8]

FAC and BSO are co-administered to the cells at concentrations that, individually, are not harmful to the cells separately, but together will result in decreased viability with a synergistic effect. This validated FRDA cell model is used frequently to study the pathology of FRDA and for screening for small molecules with potential therapeutic effects on FRDA. [6, 8, 9], and in this document will be referred to as the "FRDA (FAC+ BSO)" system. The parabenzoquinone idebenone, a compound that is under clinical evaluation for FRDA, was used to validate this FRDA (FAC+BSO) cell model and was shown to rescue the cells at 100 nM and 1 μ M. [10]

1.3 Ferroptosis

The significant hallmarks in the pathology of FRDA at the cellular level - cell death caused by iron accumulation and lipid peroxidation – are also the critical characteristics of ferroptosis. Ferroptosis, a term first coined in 2012 by Dixon et al, is a form of regulated cell death caused by the iron-dependent accumulation of lipid hydroperoxides to lethal levels. Iron is proved vital to the accumulation of lipid peroxides in the process of ferroptosis and ferroptosis can be suppressed with iron chelators. [11]

The process of ferroptosis is mainly based on the inactivation of the phospholipid peroxidase glutathione peroxidase 4 (GPX4). [1] GPX4 plays an important role in protecting cells against membrane lipid peroxidation since it metabolizes the potentially toxic hydroperoxides of polyunsaturated fatty acid (PUFA)-containing phospholipids (PL-PUFA-OOH) into its nontoxic alcohols (PL-PUFA-OH) in cells. The metabolization of PL-PUFA-OOH by GPX4 requires reduced glutathione (GSH), the synthesis of which requires cysteine. Cysteine is mainly imported into the cell by cystine/glutamate transporter (System Xc⁻), although there are also other pathways through which cysteine moves into cells. [11] [1]

GPX4 can be inhibited directly by inhibitors binding to GPX4, or indirectly by the inhibition of System Xc⁻ which results in insufficiency of cysteine and GSH. Both direct and indirect inhibition of GPX4 will lead to

overwhelming lipid peroxidation in cells and finally cell death (**Figure 1**).

[1] For example, erastin (structure showed in **Figure 2**) was found to be an indirect inhibitor of GPX4 because it can suppress the normal function of System Xc⁻.

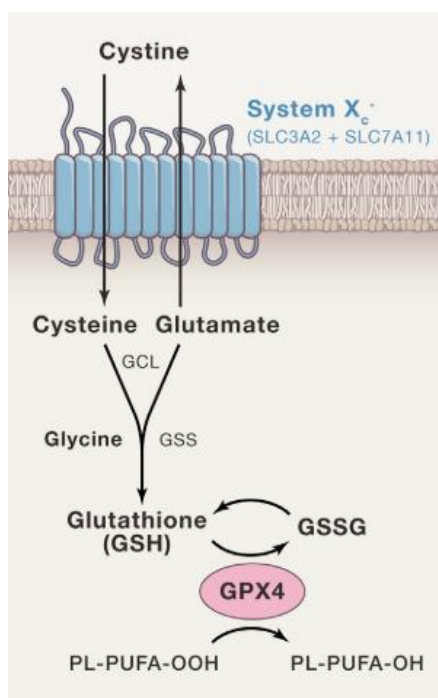


Figure 1. Mechanisms of Ferroptosis. GPX4 metabolizes PL-PUFA-OOH into PL-PUFA-OH in cells. This process requires GSH, the synthesis of which requires cysteine. Cysteine is mainly imported into the cell by System Xc⁻. GPX4 = glutathione peroxidase 4. PL-PUFA = polyunsaturated fatty acid (PUFA)-containing phospholipids. OOH = hydroperoxides. OH = alcohols. GSH = reduced glutathione. [1] Used by Permission from *Cell press*.

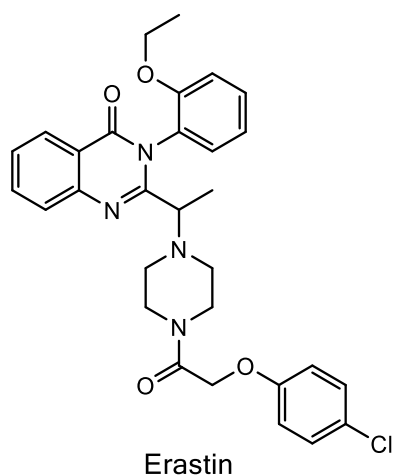


Figure 2. Structure of erastin.

To study the relationship between FRDA and ferroptosis, our colleagues Wilson and Cotticelli, in collaboration with the Huryn and

Wipf labs, tested both ferroptosis inducers and inhibitors in FRDA cell models, and in 2019 published their results suggest that inhibiting ferroptosis may be a valid therapeutic approach to FRDA. [6] They used their previously established murine cell model harboring human frataxin with the disease-associated I154F point mutation as the experimental group while using murine cells inserted with normal human frataxin gene as control group. In this study they found that FRDA cell models are sensitive to erastin, an inducer of ferroptosis; this inducer decreased survival of FRDA cells dramatically compared to control group, similar to the effects seen in cells stressed with FAC + BSO. They have since developed a new assay, in which erastin is used to stress the cells, in place of FAC + BSO in the FRDA cell model; in this document we will refer to this assay as FRDA (erastin). To extend these studies, they used their FRDA (FAC + BSO) assay to test ferroptosis inhibitors (Fer-1 and SRS11-92) and found ferroptosis inhibitors were able to rescue the stressed cells in a dose-dependent manner.

The ferroptosis inhibitors, SRS11-92, could also prevent death induced by frataxin knockdown in normal primary human fibroblasts. Cells were transfected with anti-FXN siRNA as a frataxin knockdown model and control cells were transfected with a scrambled siRNA. A significantly decreased level of the frataxin protein and cell death was observed in the frataxin knockdown model compared with the control

group. However, a ferroptosis inhibitor showed protective effects in this FRDA cell model, increasing the survival of cells. [6] Based on these data, this publication concluded that ferroptosis is likely a mechanism of cell death in FRDA, as multiple methods to prevent it (genetic and pharmacological) can protect cells, and therefore targeting ferroptosis may be a novel therapeutic target for Friedreich's ataxia. [6]

1.4 Effects of oleic acid on FRDA cell models

Ferroptosis involves peroxidation of lipids, but details about which kind of lipids are most critical to ferroptosis and how they perform their function in ferroptosis remain unclear. There is evidence that among all the lipids in cells, polyunsaturated fatty acids (PUFAs) – such as H-linoleate (structure showed in **Figure 3**) - are most susceptible to peroxidation during ferroptosis because the bis-allylic protons in their structures are prone to hydrogen atom abstraction. [12]

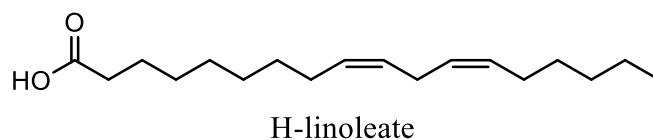


Figure 3 H-linoleate

Therefore, Yang et al. screened different fatty acids in FRDA cell

models, and oleic acid (**Figure 4**), a representative molecule of monounsaturated fatty acids (MUFA) showed protective effects. [12]

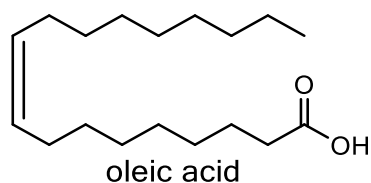
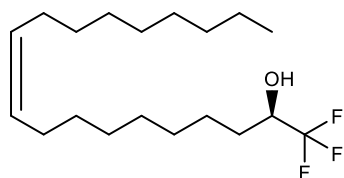


Figure 4. Structure of oleic acid.

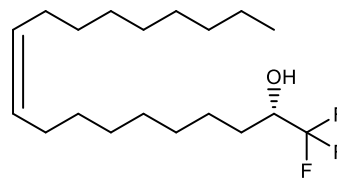
In previous work, our collaborators together with Dr. Huryn demonstrated that oleic acid is effective in the FRDA (FAC + BSO) assay.[9] They showed similar effects in the FRDA (erastin) model: oleic acid increased the viability in a dose-dependent manner.[9] In this publication, other fatty acids were also evaluated, such as stearic acid and gadoleic acid. Overall, oleic acid was most efficacious in protecting FDRA cells among all the long-chain fatty acids tested.[9]

Although the mechanisms of the protection function of oleic acid of these FRDA models are not clear, this small molecule can still serve as a good starting point for developing treatments for FRDA and molecular probes to understand the pathology of FRDA. Towards that end, previous efforts focused on a series of analogs that were prepared based on the concept of bioisosterism, which is a fundamental medicinal chemistry strategy to overcome adverse side effects and modulate physicochemical properties, including acidity, lipophilicity, water solubility, membrane permeability, plasma protein binding ability, etc.[13] Among those synthesized, the R-trifluoromethyl alcohol (**2-R**, the structure showed in **Figure 5**), but not the S-enantiomer (**2-S**, the structure showed in **Figure**

5), proved effective in the FRDA (FAC+BSO) and FRDA (erastin) assay, suggesting a specific molecular target of these molecules. [9] Based on these findings, the current project aimed to follow up on these original findings, and design and synthesize analogs of the 1) R-trifluoromethyl alcohol and 2) oleic acid to develop structure activity relationships (SAR) to improve potency and properties, such as membrane permeability, toxicity, poor PK, and potential off-target effects attributed to oleic acid, .



(R,Z)-1,1,1-trifluorononadec-10-en-2-ol (**2-R**)



(S,Z)-1,1,1-trifluorononadec-10-en-2-ol (**2-S**)

Figure 5. Structure of **2-R** and **2-S**.

2.0 Synthesis and Follow-up of Trifluoromethyl Alcohol Isosteres of Oleic acid

2.1 Background information

2.1.1 Trifluoromethyl group in drug design

The trifluoromethyl groups (**Figure 6**) have been used widely in drug design and discovery as a bioisostere of carboxylic acid since it can modify physicochemical properties of the compound and decrease the rate of metabolism in vivo. [14]



Figure 6. Structure of trifluoromethyl ketone group and trifluoromethyl alcohol group.

The trifluoromethyl ketone group usually forms stable hydrates in an aqueous solution which improves water solubility of the compound. Furthermore, the trifluoromethyl ketone group is much more lipophilic than its carboxylic acid analog. [14] Since compounds containing carboxylic acid groups may have limited permeability through biological membranes, the trifluoromethyl ketone isostere of the parent compound has the potential to overcome the drawbacks of carboxylic acid groups. In fact, the trifluoromethyl ketone isostere of oleic acid (**1**) has been

reported before as an inhibitor of oleamide hydrolase, an enzyme that catalyzes the hydrolysis of oleamide to oleic acid (**Figure 7**).[15]

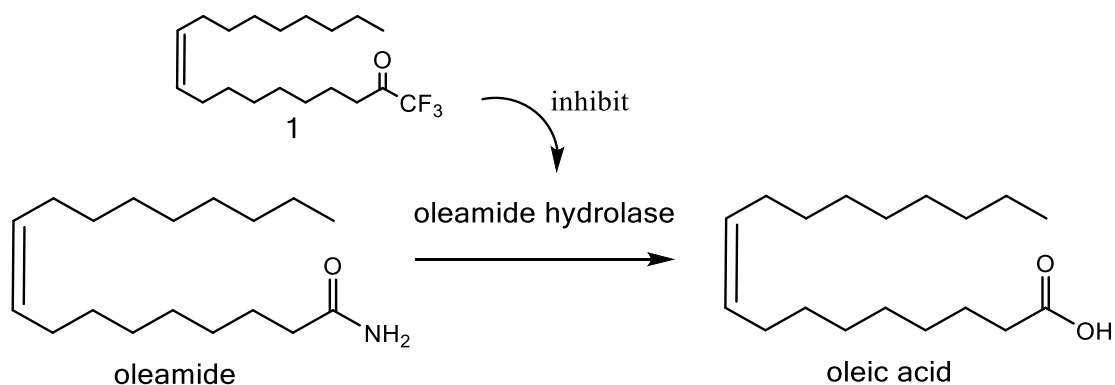


Figure 7. Trifluoromethyl ketone isostere of oleic acid (**1**) inhibits oleamide hydrolase, an enzyme that catalyzes the hydrolysis of oleamide to oleic acid.

As for the trifluoromethyl alcohol isostere, previous studies suggest that alcohols with adjacent fluorine substitution became more acidic [16], which means the trifluoromethyl alcohol group can also serve as a bioisostere of carboxylic acid group since the hydrogen of trifluoromethyl alcohol group is more likely to be ionized.

2.1.2 Original Synthesis of 1, 2-R, 2-S and 2-rac

In the original preparation of these compounds, by Roberto Forrestieri from Penn, the trifluoromethyl ketone isostere of oleic acid has been synthesized, and was reduced to trifluoromethyl alcohols (**Figure 8**). [9] When the trifluoromethyl ketone is reduced to trifluoromethyl alcohol,

a chiral carbon is introduced into the compound. In previous work, the two enantiomers (**2-R**, **2-S**) and the racemic alcohol (**2-rac**) were prepared. [9] In order to provide additional quantities of material for further testing, and to confirm the chiral purity, which was not done previously, our first goal was to prepare additional quantities of 2-R, 2-S and 2-rac.

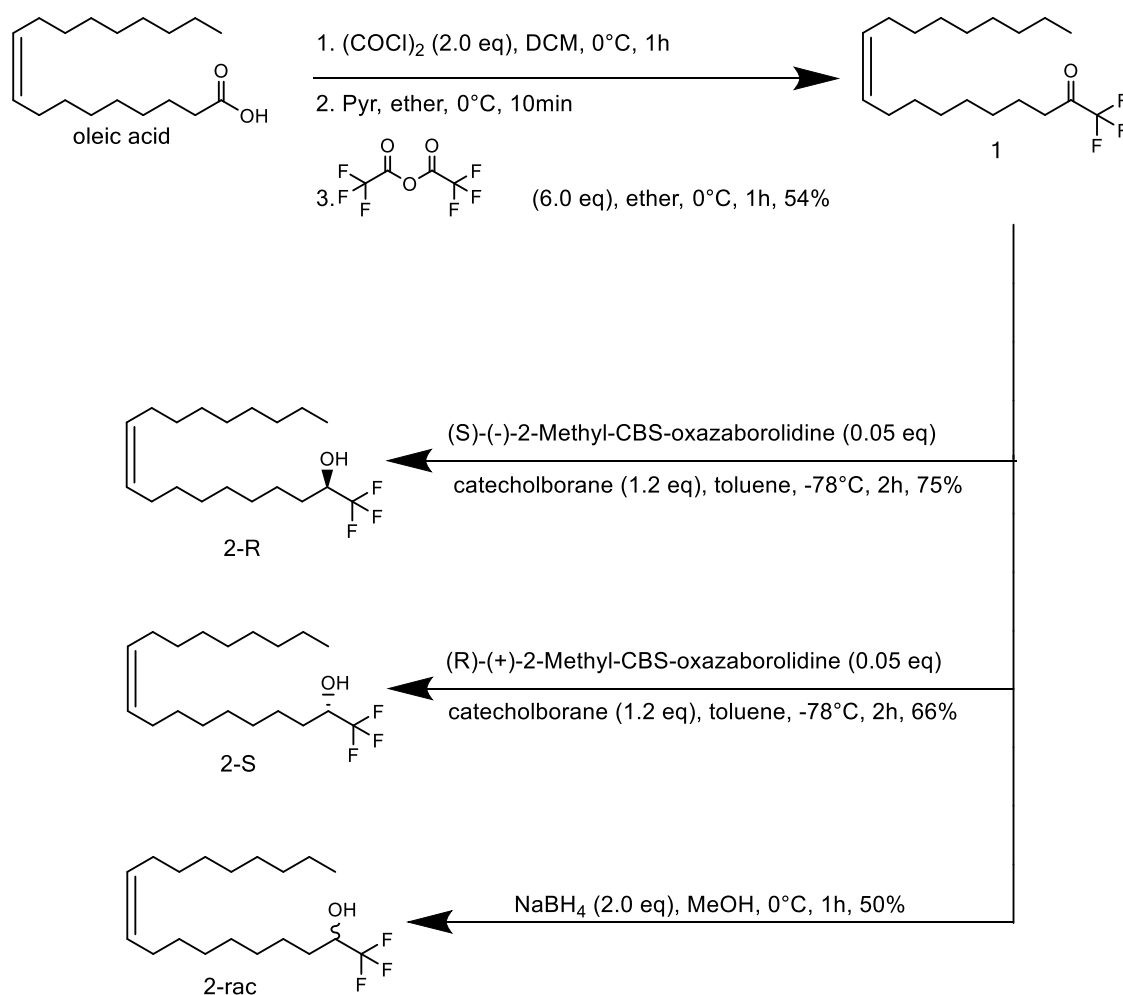
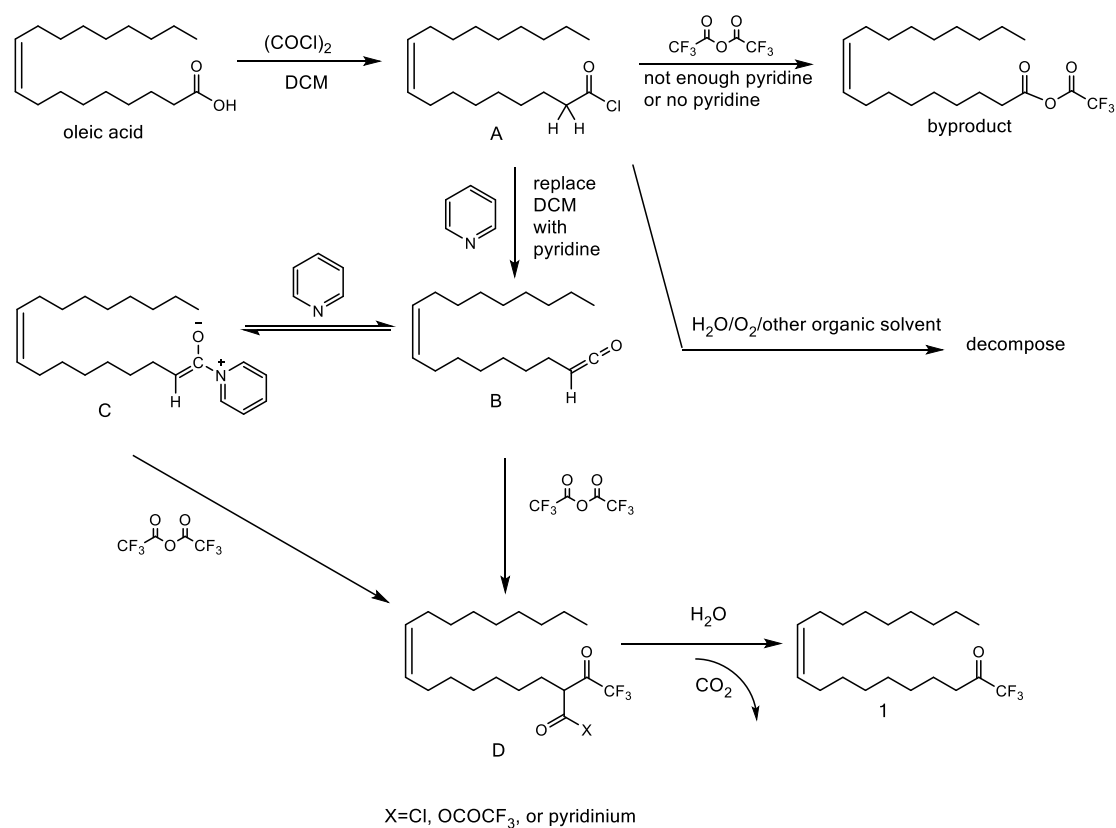


Figure 8. Synthesis scheme of compound **1**, **2-R**, **2-S**, and **2-rac**.

2.2 Scale-up synthesis of 1, 2-R, 2-S and 2-rac

As a first goal, we repeated the Forresteri synthesis of compound **1**. However, in doing so, we observed that the synthesis was not reliable, and gave variable results, including sometimes no product generated. The synthesis of compound **1** is based on a report by Jean Boivin et al. in 1992. [17] Therefore, in order to investigate the protocol and develop a more reliable one, we referred to [17]. The mechanism of the reaction to prepare the **1** is shown in **Figure 9**.



According to this mechanism, oleic acid is first transformed into the

Figure 9. Mechanism of synthesis from oleic acid to compound **1**.

acid chloride (**intermediate A**) using oxalyl chloride, then with the

addition of pyridine generates a ketene (**intermediate B**). This ketene can react with trifluoroacetic anhydride to yield compound **1** after hydrolysis and decarboxylation. The ketene can also react with excess pyridine to form **intermediate C** which is still able to be captured by trifluoroacetic anhydride and then yield compound **1**. However, if there is not enough pyridine added to the acid chloride before trifluoroacetic anhydride is added to the reaction mixture, the acid chloride will yield an unwanted byproduct (**Figure 9**), the structure of which is identified by ¹H-NMR. Further research is needed to study the mechanism of formation of this byproduct. Thus in this synthesis method, it is important not to add trifluoroacetic anhydride until the acid chloride has completely reacted with excess pyridine.

Another issue identified is that dichloromethane (DCM) is replaced with diethyl ether as the solvent of the second step (from **A** to **B**). There is a risk in this process that water and oxygen will invade the reaction system and then decompose the acyl chloride intermediate. Overall, this method to synthesize compound **1** reported in [9] is practical, however very specific reaction protocols are required to yield consistent results. Based on these studies, the following adjustments to the protocol were made:

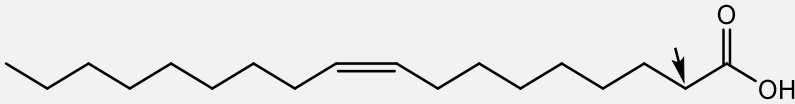
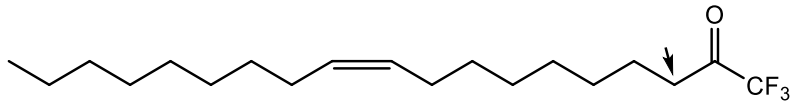
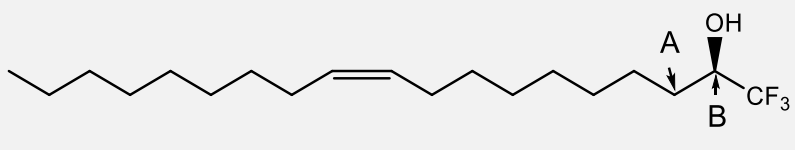
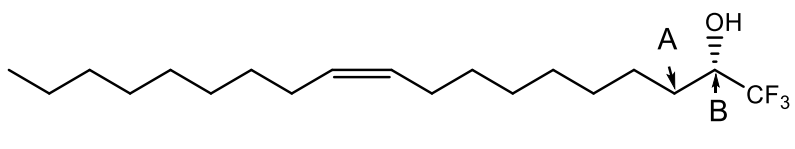
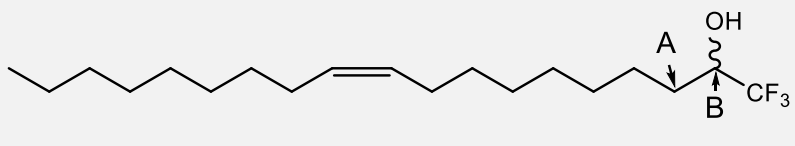
- Monitor reaction to assure complete consumption of the acid chloride before addition of (CF₃CO)₂O.
- Careful solvent exchange to exclude water and oxygen from the

reaction mixture.

We repeated the synthesis of **1** applying the adjustments to the protocol, and the yield of **1** is consistently in the 50-60% range. With ready access to this material, we also re-synthesized **2-R**, **2-S** and **2-rac** on a larger scale (**2-R**, 200 mg; **2-S**, 200 mg; **2-rac**, 630 mg). The structures of **1**, **2-R**, **2-S** and **2-rac** were confirmed using $^1\text{H-NMR}$. Chemical shift (ppm) of the $\alpha\text{-H}$ in oleic acid, $\alpha\text{-H}$ in compound **1**, and $\alpha\text{-H}$ and $\beta\text{-H}$ in compound **2-R**, **2-S** and **2-rac** are displayed in the **Table 1**.

However, $^1\text{H-NMR}$ cannot determine the optical purity of the alcohols because protons in two different enantiomers generate identical peaks on their $^1\text{H-NMR}$ spectra. Therefore, we employed Mosher's method to measure the optical purity of **2-R** and **2-S** and used **2-rac** as a standard. [18]

Table 1. Chemical shift (ppm) of the α -H in oleic acid, α -H in compound **1**, and α -H and β -H in compound **2-R**, **2-S** and **2-rac**.

Compound	Structure	Chemical shift (ppm)
Oleic acid		2.21
1		2.40
2-R		A = 1.40, B = 5.60
2-S		A = 1.40, B = 5.60
2-rac		A = 1.40, B = 5.60

Mosher's method uses α -methoxy- α -trifluoromethylphenyl-acetic acid (MTPA) to form a derivative (e.g. ester, for example) from chiral material to generate diastereomeric mixtures. [19] The characteristic NMR peaks from the Mosher reagent are typically distinct in each diastereomer, and can then be used to determine optical purity. In our experiments, we combined the alcohols (**2-R**, **2-S** and **2-rac**) with MTPA to form diastereomeric Mosher's esters (**Figure 10**). The protons in Mosher's esters with different optical configurations display different chemical shifts in their ^1H -NMR spectra. Here, we selected the protons

on the methoxy groups since their peaks in the $^1\text{H-NMR}$ spectra were easy to identify and not overlapped with other peaks.

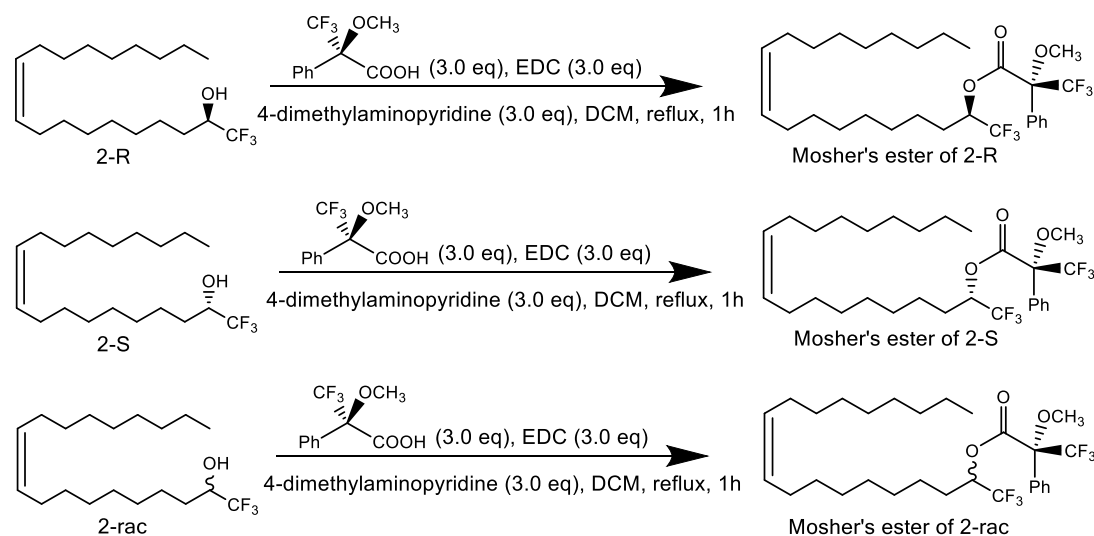


Figure 10. Mosher's method was used to determine the optical purity of **2-R**, **2-S**, and **2-rac**. **2-R**, **2-S**, and **2-rac** reacted with α -methoxy- α -trifluoromethylphenylacetic acid (MTPA) to form Mosher's ester of **2-R**, **2-S**, and **2-rac** respectively.

Two different peaks appeared in the $^1\text{H-NMR}$ spectrum of **2-rac**, the racemic alcohol, one at $\sim\delta$ 3.4 ppm and one at 3.5 ppm, in a ratio close to 1:1, indicating that the diastereomers could be differentiated, and this method used to assess chiral purity of R-2 and S-2 by calculating the $^1\text{H-NMR}$ peak integration of the protons on the methoxy groups. (**Table 2**) There was only one peak around 3.60 ppm in the Mosher's ester of **2-R**, and only one peak around 3.45 ppm in the Mosher's ester of **2-S**, indicating that these two enantiomers are optically pure, at least at the level of >95:5 (the sensitivity of NMR) This experiment confirmed the optical purity of **2-R** and **2-S**.

Table 2. $^1\text{H-NMR}$ spectra from $\sim 3\text{ppm}$ to 4.2ppm of **2-R**, **2-S** and **2-rac**.

	<p>Mosher's ester of 2-R</p>
	<p>Mosher's ester of 2-S</p>
	<p>Mosher's ester of 2-rac</p>

2.3 Synthesis of Methyl Ethers of 2-R, 2-S and 2-rac

To further understand the structure-activity relationship of the trifluoromethyl isosteres of oleic acid, and evaluate the role of the alcohol O-H, we designed and synthesized three methyl ethers **3-R**, **3-S** and **3-rac** based on **2-R**, **2-S** and **2-rac** (**Figure 9**).

The reaction from alcohol to methyl ether usually employs a basic reagent to remove the proton on the hydroxyl group, followed by addition of a methylating agent. [20-22] As reported in [21], trifluoromethyl alcohol was transformed into its methyl ether using KOH as a base and water as the solvent. We started from potassium hydroxide and iodomethane in H₂O, under 0 °C for 2h, but no reaction was observed. As we increased the temperature to 20, 40, 60, 80°C and 100°C to reflux, there was still no product. We then referred to the synthesis method reported in [20], in which the alcohol was transformed into its methyl ether using KOH as a base and dimethyl sulfoxide(DMSO) as solvent, while the carbon-carbon double bond in the structure of the starting material remained stable. We then replaced the solvent with DMSO and kept the reaction mixture under 0, 20, 40, 60, 80, 100 and 120°C, but there was no reaction observed. Therefore, we decided to use a stronger base to remove the proton. As reported in [22], a trifluoromethyl alcohol was transformed into its methyl ether using potassium tert-butoxide [KOC(CH₃)₃] as a base and

tetrahydrofuran (THF) as the solvent. We attempted to use potassium tert-butoxide, but still no reaction was observed.

There are several examples in which alcohol was transformed into its methyl ether using sodium hydride (NaH) as the reagent and THF as the solvent.[23-27] Results in [23] and [27] showed that alkenes are stable when exposed to NaH at 0°C in THF for around six hours. Results in [24] and [24, 25] showed that a starting material with a long alkyl chain (eleven carbons in [24] while ten carbons in [25]) was amenable to these reaction conditions. Based on this precedent, we used NaH as a base, which proved successful. In the case of **3-R** we achieved a satisfactory yield of 83% but in the cases of **3-rac** and **3-S** the yield was much lower (~45%) than the yield of **3-R**. (**Figure 11**) Since the reactivity of all three are identical, one possibility is that in the case of 3-rac and 3-S, the reagents and reaction conditions were not completely dry since the reactivity of NaH can easily be affected by water. According to the results, we found that NaH is the optimal base to transform trifluoromethyl alcohol to its ether when there is a long alkyl chain and carbon-carbon double bond in the structure of the starting material, although vigorously anhydrous conditions are required during operation for optimal yields.

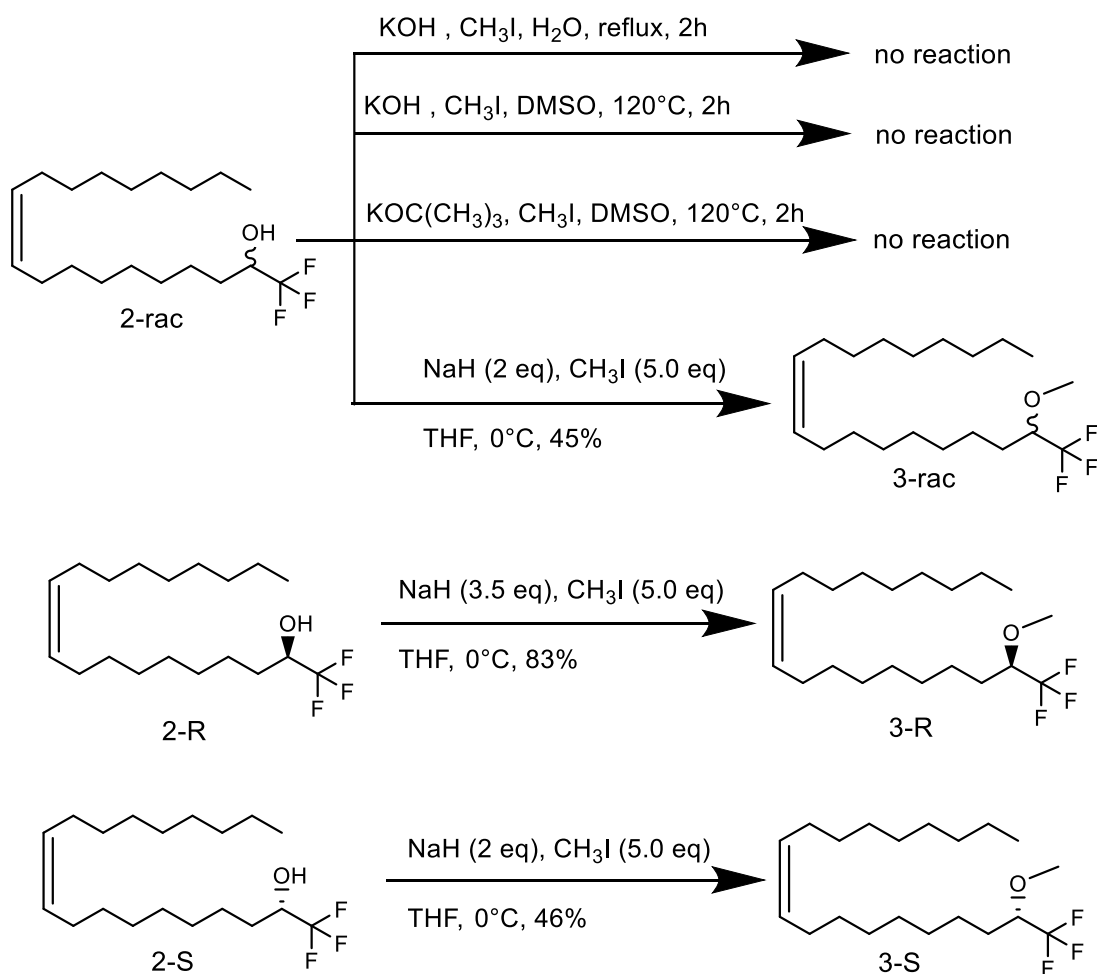


Figure 11. Synthesis scheme of compound **3-R**, **3-S**, and **3-rac**.

2.4 Bioevaluation of Methyl Ethers of 2-R, 2-S and 2-rac

Our collaborators tested **3-R**, **3-S** and **3-rac** at 20uM in the FRDA (erastin) model using **2-R** as a positive control (**Figure 12**, **Figure 13**). Under conditions where + erastin resulted in nearly complete loss of survival (~9% survival) the three ethers, **3-R**, **3-S** and **3-rac** are virtually

inactive ($\leq 20\%$ protection). In the same assay, the alcohol, **2-R**, resulted in $\sim 50\%$ survival. These results suggest that the proton on the trifluoromethyl alcohol is essential for the biological effects of this scaffold, perhaps acting as a H-bond donor or through an ionic interaction[28], although the specific molecular target of these compounds remain unclear.

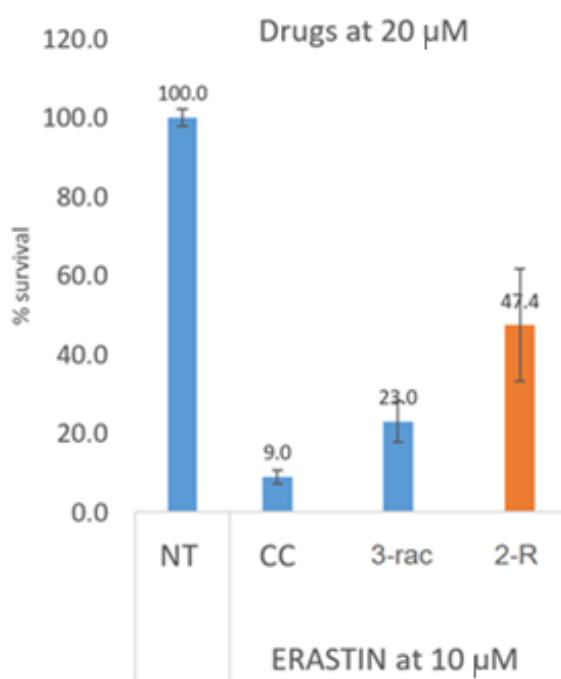


Figure 12. Efficacy of compound **3-rac** and **2-R** in protecting FRDA cells treated with erastin. NT = not treated. CC = control carrier. Data courtesy of M. Coticelli and R. Wilson

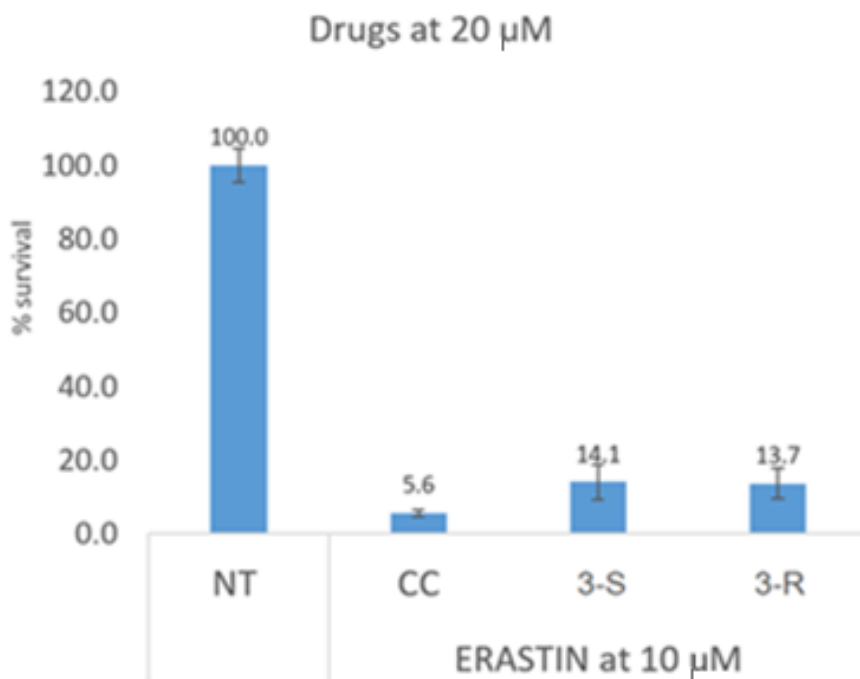


Figure 13. Efficacy of compound **3-S** and **3-R** in protecting FRDA cells treated with erastin. NT = not treated. CC = control carrier. Courtesy of M. Cotticelli and R. Wilson

2.5 Future plans based on trifluoromethyl alcohol scaffold

2.5.1 Other Analogs of 2-R

Based on the results above, our future synthesis plan will focus on further exploring the structure-activity relationship of **2-R** since it showed promising efficacy in FRDA models. Given the requirement for either an ionizable group or a proton donor, new molecules will focus on retaining this feature. An example of future compounds includes methyl alcohol which would test the importance of pKa of the OH (e.g. methanol pKa ~29 in DMSO; trifluoromethanol pKa ~23, DMSO) [29], and also lipophilicity at

the terminal position.

2.5.2 Long-chain unsaturated fatty acids other than oleic acid

Previous studies suggest that in addition to oleic acid, other fatty acids including Cis-Vaccenic Acid, Erucic acid, Gadoleic Acid, Petroselinic Acid, Palmitoleic Acid and cis-10-Heptadecenoic Acid (structure showed in **Figure 14**) also display protective effects on FRDA cell models, although to a slightly lesser degree than oleic acid.[9] Future plans include the synthesis of the trifluoromethyl ketone and alcohols of these molecules to determine the optimal chain length and olefin position. In addition, we will be able to determine if the trends we observed in the oleic acid series can be transferred to other fatty acid scaffolds.

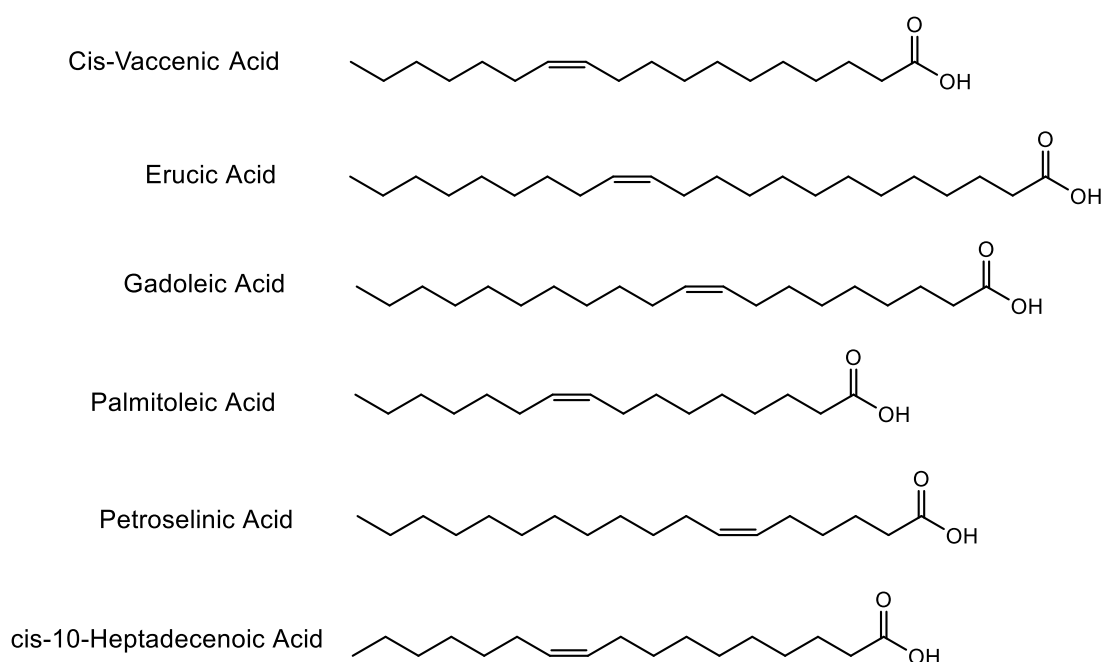


Figure 14. Structure of Cis-Vaccenic Acid, Petroselinic Acid, Petroselinic Acid, Erucic acid, Heptadecenoic acid and Palmitoleic Acid.

3.0 Design and synthesis of other isosteres of oleic acid

Since previous approach applying isosteric replacement was successful, we decided to investigate further the activity of novel isosteres of oleic acid in FRDA models. Also, there are some shortcomings in the carboxylic acid functional group, including rapid metabolism in vivo and toxic metabolites in some cases. [30] Therefore, to further study the structure-activity relationships of isosteres of oleic acid, we planned to design and synthesize novel compounds based on previous work.

To further study the effects of different isosteres in FRDA model, we designed five novel isosteres of oleic acid (**Figure 15**). Previous studies provide successful examples of various categories of isosteres of carboxylic acid, including amino groups, substituted phenols, sulfonamides and acylureas. [13] [31], and compounds **4**, **5**, **6**, **7** and **8** provide a typical representation of each category separately (**4** - amino group; **5** - substituted phenol; **6** and **7** – sulfonamides; **8** – acylureas). The other reason why we designed **4**, **5**, **6**, **7** and **8** was to further study the effects of different physicochemical properties on the activity. Compound **2-R** was more active than other compounds in the assay mentioned, so we calculated the value of pK_a (298K in aqueous solution), numbers of H-bond donor (HBD) and H-bond acceptor (HBA), logP and logD_{7.4} of **2-R** using MarvinSketch (**Table 3**). Data showed that **2-R** displays notably

higher values of pK_a and $\log D_{7.4}$ than oleic acid. We calculated the value of pK_a (298K in aqueous solution), numbers of H-bond donor (HBD) and H-bond acceptor (HBA), $\log P$ and $\log D_{7.4}$ of compounds **1**, **2-rac**, **2-S**, **3-rac**, **3-R**, **3-S**, **4**, **5**, **6**, **7**, **8** and oleic acid using MarvinSketch (**Table 3**). Compounds **4**, **5**, **6**, **7** and **8** display higher values of pK_a and $\log D_{7.4}$ than oleic acid except for the values of pK_a of **4**, which is similar to compound **2-R**. We expected to further study the structure-activity relationships of isosteres of oleic acid and learn the effects of different physicochemical properties of isosteres on their effectiveness in FRDA cell models.

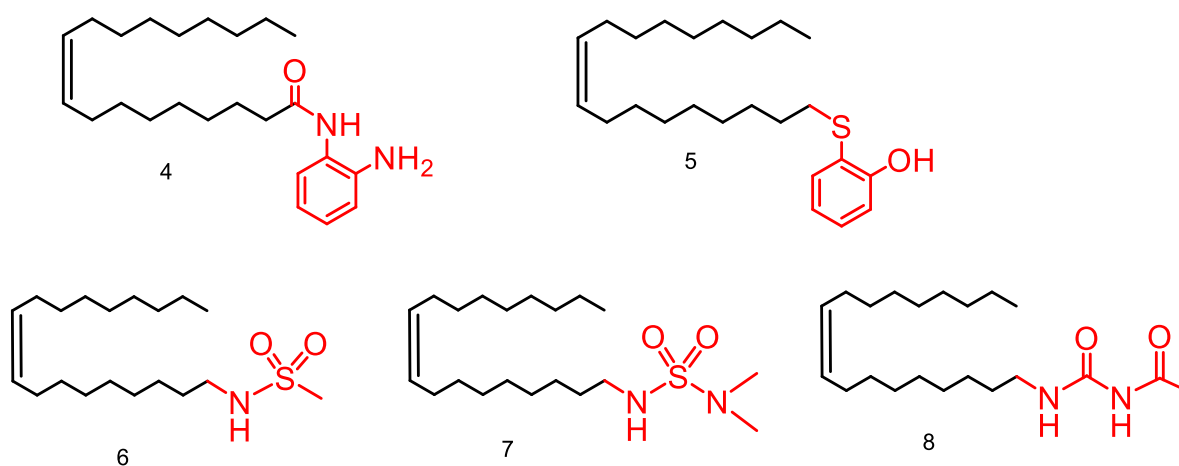


Figure 15. Structure of compounds **4**, **5**, **6**, **7** and **8**.

Table 3. Prediction of the value of pKa(298K), numbers of H-bond donor (HBD) and H-bond acceptor (HBA), logP and logD_{7.4} of compounds **1**, **2-rac**, **2-R**, **2-S**, **3-rac**, **3-R**, **3-S**, **4**, **5**, **6**, **7**, **8** and oleic acid using MarvinSketch at 298K.

Compound	pKa(298K)	HBD	HBA	logP	logD _{7.4}
Oleic acid	4.99	1	2	6.78	4.4
1	-	0	1	8.25	8.25
2-rac , 2-R , 2-S	11.41	1	1	7.68	7.68
3-rac , 3-R , 3-S	-	0	1	8.33	8.33
4	3.45 (conjugate acid)	2	2	7.39	7.39
5	9.20	1	1	9.38	9.37
6	12.08	1	2	5.87	5.87
7	12.10	1	3	5.87	5.87
8	11.78	2	2	6.03	6.03

3.1 Synthesis of N-(2-aminophenyl)oleamide (**4**)

We designed and synthesized N-(2-aminophenyl) amide of oleic acid (**4**) as a bioisostere of the carboxylic acid of oleic acid. The value of pK_a and ionization state of compound **4** was predicted using MarvinSketch at 298K (**Figure 16**). Predicted value of pK_a of the conjugate acid of the aniline group of compound **4** is 3.45. Also, the aniline group of compound **4** can be H-bond donors, acceptors, and can participate in dipole interactions. Therefore, this group may serve as a replacement of the carboxylic acid functional group.

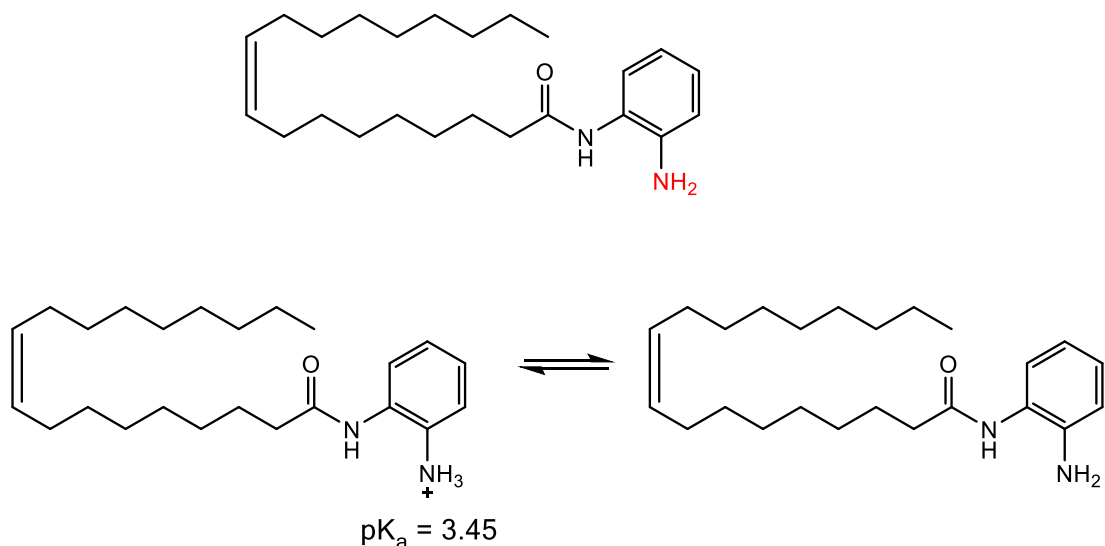


Figure 16. Prediction of the value of pK_a and ionization state of compound **4** using MarvinSketch at 298K.

Compound **4** was synthesized previously, as reported in [32]. Here we employed the method reported in [33] since our lab has successfully used this method before. Oleic acid was combined with benzene-1,2-diamine using N-Methylmorpholine and propanephosphonic acid anhydride to yield the known final product, N-(2-aminophenyl)oleamide. (**Figure 17**).

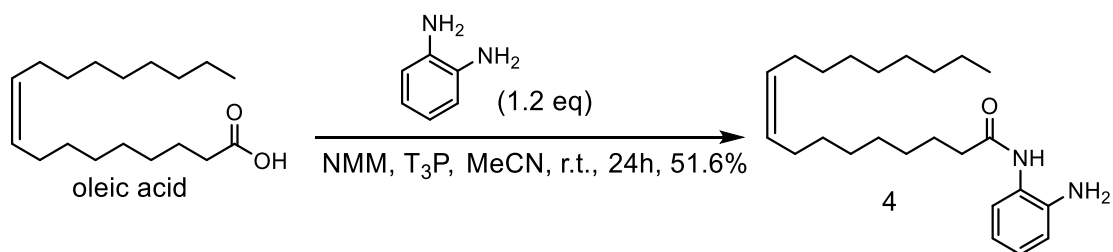


Figure 17. Synthesis scheme of compound **4**.

3.2 Synthesis of (Z)-2-(octadec-9-en-1-ylthio)phenol (5)

According to previous studies, substituted phenols are slightly acidic and can serve as bioisosteres of carboxylic acids.[31] Therefore, we designed and synthesized the substituted phenol isostere, compound **5** (**Figure 16**). We confirmed that compound **5** was a novel molecule using SciFinder.

As reported in [34], 2-mercaptophenol can react with a primary alkyl bromide and sodium bicarbonate (NaHCO_3) in dimethylformamide (DMF) to yield its alkyl thiophenol while the carbon-carbon double bond in the starting material remained stable during the reaction. In addition, there are several examples that oleyl bromide (structure showed in **Figure 18**) can be synthesized from oleyl alcohol (structure showed in **Figure 18**) using tetrabromomethane (CBr_4) and triphenylphosphine (PPh_3) in dichloromethane (DCM). [35-39] Oleyl alcohol and oleyl bromide are both commercially available, but oleyl alcohol is much more affordable than oleyl bromide. Therefore, we designed the synthesis scheme of compound **5** as showed in **Figure 18**.

We first repeated the synthesis method of oleyl bromide reported in [35-39] and the yield of oleyl bromide is 99%, suggesting this is an efficient method to synthesize oleyl bromide in lab. We then synthesized compound **5** from oleyl bromide according to the method reported in [34].

The yield of compound **5** was only 46% but the operation during reaction was quite simple, which means this is a convenient method to synthesize compound **5** except for the modest yield.

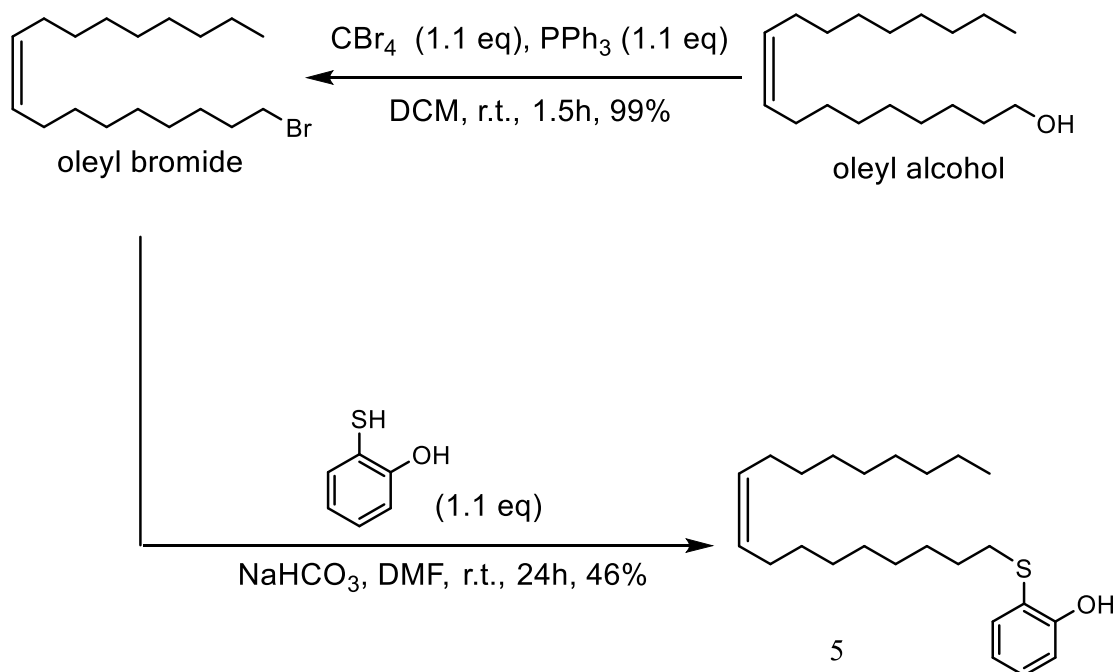


Figure 18. Synthesis scheme of compound **5**.

3.3 Synthesis of (Z)-N-(octadec-9-en-1-yl)methanesulfonamide (**6**) and (Z)-N'-(octadec-9-en-1-yl)-N,N-dimethylsulfamide (**7**)

Previous studies showed that sulfonamides could substitute for a carboxylic due to the geometric similarity and the pKa between the sulfonamide functional group and the carboxylic acid functional group. [31] In addition, the replacement of carboxylic acid groups with sulfonamides

was shown to improve the permeability through biological membrane of the original carboxylic acids in some cases. [13] Therefore, we designed and synthesized compounds **6** and **7** (**Figure 19**) to evaluate if the sulfonamide functional group can also show protective effects in the FRDA assay. We confirmed that compounds **6** and **7** were novel molecules using SciFinder.

Synthesis of compound **6** was based on a method reported in [40], in which the primary amine reacted with methanesulfonyl chloride to yield the product while the carbon-carbon double bond in the starting material remained stable during the reaction. Towards this end, Oleylamine was combined with methanesulfonyl chloride to yield compound **6**. Synthesis of compound **7** relied on an identical method reported in [41], in which the primary amine reacted with sulfamoyl chloride to yield the product while the carbon-carbon double bond in the starting material remained stable during the reaction. Oleylamine was combined with N,N - dimethylsulfamoyl chloride to yield compound **7**. High yields of compounds **6** and **7** indicated that these two synthesis methods are ideal to produce the final products. In addition, these two synthesis methods are operationally simple.

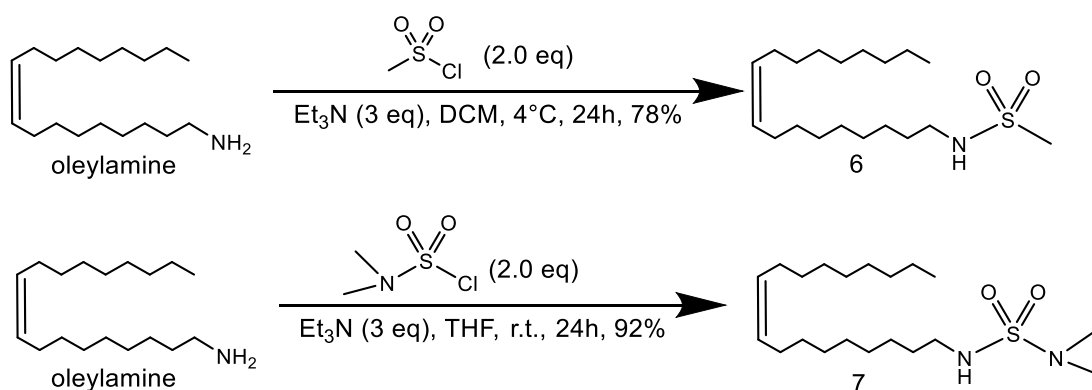


Figure 19. Synthesis scheme of compounds **6** and **7**.

3.4 Synthesis of (Z)-N-(octadec-9-en-1-ylcarbamoyl)acetamide (**8**)

Acylurea functional group can also serve as a carboxylic acid isostere, and sometimes affords higher permeability through biological membranes. [13] Therefore we designed and synthesized compound **8** (**Figure 20**). We confirmed that compound **8** was a novel molecule using SciFinder.

As reported in [42], the scientists synthesized (Z)-1-(octadec-9-en-1-yl)urea from oleylamine using nitrourea, while nitrourea was synthesized from urea and nitric acid *in situ* and used without further purification. Here we repeated this synthesis method and achieved an excellent yield of 92%. The urea group in (Z)-1-(octadec-9-en-1-yl)urea was acetylated by adding acetic anhydride to yield the final product, compound **8**, which is an identical method reported in [43].

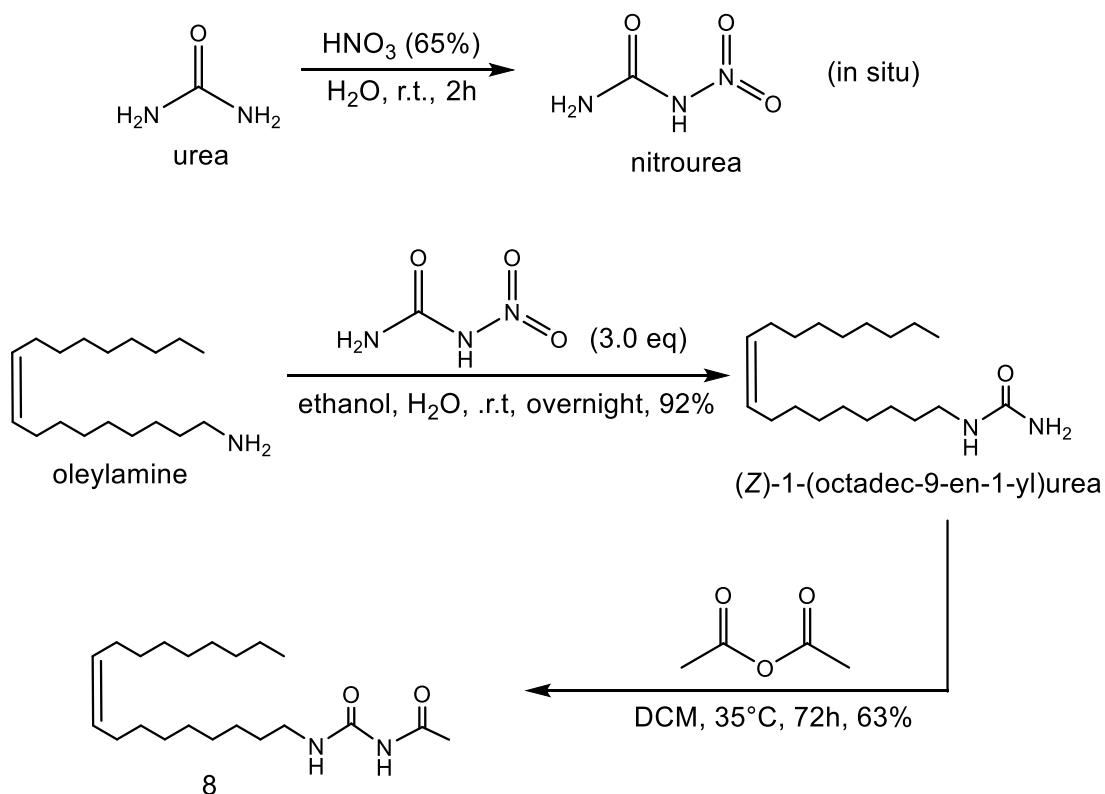


Figure 20 Synthesis scheme of compound **8**.

3.5 Bioevaluation of 4, 5, 6, 7 and 8

3.5.1 Bioevaluation of Compound 4, 5, 6, 7 and 8

Our collaborators tested the effectiveness of compounds using the FRDA (erastin) assay as described in Chapter 1.

Compounds **4**, **5**, **6**, **7**, **8** along with **3-rac** and **2-R** (as a control) were tested at 20 μm (**Figure 21**). Results showed that **4** and **5** were more efficacious than the other compounds in this assay, improving the survival of cells to 3~4 times of the survival of cells treated with **6**, **7**, **8** and **3-rac**.

Of interest, **4** and **5**, were much effective than our previous ‘best’ compound **2-R** under these assay conditions.

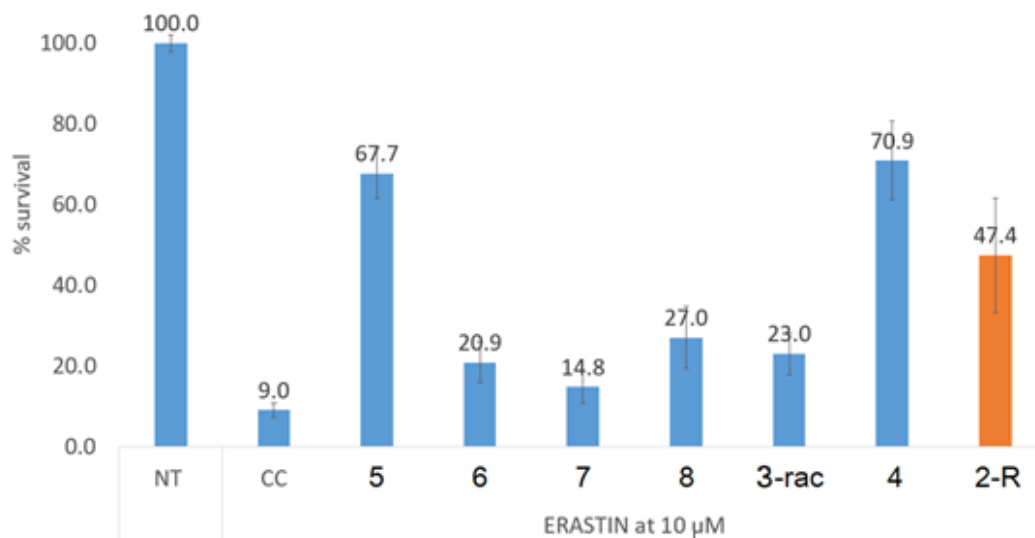


Figure 21. Efficacy of compound **2-R**, **3-rac**, **4**, **5**, **6**, **7** and **8** in protecting FRDA cells treated with erastin at 20 μ M. NT = not treated. CC = control carrier. Data courtesy of R. Wilson and G. Cotticelli

Further testing of **4** showed the effects to be dose-dependent, with protective effects observed at 1 (~50%) and 5 μ M (~95%), but no significant effect at 0.5 μ M or 0.1 μ M (**Figure 22**).

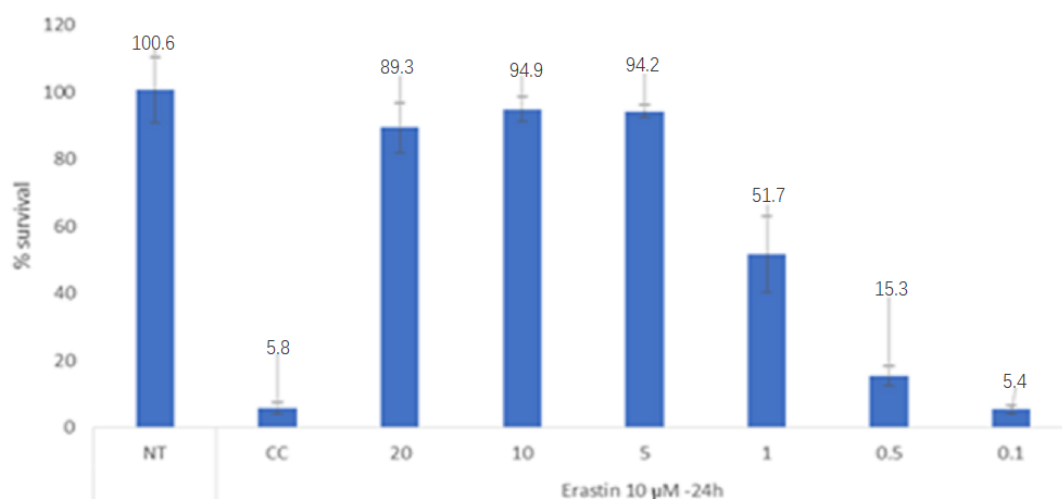


Figure 22. Efficacy of compound 4 in protecting FRDA cells treated with erastin. Compound 4 was tested at 20, 10, 5, 1, 0.5 and 0.1 μ m. NT = not treated. CC = control carrier. Data courtesy of R. Wilson and G. Cotticelli

Compound 4 was also tested side by side with 2-R, 2-S and oleic acid. Interestingly, compound 4 was the most potent among these molecules. At 5 μ m, the survival of cells treated with compound 4 was more than four times of the survival of cells treated with compound 2-R. Even at 1 μ m, compound 4 still showed notable protective effects on FRDA cell models (Figure 23).

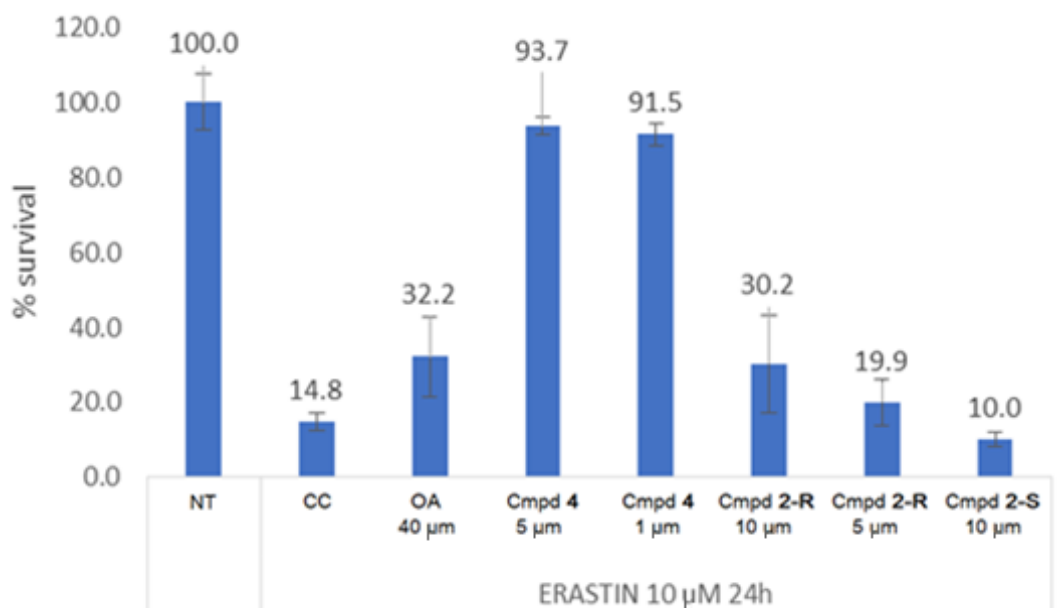


Figure 23. Efficacy of compounds **4**, **2-R**, **2-S** and oleic acid in protecting FRDA cells treated with erastin. NT = not treated. CC = control carrier.

A previous study suggested that compound **4** can be hydrolyzed into oleic acid and nitrogen-containing heterocycle when exposed to nitric oxide and oxygen (**Figure 24**). [32] Benzamides are also known to be pro-drugs, and can be hydrolyzed in cells to deliver the carboxylic acid.[44] Therefore, we decided to evaluate the chemical stability of compound **4** under conditions of the assay to evaluate if the compound was acting as a pro-drug to deliver oleic acid.

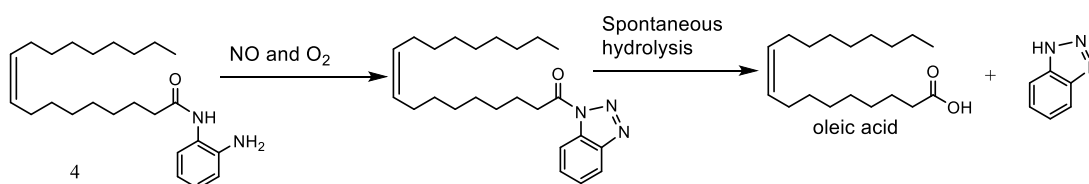


Figure 24. Mechanism of hydrolysis of compound **4** into oleic acid when exposed to nitric oxide and oxygen.

We dissolved **4** in DMSO at 4 mM and diluted this solution in the medium

which was used in the bioassays to culture cells. The resulting mixture was kept at room temperature for 24 h. Then we employed Thin-Layer Chromatography (TLC) to monitor the stability using oleic acid as a TLC standard. Although TLC cannot be used to determine the purity or concentration in the structure, it is a convenient method in the lab to identify the appearance of certain molecules with a standard. In addition, the lack of a chromophore in oleic acid, makes its detection challenging by more typical methods. We found that **4** was stable under these conditions after checking for three times at the same time, and no spot of oleic acid was observed. While we have not determined the stability of **4** in cells, we are confident that at least in the assay media, no hydrolysis is occurring.

3.5.2 Studies towards additional novel isosteres

To further evaluate the structure requirements for activity based on compound **4**, we plan to replace the nitrogen atom in the amide bond with a carbon atom (**Figure 25**). In addition, this compound cannot be hydrolyzed to oleic acid, therefore it would serve to further evaluate the potential for Compound **4** to be acting as a pro-drug. For example, if the new compound was inactive, it suggests the need for the NH and we would not rule out the pro-drug possibility for **4**. Therefore, this compound would give us important SAR information.

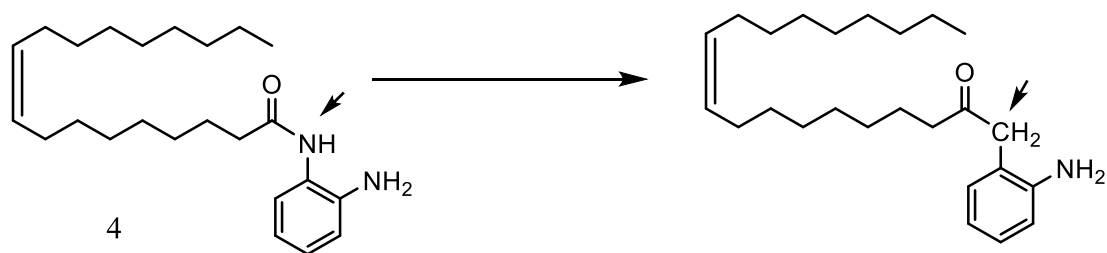


Figure 25. Modification of compound **4** by replacing the nitrogen atom in the amide bond with a carbon atom.

In order to form a new carbon-carbon bond in the molecule structure, we plan to employ a Grignard reaction, a method of adding organomagnesium halide (Grignard reagent) to a ketone or aldehyde. The carbon in a cyanide group can also be attacked by Grignard reagent and then form a new carbon-carbon bond. [45] To prepare the electrophile (ketone, aldehyde or nitrile), we will use oleic acid; an organometallic reagent based on 2-aminophenylmethanol will be used as the Grignard reagent. Since the protons on the amino group of 2-aminophenylmethanol are reactive, a protection group is needed. **(Figure 26).**

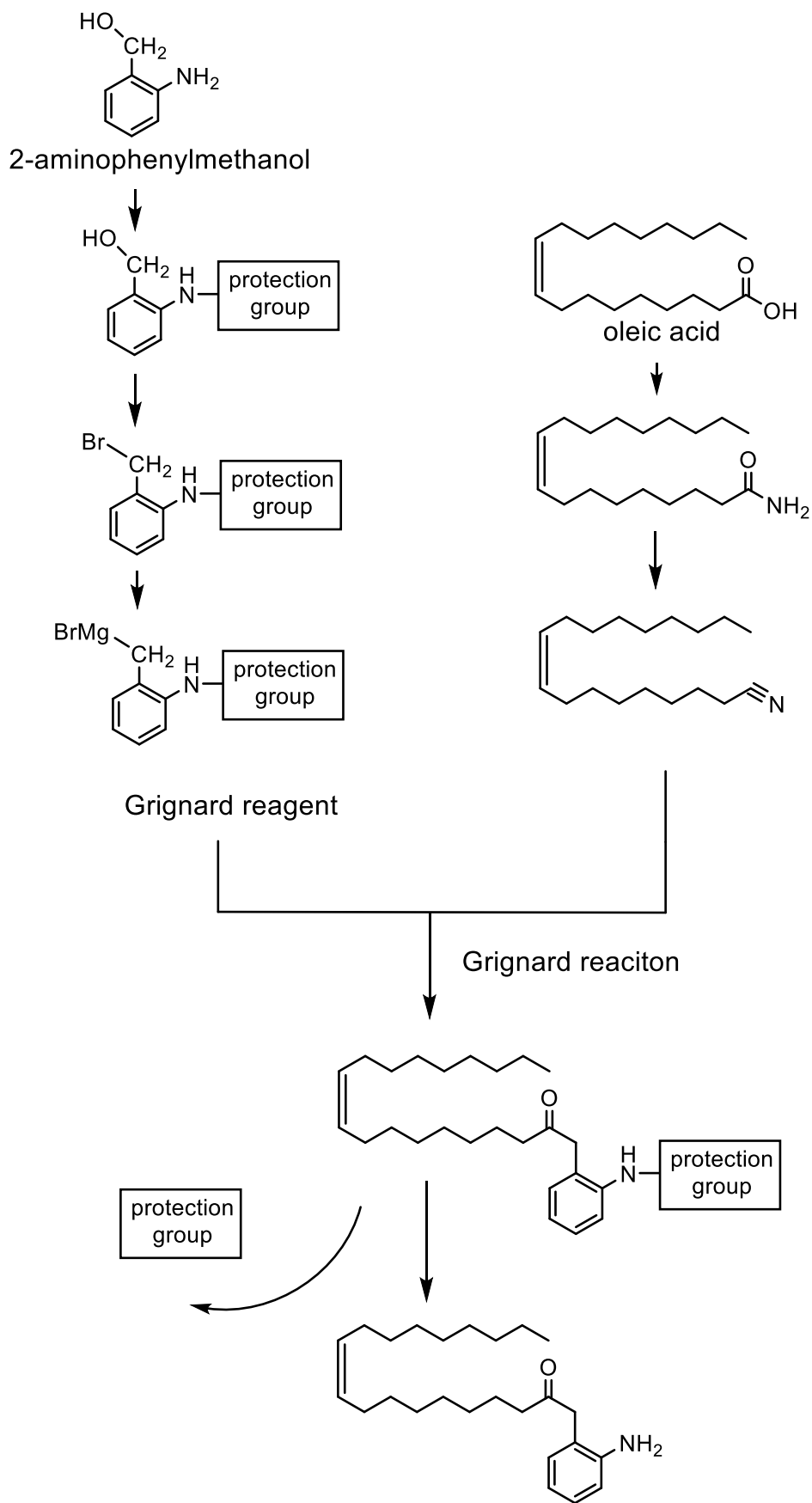


Figure 26. Synthesis plan of a new isostere of oleic acid by Grignard reaction.

Oleylnitrile was synthesized according to a method reported in [46]. Specifically, oleic acid was converted to its chloride using oxalyl chloride and then yielded oleylamide after adding ammonia monohydrate. Then oleylamide was converted to oleylnitrile using thionyl chloride (**Figure 27**).

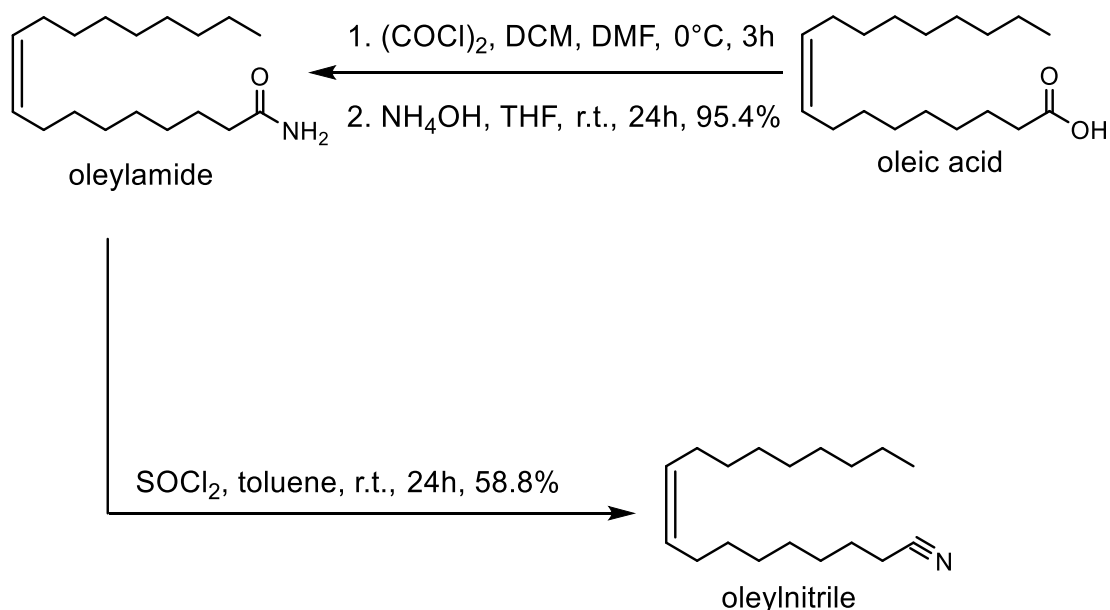


Figure 27. Synthesis scheme of oleylnitrile.

For the Grignard reagent, we first used Di-tert-butyl dicarbonate as a protection group to mask the amino group in 2-aminophenylmethanol and then replaced the hydroxyl group in 2-aminophenylmethanol with a bromine atom. However, conversion of the bromide to the Grignard reagent was unsuccessful, despite the reaction being run under strict water-free conditions. Further literature indicated that Di-tert-butyl

dicarbonate as an amino protection group is unstable under the conditions of Grignard reaction (**Figure 28**), suggesting why this reaction was unsuccessful. In addition, ring closure may also occur. [47] Thus we are now considering other amino protection groups and alternative methods of synthesis.

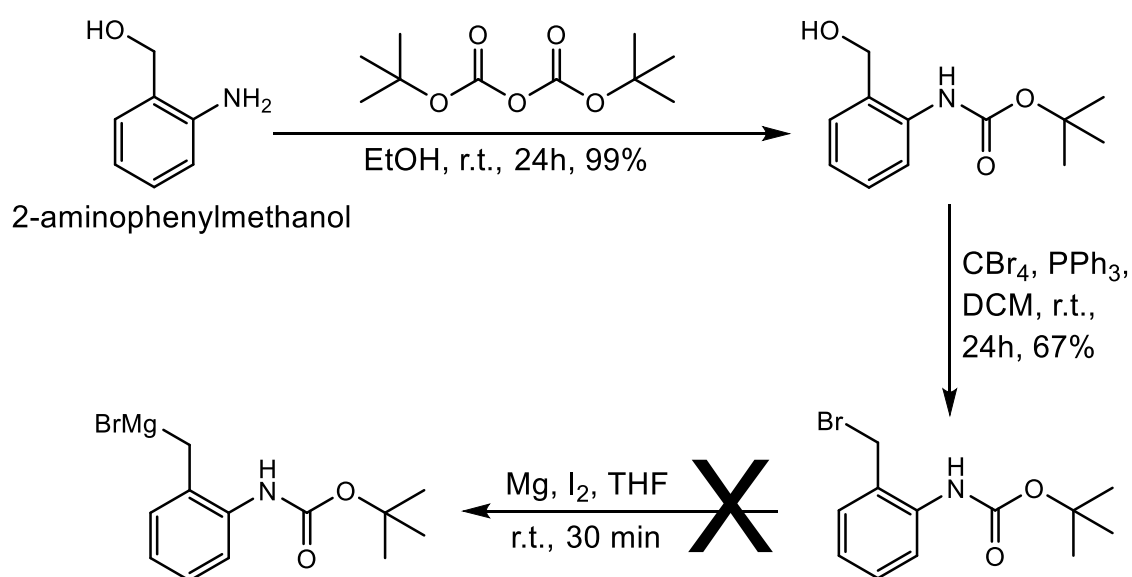


Figure 28. Failed synthesis scheme of a Grignard reagent.

4.0 Conclusion

In this project, we re-synthesized 3 compounds so they would be available for further testing, and also assessed enantiomeric purity of two of them. We also prepared 8 novel compounds (**Figure 29**): **3-rac**, **3-R**, **3-S**, **4**, **5**, **6**, **7** and **8**, based on the previous findings on compounds **1**, **2-rac**, **2-R**, **2-S**. Based on the biological testing of the new compounds, we have a more refined understanding of the structure-activity relationship of these oleic acid isosteres. Importantly, we identified two new compounds with more potent activity than the previous best compound, **2-R**.

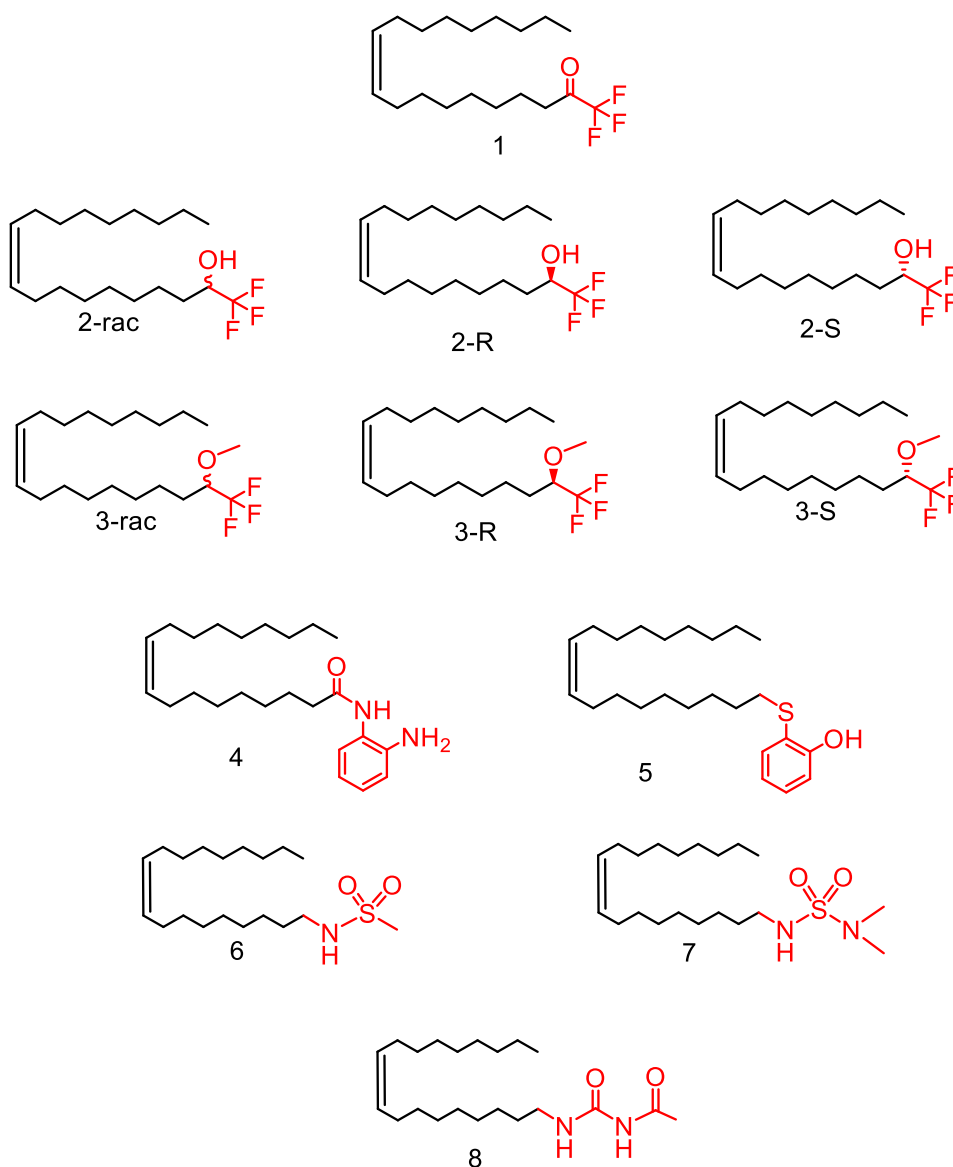


Figure 29. Structure of compound **1**, **2-rac**, **2-R**, **2-S**, **3-rac**, **3-R**, **3-S**, **4**, **5**, **6**, **7** and **8**.

Among these 12 compounds, **1**, **2-R**, **2-rac**, **4** and **5** were proved active while **2-S**, **3-R**, **3-S**, **3-rac**, **6**, **7** and **8** were not active. In all the active compounds (**1**, **2-R**, **2-rac**, **4** and **5**), each structure contains both a lipophilic group (phenyl group in **4** and **5**, trifluoromethyl group in **1**, **2-R** and **2-rac**) and a hydrogen bond donor or Lewis acid (hydroxyl group in **2-R**, **2-rac** and **5**, amino group in **4**, carbonyl group in **1** which may form a

hydrate) (**Figure 30**). In case of **3-R**, **3-S** and **3-rac** there is no hydrogen bond donor or Lewis acid while in **6**, **7** and **8** there is no lipophilic group, and these compounds are proved inactive in the FRDA cell models. However, oleic acid doesn't contain a lipophilic group but it was proved active. Further research is needed to study oleic acid as an exception.

2-R, **2-S** and **2-rac** are enantiomers but **2-S** was proved inactive in previous [9] study, indicating the stereoselectivity should be taken into consideration when designing compounds.

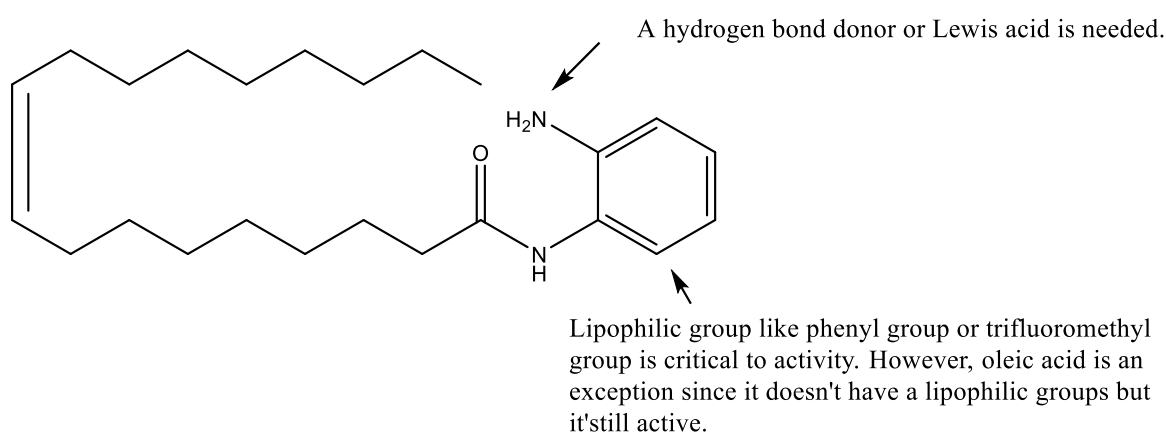


Figure 30. Structure-Activity Relationships (SAR) model based on the bioassay of **1**, **2-rac**, **2-R**, **2-S**, **3-rac**, **3-R**, **3-S**, **4**, **5**, **6**, **7** and **8**.

This project, and particularly compound **4**, the most potent compound to date, provides a good starting point for designing and synthesizing compounds for the treatment of FRDA and for molecular probes used in studying pathology. Future studies will focus on the mechanism of action studies and structure-activity researches to further improve physicochemical properties and therapeutic effects of the molecules.

5.0 Experimental Section

General Information

Reagent: All reagents were purchased at the highest commercial quality and used without further purification, unless otherwise stated. All solvents were reagent grade, unless otherwise stated.

Thin layer chromatography : Thin layer chromatography (TLC) was performed using 0.25 mm E. Merck precoated silica gel plates. TLC spots were detected using UV light and/or a solution of p-anisaldehyde in ethanol with H₂SO₄ and heat as color-developing agents.

NMR: ¹H-NMR was used to confirm the purity of all the final products. Chloroform-D was used as the solvent. ¹H-NMR and ¹³C-NMR spectra were recorded on a Bruker AMX-500 spectrometer. ¹H and ¹³C chemical shifts were reported relative to the residual solvent's peak.

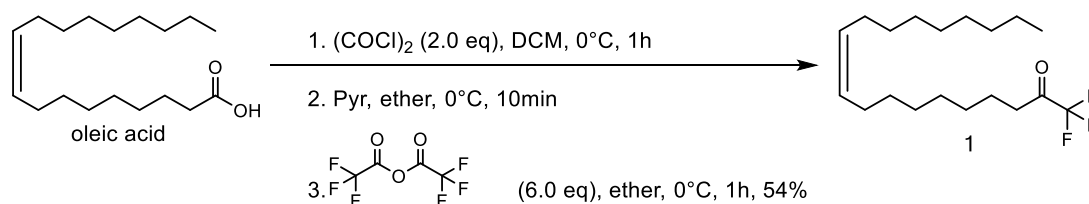
Mass Spectra: High resolution mass spectrometry (HRMS) was performed on a Thermo TSQ Quantum Ultra spectrometer.

Compounds

Oleic acid and oleyl alcohol were purchased from commercial sources at the highest commercial quality and used as received. Oleylamine purchased from commercial sources and used after further purification in lab.

Purification of oleylamine: Add 5g crude oleylamine to the Erlenmeyer flask. Then add 400mL NaOH solution (800mg NaOH in 300mL H₂O) and 50mL ethyl acetate. Ethyl acetate layer was separated, aqueous layer was extracted with ethyl acetate (3 x 50.0 mL). The combined organic layers were dried over anhydrous Na₂SO₄, filtered, and concentrated in *vacuo*. The resulting crude product was purified using silica gel chromatography (Combi flash *Rf*, 40% MeOH-DCM with NH₃). ¹H NMR (600 MHz, CDCl₃): δ 5.43-5.33 (m, 2H), 2.71-2.69 (m, 2H), 2.08-1.91 (m, 4H), 1.52-1.48 (m, 2H), 1.39-1.20 (m, 22H), 0.92-0.84 (m, 3H) ppm; ¹³C NMR (CDCl₃, 150 MHz) δ 130.5, 130.4, 130.3, 130.2, 129.9, 129.8, 128.7, 60.4, 42.2, 39.7, 33.8, 32.6, 31.9, 31.8, 31.5, 30.9, 29.7, 29.6, 29.5, 29.4, 29.3, 28.9, 27.7, 27.2, 26.8, 23.3, 22.7, 22.5, 21.0, 18.3, 14.2, 14.1 ppm.

(Z)-1,1,1-trifluorononadec-10-en-2-one (1):

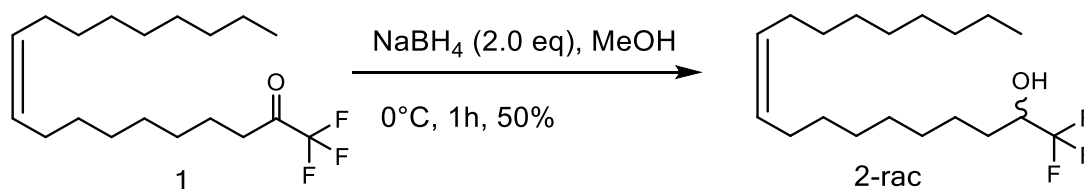


Step 1: To a solution of oleic acid (1g, 3.5 mmol, 1.0 equiv) in DCM (20.0 mL) was added oxalyl chloride (1.3g, 0.88 mL, 10.6 mmol, 3.0 equiv) dropwise over 30min under nitrogen atmosphere at 0°C . The resulting reaction mixture was stirred at room temperature in dark for 1 h.

Step 2 and 3: The collector of rotovap was cleaned thoroughly with acetone and dried before use. The solvent was removed by *vacuo* at 45°C . Then the flask was capped quickly and protected the concentrate with nitrogen atmosphere. The concentrate was desolved with ether (20.0 mL) under nitrogen atmosphere at 0°C while stirred. To the mixture add pyridine (2.2mL) and after stirring for 10 min, trifluoroacetic anhydride (2.90 mL, 21.2 mmol, 6.0 equiv) was added dropwise. The resulting reaction mixture was stirred at 0°C for 2h. TLC analysis of the reaction shows complete disappearance of starting material. The reaction mixture was quenched with the addition of H_2O (50.0 mL) very slowly in a large Erlenmeyer flask. The ether layer was separated, aqueous layer was extracted with ethyl acetate (3 x 15.0 mL). The combined organic layers were dried over anhydrous Na_2SO_4 , filtered, and concentrated in *vacuo*. The resulting crude product was purified using silica gel chromatography (Combi flash *Rf*, 5% Hex-EA) to produce (Z)-1,1,1-trifluorononadec-10-en-

2-one (**1**, 630 mg, 1.90 mmol, 54%) as light yellow liquid. ¹H NMR (600 MHz, CDCl₃): δ 5.42-5.35 (m, 2H), 2.79-2.72 (m, 2H), 2.06-2.01 (m, 4H), 1.72-1.68 (m, 2H), 1.45-1.26 (m, 22H), 0.93-0.86 (m, 3H) ppm; CIMS m/z 332.976 (calcd for C₁₉H₃₃F₃O, 334.47).

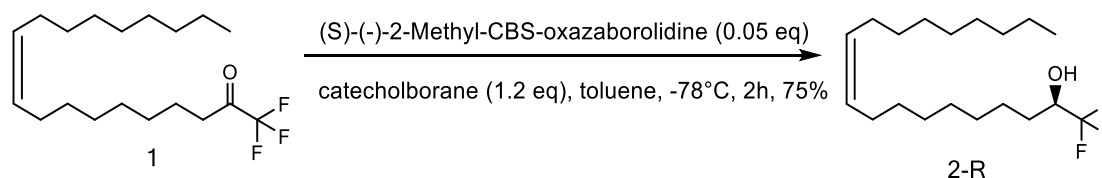
(Z)-1,1,1-trifluorononadec-10-en-2-ol (2-rac):



To a solution of (Z)-1,1,1-trifluorononadec-10-en-2-one (**1**, 630 mg, 1.9 mmol, 1.0 equiv) in methanol (20.0 mL) was added sodium borohydride (144 mg, 3.8 mmol, 2.0 equiv) under nitrogen atmosphere at 0 °C. The resulting reaction mixture was stirred at 0 °C for 1 h. TLC analysis of the reaction shows complete disappearance of starting material. The reaction mixture was concentrated in *vacuo* and then quenched with the addition of H₂O (30.0 mL). Then the aqueous layer was extracted with ethyl acetate (3 x 15.0 mL). The combined organic layers were dried over anhydrous Na₂SO₄, filtered, and concentrated in *vacuo*. The resulting crude product was purified using silica gel chromatography (Combi flash *Rf*, 15% Hex-EA) to produce (Z)-1,1,1-trifluorononadec-10-en-2-ol (**2-rac**, 280 mg, 0.83 mmol, 50%) as light yellow liquid. ¹H NMR (600 MHz, CDCl₃): δ 5.45-5.36 (m, 2H), 3.89-3.83 (m, 1H), 2.12-1.92 (m, 4H), 1.68-1.62 (m, 1H), 1.52-1.48

(m, 2H), 1.45-1.19 (m, 22H), 0.88-0.78 (m, 3H) ppm; ¹³C NMR (CDCl₃, 150 MHz) δ 130.1, 129.7, 128.0, 126.2, 124.3, 122.4, 70.8, 70.7, 70.5, 70.3, 31.9, 31.8, 29.8, 29.7, 29.6, 29.5, 29.3, 29.3, 29.2, 29.2, 27.2, 27.2, 24.9, 22.7, 22.6, 21.0, 14.1, 14.1 ppm. CIMS m/z 338.32 (calcd for C₁₉H₃₅F₃O, 336.48).

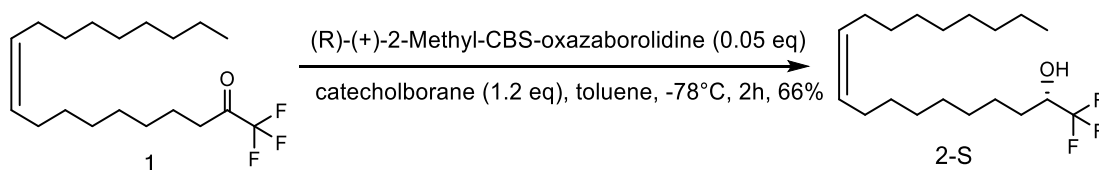
(R,Z)-1,1,1-trifluorononadec-10-en-2-ol (2-R):



To a solution of (Z)-1,1,1-trifluorononadec-10-en-2-one (**1**, 200 mg, 0.6 mmol, 1.0 equiv) in toluene (5.0 mL) was added (S)-(-)-2-Methyl-CBS-oxazaborolidine (0.03 mL, 1 mol/L, 0.03 mmol, 0.05 equiv) and the resultant solution was stirred under nitrogen atmosphere at -78°C for 10 min. Catecholborane (1.2 mL, 1 mol/L, 1.2 mmol, 2.0 eq) was then added dropwise over 2 h at -78°C, and the reaction mixture was stirred at room temperature for 1 h. TLC analysis of the reaction shows complete disappearance of starting material. The reaction mixture was quenched with the addition of H₂O (20.0 mL). The organic layer was separated, then the aqueous layer was extracted with ethyl acetate (3 x 10.0 mL). The combined organic layers were dried over anhydrous Na₂SO₄, filtered, and concentrated in *vacuo*. The resulting crude product was purified using silica gel chromatography (Combi flash *R_f*, 15% Hex-EA) to produce (R,Z)-

1,1,1-trifluorononadec-10-en-2-ol (**2-R**, 150 mg, 0.45 mmol, 75%) as light yellow liquid. ¹H NMR (600 MHz, CDCl₃): δ 5.39-5.33 (m, 2H), 3.96-3.92 (m, 1H), 2.08-2.02 (m, 4H), 1.78-1.72 (m, 1H), 1.62-1.58 (m, 2H), 1.50-1.21 (m, 22H), 0.92-0.88 (m, 3H) ppm; ¹³C NMR (CDCl₃, 150 MHz) δ 130.1, 129.7, 128.0, 126.2, 124.3, 122.4, 70.9, 70.7, 70.5, 70.3, 31.9, 29.8, 29.7, 29.6, 29.5, 29.3, 29.3, 29.3, 29.2, 29.2, 27.2, 27.2, 26.7, 24.9, 22.7, 14.1 ppm. CIMS m/z 339.86 (calcd for C₁₉H₃₅F₃O, 336.48).

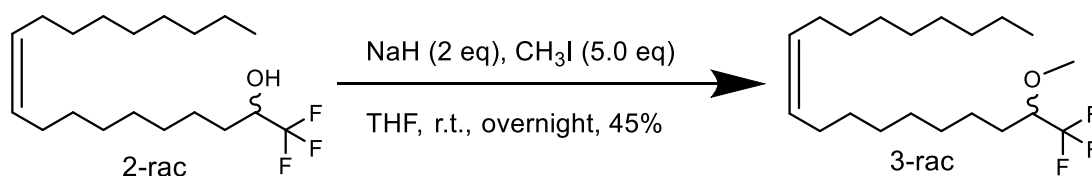
(S,Z)-1,1,1-trifluorononadec-10-en-2-ol (2-S):



To a solution of (Z)-1,1,1-trifluorononadec-10-en-2-one (**1**, 200 mg, 0.6 mmol, 1.0 equiv) in toluene (5.0 mL) was added (R)-(+)-2-Methyl-CBS-oxazaborolidine (0.03 mL, 1 mol/L, 0.03 mmol, 0.05 equiv) and the resultant solution was stirred under nitrogen atmosphere at -78°C for 10 min. Catecholborane (1.2 mL, 1 mol/L, 1.2 mmol, 2.0 eq) was then added dropwise over 2 h at -78°C, and the reaction mixture was stirred at room temperature for 1 h. TLC analysis of the reaction shows complete disappearance of starting material. The reaction mixture was quenched with the addition of H₂O (20.0 mL). The organic layer was separated, then the aqueous layer was extracted with ethyl acetate (3 x 10.0 mL). The

combined organic layers were dried over anhydrous Na₂SO₄, filtered, and concentrated in *vacuo*. The resulting crude product was purified using silica gel chromatography (Combi flash *Rf*, 15% Hex-EA) to produce (S,Z)-1,1,1-trifluorononadec-10-en-2-ol (**2-S**, 130 mg, 0.39 mmol, 66%) as light yellow liquid. ¹H NMR (600 MHz, CDCl₃): δ 5.42-5.36 (m, 2H), 3.96-3.88 (m, 1H), 2.10-2.03 (m, 4H), 1.79-1.73 (m, 1H), 1.65-1.53 (m, 2H), 1.50-1.23 (m, 22H), 0.93-0.87 (m, 3H) ppm; ¹³C NMR (CDCl₃, 150 MHz) δ 130.0, 129.7, 128.0, 126.1, 124.3, 122.4, 70.9, 70.8, 70.5, 70.3, 31.9, 29.8, 29.7, 29.6, 29.3, 29.3, 29.2, 29.2, 27.3, 27.2, 24.9, 22.7, 22.6, 18.4, 14.1 ppm. CIMS m/z 338.18 (calcd for C₁₉H₃₅F₃O, 336.48).

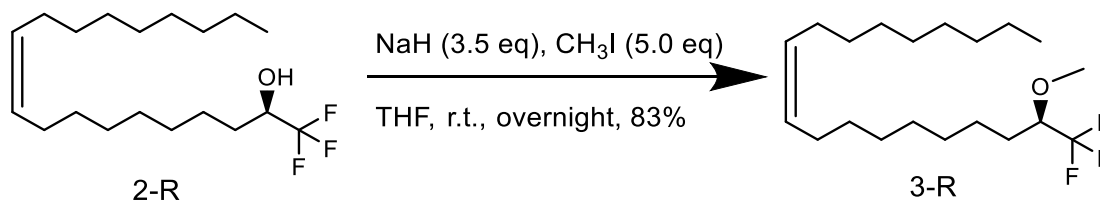
(Z)-19,19,19-trifluoro-18-methoxynonadec-9-ene (3-rac):



To a solution of (Z)-1,1,1-trifluorononadec-10-en-2-ol (**2-rac**, 280 mg, 0.83 mmol, 1.0 eq) in 10 mL anhydrous THF was added CH₃I (1179 mg, 0.5 mL, 8.3 mmol, 10.0 eq) under nitrogen protection. To a dry round flask was added NaH (68mg, 1.7 mmol, 2.0 eq, dispersed in oil). NaH was washed with hexanes three times under nitrogen protection. Pure NaH was dispersed in 2 mL THF into the reaction mixture at 0°C. The resulting reaction mixture was stirred under nitrogen protection at room

temperature overnight. TLC analysis of the reaction shows complete disappearance of starting material. The reaction mixture was quenched with excess NH_4Cl solution slowly in a large Erlenmeyer flask. Then the aqueous layer was extracted with ethyl acetate (3 x 15.0 mL). The combined organic layers were dried over anhydrous Na_2SO_4 , filtered, and concentrated in *vacuo*. The resulting crude product was purified using silica gel chromatography (Combi flash *Rf*, 100% Hex) to produce (Z)-19,19,19-trifluoro-18-methoxynonadec-9-ene (**3-rac**, 130 mg, 0.37 mmol, 45%) as light yellow liquid. ^1H NMR (600 MHz, CDCl_3): δ 5.43-5.37 (m, 2H), 3.61-3.52 (m, 3H), 3.49-3.39 (m, 1H), 2.11-2.05 (m, 4H), 1.70-1.62 (m, 1H), 1.62-1.56 (m, 2H), 1.48-1.21 (m, 22H), 0.94-0.89 (m, 3H) ppm; ^{13}C NMR (CDCl_3 , 150 MHz) δ 130.0, 129.8, 79.6, 79.5, 60.6, 58.5, 31.9, 29.8, 29.70, 29.53, 29.3, 29.3, 29.2, 28.8, 27.2, 27.2, 25.0, 22.7, 18.5, 14.2, 14.1 ppm. CIMS *m/z* 355.18 (calcd for $\text{C}_{20}\text{H}_{37}\text{F}_3\text{O}$, 350.51).

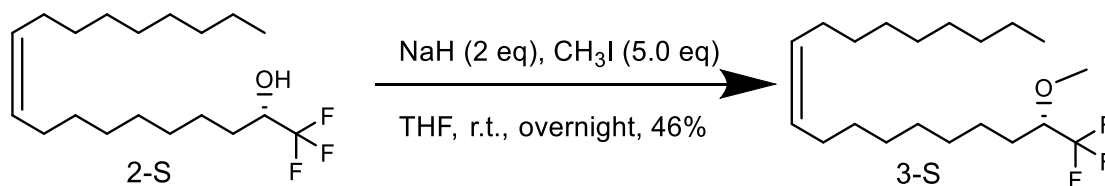
(R,Z)-19,19,19-trifluoro-18-methoxynonadec-9-ene (3-R):



To a solution of (R,Z)-1,1,1-trifluorononadec-10-en-2-ol (**2-R**, 80 mg, 0.24 mmol, 1.0 eq) in 5 mL anhydrous THF was added CH_3I (170 mg, 1.2 mmol, 5.0 eq) under nitrogen protection. To a dry round flask was added NaH

(20mg, 0.83 mmol, 3.5 eq, dispersed in oil). NaH was washed with hexanes three times under nitrogen protection. Pure NaH was dispersed in 2 mL THF into the reaction mixture at 0°C. The resulting reaction mixture was stirred under nitrogen protection at room temperature overnight. TLC analysis of the reaction shows complete disappearance of starting material. The reaction mixture was quenched with excess NH₄Cl solution slowly in a large Erlenmeyer flask. Then the aqueous layer was extracted with ethyl acetate (3 x 10.0 mL). The combined organic layers were dried over anhydrous Na₂SO₄, filtered, and concentrated in *vacuo*. The resulting crude product was purified using silica gel chromatography (Combi flash *R_f*, 100% Hex) to produce (R,Z)-19,19,19-trifluoro-18-methoxynonadec-9-ene (**3-R**, 70 mg, 0.2 mmol, 83%) as light yellow liquid. ¹H NMR (600 MHz, CDCl₃): δ 5.42-5.35 (m, 2H), 3.60-3.56 (m, 3H), 3.49-3.38 (m, 1H), 2.10-2.03 (m, 4H), 1.69-1.63 (m, 1H), 1.61-1.54 (m, 2H), 1.46-1.20 (m, 22H), 0.92-0.86 (m, 3H) ppm; ¹³C NMR (CDCl₃, 150 MHz) δ 130.0, 129.8, 79.6, 79.5, 60.6, 60.4, 58.5, 31.9, 29.8, 29.7, 29.5, 29.3, 29.3, 29.2, 28.8, 27.2, 27.2, 25.0, 22.7, 21.1, 18.5, 14.2, 14.1 ppm. CIMS m/z 349.87 (calcd for C₂₀H₃₇F₃O, 350.51).

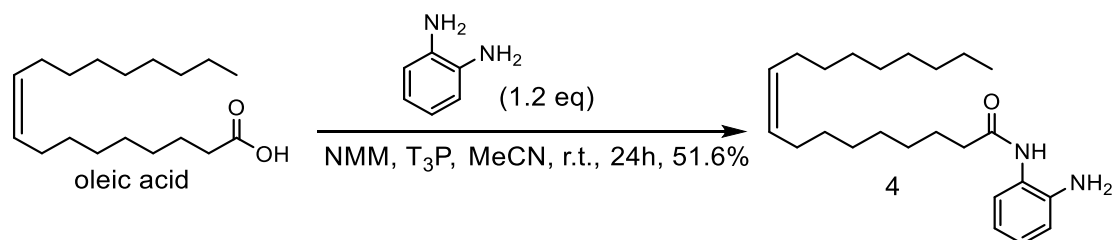
(S,Z)-19,19,19-trifluoro-18-methoxynonadec-9-ene (3-S):



To a solution of (S,Z)-1,1,1-trifluorononadec-10-en-2-ol (**2-S**, 100 mg, 0.3 mmol, 1.0 eq) in 5 mL anhydrous THF was added CH₃I (213 mg, 1.5 mmol, 5.0 eq) under nitrogen protection. To a dry round flask was added NaH (14.4 mg, 0.6 mmol, 2 eq, dispersed in oil). NaH was washed with hexanes three times under nitrogen protection. Pure NaH was dispersed in 2 mL THF into the reaction mixture at 0°C. The resulting reaction mixture was stirred under nitrogen protection at room temperature overnight. TLC analysis of the reaction shows complete disappearance of starting material. The reaction mixture was quenched with excess NH₄Cl solution slowly in a large Erlenmeyer flask. Then the aqueous layer was extracted with ethyl acetate (3 x 10.0 mL). The combined organic layers were dried over anhydrous Na₂SO₄, filtered, and concentrated in *vacuo*. The resulting crude product was purified using silica gel chromatography (Combi flash *Rf*, 100% Hex) to produce ((S,Z)-19,19,19-trifluoro-18-methoxynonadec-9-ene (**3-S**, 50 mg, 0.14 mmol, 46%) as light yellow liquid. ¹H NMR (600 MHz, CDCl₃): δ 5.41-5.36 (m, 2H), 3.60-3.54 (m, 3H), 3.48-3.36 (m, 1H), 2.09-2.06 (m, 4H), 1.68-1.61 (m, 1H), 1.58-1.53 (m, 2H), 1.43-1.21 (m, 22H), 0.91-0.84 (m, 3H) ppm; ¹³C NMR (CDCl₃, 150 MHz) δ 130.0, 129.8, 127.2,

36.9, 31.9, 29.8, 29.8, 29.6, 29.3, 29.3, 29.2, 27.2, 27.2, 25.7, 22.7, 14.1 ppm. CIMS m/z 354.84 (calcd for C₂₀H₃₇F₃O, 350.51).

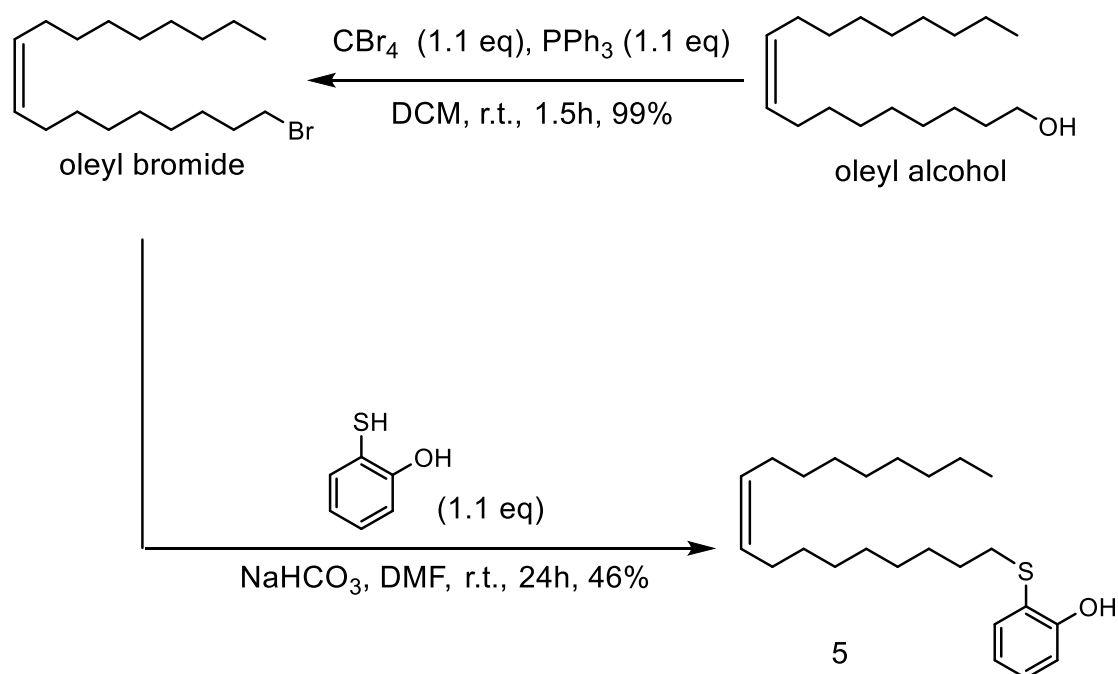
N-(2-aminophenyl)oleamide (**4**):



To a solution of oleic acid (300 mg, 1.04 mmol, 1.0 equiv) in MeCN (6.0 mL) was added o-Phenylenediamine (142 mg, 1.3 mmol, 1.2 equiv), 2,4,6-Tripropyl-1,3,5,2^{λ5},4^{λ5},6^{λ5}-trioxatriphosphinane 2,4,6-trioxide (1.0 mL) and N-Methylmorpholine (1.0 mL). The resulting mixture was stirred under nitrogen atmosphere at room temperature overnight. TLC analysis of the reaction shows complete disappearance of starting material. The reaction mixture was concentrated in vacuo and then quenched with the addition of H₂O (30.0 mL). Then the aqueous layer was extracted with ethyl acetate (3 x 15.0 mL). The combined organic layers were dried over anhydrous Na₂SO₄, filtered, and concentrated in vacuo. The resulting crude product was purified using silica gel chromatography (Combi flash *R_f*, 15% Hex-EA) to produce N-(2-aminophenyl)oleamide (**4**, 200 mg, 0.54 mmol, 51.6%) as light yellow liquid. ¹H NMR (600 MHz, CDCl₃): δ 7.41-7.39 (m, 1H), 7.38-7.36 (m, 1H), 7.12-7.09 (m, 1H), 7.12-7.09 (m, 1H), 5.41-5.32 (m, 2H), 2.48-

2.43 (m, 2H), 2.09-1.96 (m, 4H), 1.49-1.21 (m, 22H), 0.95-0.84 (m, 3H) ppm;
13C NMR (CDCl₃, 150 MHz) δ130.0, 129.7, 127.2, 36.9, 31.9, 29.8, 29.8,
29.6, 229.3, 29.3, 29.2, 27.6, 27.2, 25.7, 22.7, 14.1 ppm. CIMS m/z 373.30
(calcd for C₂₄H₄₀N₂O, 372.60).

(Z)-2-(octadec-9-en-1-ylthio)phenol (5):



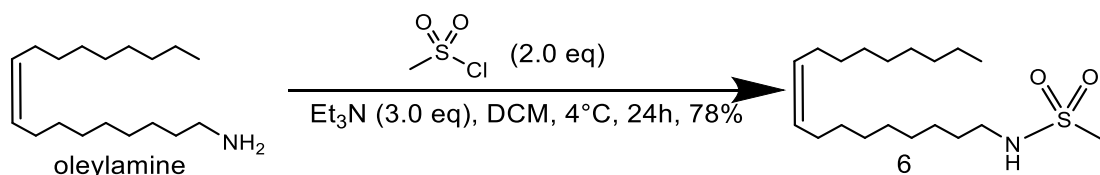
To a solution of oleyl alcohol (3 g, 11.2 mmol, 1.0 equiv) in DCM (40 mL) was added tetrabromomethane (4.07 g, 12.3 mmol, 1.1 equiv). Then triphenylphosphine (3.22 g, 12.3 mmol, 1.1 equiv, dissolved in 20 mL DCM) was added dropwise under nitrogen atmosphere at 0 °C over 0.5 h. After adding triphenylphosphine, the ice-water bath was removed. The resulting reaction mixture was stirred at room temperature for 1.5 h. TLC analysis of the reaction shows complete disappearance of starting

material. The reaction mixture was concentrated in vacuo and then quenched with the addition of H₂O (80.0 mL). Then the aqueous layer was extracted with ethyl acetate (3 x 30.0 mL). The combined organic layers were dried over anhydrous Na₂SO₄, filtered, and concentrated in vacuo. The resulting crude product was purified using silica gel chromatography (Combi flash *Rf*, 5% Hex-EA) to produce (Z)-1-bromooctadec-9-ene (3.5 g, 12.2 mmol, 99%) as colorless liquid. ¹H NMR (600 MHz, CDCl₃): δ 5.49-5.33 (m, 2H), 3.51-3.39 (m, 2H), 2.12-2.01 (m, 4H), 1.92-1.88 (m, 2H), 1.49-1.20 (m, 22H), 0.98-0.84 (m, 3H) ppm; ¹³C NMR (CDCl₃, 150 MHz) δ 130.5, 130.2, 130.0, 129.8, 53.4, 35.2, 34.1, 32.9, 32.6, 32.6, 31.9, 29.8, 29.7, 29.7, 29.6, 29.6, 29.5, 29.5, 29.5, 29.3, 29.3, 29.2, 29.0, 28.9, 28.8, 28.8, 28.2, 27.2, 27.2, 22.7, 14.1 ppm.

To a solution of (Z)-1-bromooctadec-9-ene (200 mg, 0.6 mmol, 1.0 equiv) in DMF (20 mL) was added 2-mercaptophenol (83mg, 0.66 mmol, 1.1 equiv) and NaHCO₃ (60mg, 0.72 mmol, 1.2 equiv). The resulting reaction mixture was stirred under nitrogen atmosphere at room temperature in dark for 24 h. TLC analysis of the reaction shows complete disappearance of starting material. The reaction mixture was concentrated in vacuo and then quenched with the addition of H₂O (30.0 mL). Then the aqueous layer was extracted with ethyl acetate (3 x 10.0 mL). The combined organic layers were dried over anhydrous Na₂SO₄, filtered, and concentrated in vacuo. The resulting crude product was purified using silica gel

chromatography (Combi flash *Rf*, 15% Hex-EA) to produce (Z)-2-(octadec-9-en-1-ylthio)phenol (**5**, 110 mg, 0.29 mmol, 46%) as light yellow sticky solid. ¹H NMR (600 MHz, CDCl₃): δ 7.49-7.43 (m, 1H), 7.00-6.96 (m, 1H), 6.82-6.79 (m, 1H), 6.72-6.69 (m, 1H), 5.40-5.34 (m, 2H), 2.18-2.13 (m, 2H), 2.06-1.97 (m, 4H), 1.58-1.53 (m, 2H), 1.48-1.19 (m, 22H), 0.92-0.84 (m, 3H) ppm; ¹³C NMR (CDCl₃, 150 MHz) δ 156.9, 136.0, 131.0, 130.0, 129.8, 120.7, 119.2, 114.7, 36.9, 31.9, 29.8, 29.7, 29.7, 29.5, 29.4, 29.3, 29.2, 29.1, 28.6, 27.2, 27.2, 22.7, 14.1 ppm. CIMS *m/z* 377.10 (calcd for C₂₄H₄₀OS, 376.64).

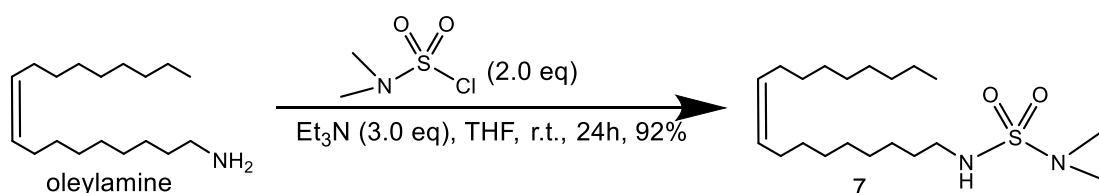
(Z)-N-(octadec-9-en-1-yl)methanesulfonamide (6):



To a solution of oleylamine (534 mg, 2 mmol, 1.0 equiv) in DCM (20 mL) was added triethylamine (606 mg, 6 mmol, 3.0 equiv) under nitrogen atmosphere at 0 °C. Then methanesulfonyl chloride (460mg, 4mmol, 2.0 equiv) was added dropwise under nitrogen atmosphere at 0 °C. The resulting reaction mixture was kept at 4 °C for 24 h in the fridge. TLC analysis of the reaction shows complete disappearance of starting material. The reaction mixture was concentrated in vacuo and then quenched with the addition of H₂O (60.0 mL). Then the aqueous layer was

extracted with ethyl acetate (3 x20.0 mL). The combined organic layers were dried over anhydrous Na₂SO₄, filtered, and concentrated in vacuo. The resulting crude product was purified using silica gel chromatography (Combi flash *Rf*, 5% MeOH-DCM with NH₃) to produce (Z)-N-(octadec-9-en-1-yl)methanesulfonamide (**6**, 540 mg, 1.56 mmol, 78%) as light colorless oil. ¹H NMR (600 MHz, CDCl₃): δ 5.43-5.33 (m, 2H), 4.19-4.09 (m, 2H), 3.21-3.12 (m, 3H), 2.09-1.92 (m, 4H), 1.53-1.51 (m, 2H), 1.39-1.21 (m, 22H), 0.91-0.83 (m, 3H) ppm; ¹³C NMR (CDCl₃, 150 MHz) δ165.8, 125.4, 56.8, 56.6, 56.3, 56.2, 56.1, 387, 38.5, 38.2, 34.9, 34.6, 34.5, 27.8, 27.6, 24.7, 24.6, 24.5, 23.6, 22.7, 21.7, 21.4, 18.2, 17.9, 17.5, 13.4, 9.2 ppm. CIMS m/z 346.29 (calcd for C₁₉H₃₉NO₂S, 345.59).

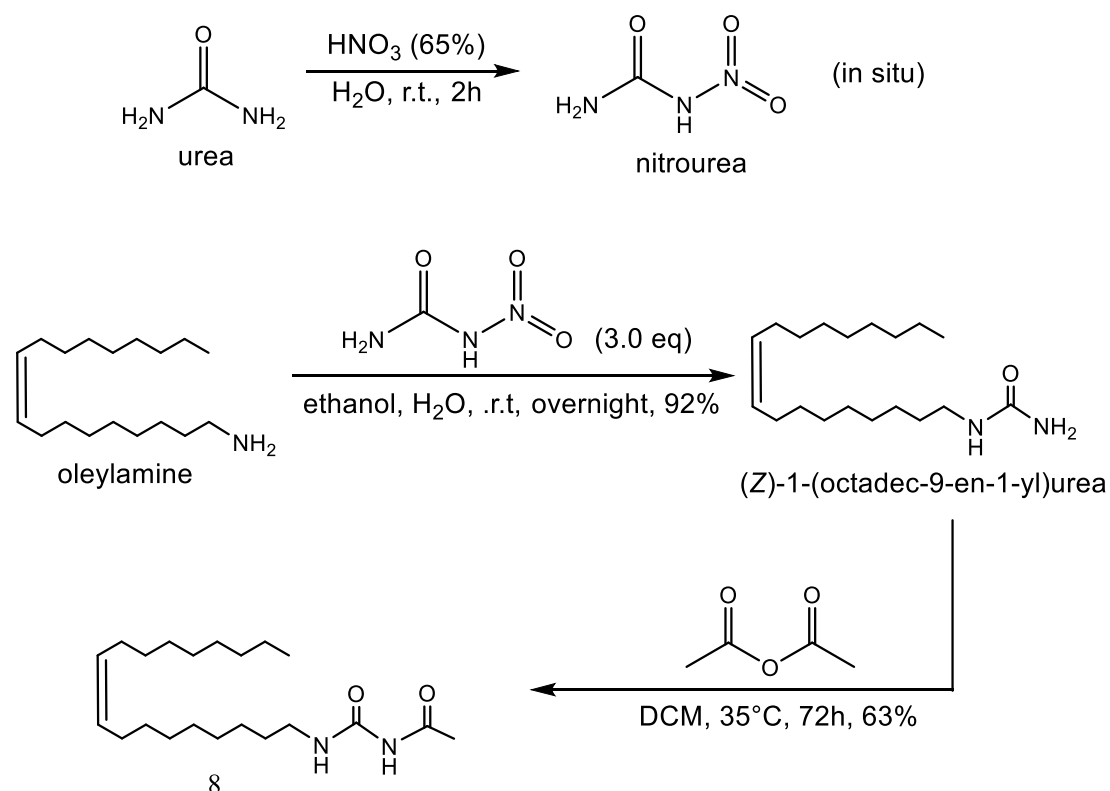
(Z)-N'-(octadec-9-en-1-yl)-N,N-dimethylsulfamide (7):



To a solution of oleylamine (534 mg, 2 mmol, 1.0 equiv) in THF (20 mL) was added triethylamine (606 mg, 6 mmol, 3.0 equiv) under nitrogen atmosphere at room temperature. Then N,N -dimethylsulfamoyl chloride (572mg, 4mmol, 2.0 equiv) was added dropwise under nitrogen atmosphere at room temperature. The resulting reaction mixture was stirred at room temperature for 24h. TLC analysis of the reaction shows

complete disappearance of starting material. The reaction mixture was concentrated in vacuo and then quenched with the addition of H₂O (60.0 mL). Then the aqueous layer was extracted with ethyl acetate (3 x 20.0 mL). The combined organic layers were dried over anhydrous Na₂SO₄, filtered, and concentrated in vacuo. The resulting crude product was purified using silica gel chromatography (Combi flash *R_f*, 20% Hex-EA) to produce (Z)-N'-(octadec-9-en-1-yl)-N,N-dimethylsulfamide (**7**, 690 mg, 1.84 mmol, 92%) as colorless oil. ¹H NMR (600 MHz, CDCl₃): δ 5.42-5.34 (m, 2H), 3.09-3.01 (m, 2H), 2.90-2.73 (m, 6H), 2.08-1.93 (m, 4H), 1.59-1.51 (m, 2H), 1.38-1.22 (m, 22H), 0.90-0.81 (m, 3H) ppm; ¹³C NMR (CDCl₃, 150 MHz) δ 130.5, 130.3, 130.2, 130.0, 129.8, 60.4, 43.7, 39.6, 38.1, 32.6, 32.6, 31.9, 31.9, 29.9, 29.8, 29.7, 29.7, 29.6, 29.6, 29.5, 29.4, 29.4, 29.3, 29.2, 29.2, 29.1, 27.2, 27.2 ppm. CIMS m/z 375.26 (calcd for C₂₀H₄₂N₂O₂S, 374.63).

(Z)-N-(octadec-9-en-1-ylcarbamoyl)acetamide (8):



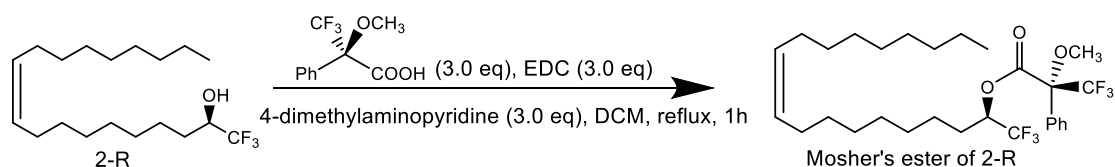
Urea (858 mg) was dissolved in 2 mL water and then HNO_3 solution (0.4 mL) was added to urea. The resulting mixture was stirred at r.t. for 2 h to produce crude nitrourea, which was used without further purification. The nitrourea solution was diluted in ethanol (20 mL) and then added oleylamine (534 mg, 2 mmol, 1.0 equiv). The resulting mixture was stirred at r.t. for overnight. TLC analysis of the reaction shows complete disappearance of starting material. The reaction mixture was concentrated in vacuo and then quenched with the addition of H_2O (60.0 mL). Then the aqueous layer was extracted with ethyl acetate (3 x 20.0 mL). The combined organic layers were dried over anhydrous Na_2SO_4 , filtered, and concentrated in vacuo. The resulting crude product was purified using

silica gel chromatography (Combi flash *Rf*, 10% MeOH-DCM with NH₃) to produce (Z)-1-(octadec-9-en-1-yl)urea (600 mg, 1.93 mmol, 96%) as yellow oil. ¹H NMR (600 MHz, CDCl₃): δ 5.46-5.30 (m, 2H), 2.95-2.91 (m, 2H), 2.09-1.95 (m, 4H), 1.69-1.61 (m, 2H), 1.41-1.19 (m, 22H), 0.91-0.83 (m, 3H) ppm;

To a solution of (Z)-1-(octadec-9-en-1-yl)urea (600 mg, 1.93 mmol, 1.0 equiv) in DCM (20 mL) was added acetic anhydride (1.6g, 1.5mL, 15 mmol, 8.0 equiv) under nitrogen atmosphere at room temperature. Then N,N - dimethylsulfamoyl chloride (572mg, 4mmol, 2.0 equiv) was added dropwise under nitrogen atmosphere at room temperature. The resulting reaction mixture was stirred at room temperature for 72h. TLC analysis of the reaction shows complete disappearance of starting material. The reaction mixture was concentrated in vacuo and then quenched with the addition of H₂O (50.0 mL). Then the aqueous layer was extracted with ethyl acetate (3 x15.0 mL). The combined organic layers were dried over anhydrous Na₂SO₄, filtered, and concentrated in vacuo. The resulting crude product was purified using silica gel chromatography (Combi flash *Rf*, 5% MeOH-DCM with NH₃) to produce (Z)-N-(octadec-9-en-1-ylcarbamoyl)acetamide (**8**, 430 mg, 1.22 mmol, 63%) as yellow oil. ¹H NMR (600 MHz, CDCl₃): δ 5.44-5.39 (m, 2H), 3.28-3.22 (m, 3H), 1.61-1.57 (m, 2H), 1.49-1.43 (m, 4H), 1.42-1.22 (m, 24H), 0.93-0.88 (m, 3H) ppm; ¹³C NMR (CDCl₃, 150 MHz) δ170.1, 130.5, 130.3, 39.8, 39.7, 32.6, 31.9,

31.9, 29.7, 29.6, 29.6, 29.5, 29.4, 29.3, 29.3, 29.2, 29.1, 29.1, 26.9, 26.7, 23.4, 22.7, 22.6, 14.1 ppm. CIMS m/z 355.26 (calcd for C₂₁H₄₀N₂O₂, 352.56).

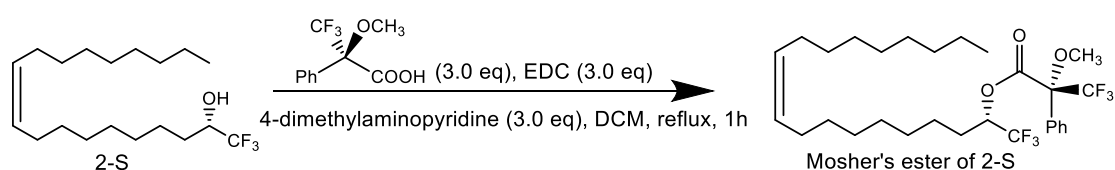
Mosher's ester of 2-R:



To a solution of (R,Z)-1,1,1-trifluorononadec-10-en-2-ol (2-R, 10mg, 0.029 mmol) in DCM (3 mL) were added α-methoxy-α-trifluoromethylphenylacetic acid (22mg, 0.087 mmol, 3.0 eq), 1-Ethyl-3-(3-dimethylaminopropyl)carbodiimide (17.4 mg, 0.087 mmol, 3.0 eq) and 4-dimethylaminopyridine (11mg, 0.087 mmol, 3.0eq). The resulting mixture was refluxed for 1 hour. TLC analysis of the reaction shows complete disappearance of starting material. The reaction mixture was concentrated in vacuo and then quenched with the addition of H₂O (5.0 mL). Then the aqueous layer was extracted with ethyl acetate (3 x5.0 mL). The combined organic layers were dried over anhydrous Na₂SO₄, filtered, and concentrated in vacuo. The resulting crude product was purified using silica gel chromatography (Combi flash *R_f*, 15% Hex-EA) to produce **Mosher's ester of 2-R** (2 mg, 0.004 mmol, 12%) as colorless oil. ¹H NMR (600 MHz, CDCl₃): δ 7.47-7.46 (m, 2H), 7.35-7.34 (m, 2H), 7.22-7.19 (m, 1H), 5.40-5.39 (m, 1H), 5.39-5.33 (m, 2H), 3.52-3.51 (m, 3H), 1.98-1.92 (m,

4H), 1.76-1.71 (m, 1H), 1.61-1.59 (m, 2H), 1.51-1.20 (m, 22H), 0.90-0.85 (m, 3H) ppm;

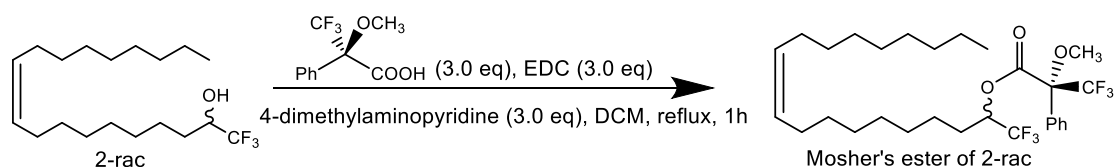
Mosher's ester of 2-S:



To a solution of (S,Z)-1,1,1-trifluorononadec-10-en-2-ol (2-S, 10mg, 0.029 mmol) in DCM (3 mL) were added α-methoxy-α-trifluoromethylphenylacetic acid (22mg, 0.087 mmol, 3.0 eq), 1-Ethyl-3-(3-dimethylaminopropyl)carbodiimide (17.4 mg, 0.087 mmol, 3.0 eq) and 4-dimethylaminopyridine (11mg, 0.087 mmol, 3.0eq). The resulting mixture was refluxed for 1 hour. TLC analysis of the reaction shows complete disappearance of starting material. The reaction mixture was concentrated in vacuo and then quenched with the addition of H₂O (5.0 mL). Then the aqueous layer was extracted with ethyl acetate (3 x 5.0 mL). The combined organic layers were dried over anhydrous Na₂SO₄, filtered, and concentrated in vacuo. The resulting crude product was purified using silica gel chromatography (Combi flash *R_f*, 15% Hex-EA) to produce **Mosher's ester of 2-S** (3 mg, 0.005 mmol, 19%) as colorless oil. ¹H NMR (600 MHz, CDCl₃): δ 7.49-7.47 (m, 2H), 7.39-7.38 (m, 2H), 7.26-7.18 (m, 1H), 5.41-5.38 (m, 1H), 5.36-5.32 (m, 2H), 3.56-3.53 (m, 3H), 1.99-1.96 (m,

4H), 1.73-1.71 (m, 1H), 1.64-1.59 (m, 2H), 1.53-1.21 (m, 22H), 0.95-0.88 (m, 3H) ppm;

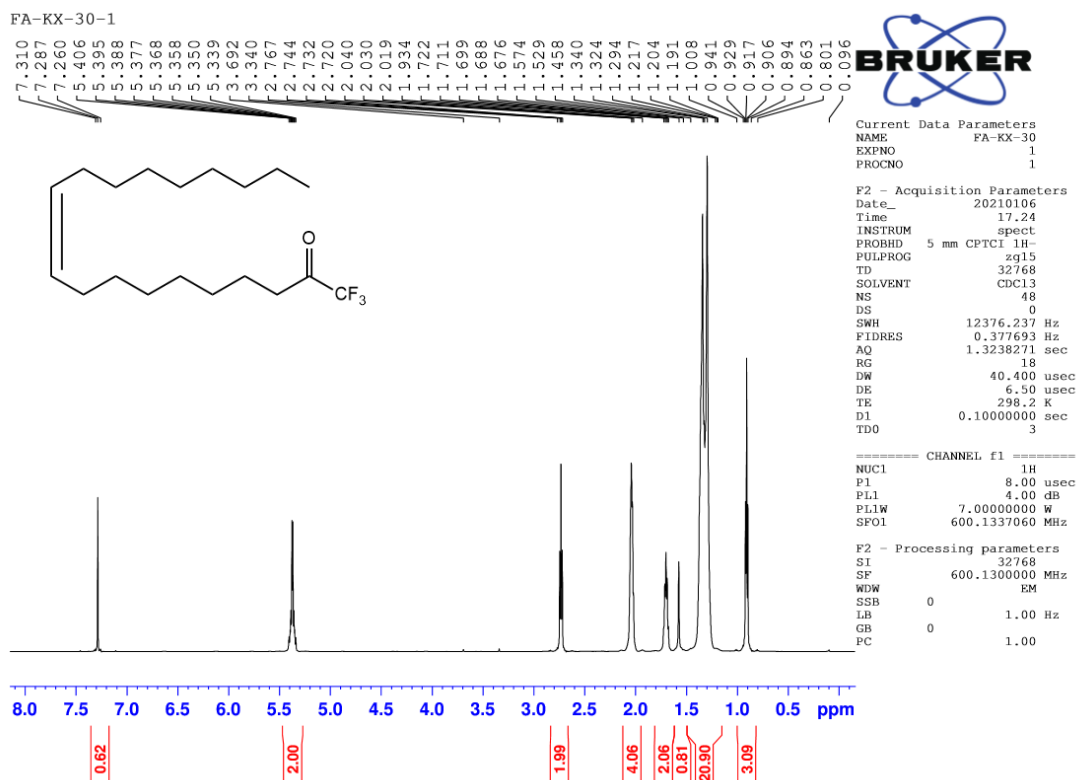
Mosher's ester of 2-rac:



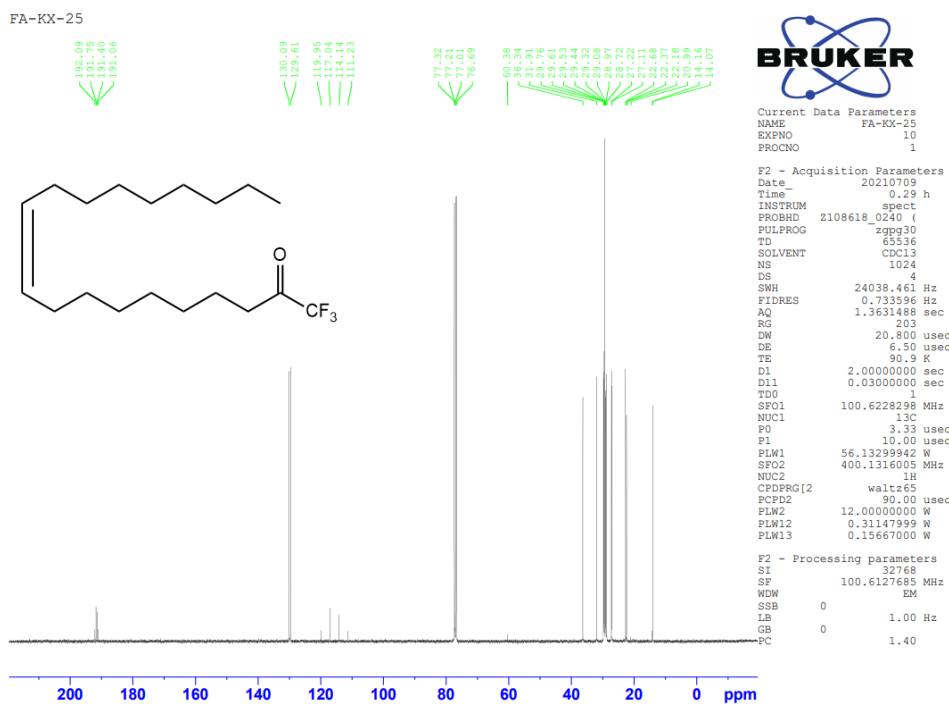
To a solution of (Z)-1,1,1-trifluorononadec-10-en-2-ol (2-rac, 10mg, 0.029 mmol) in DCM (3 mL) were added α-methoxy-α-trifluoromethylphenylacetic acid (22mg, 0.087 mmol, 3.0 eq), 1-Ethyl-3-(3-dimethylaminopropyl)carbodiimide (17.4 mg, 0.087 mmol, 3.0 eq) and 4-dimethylaminopyridine (11mg, 0.087 mmol, 3.0eq). The resulting mixture was refluxed for 1 hour. TLC analysis of the reaction shows complete disappearance of starting material. The reaction mixture was concentrated in vacuo and then quenched with the addition of H₂O (5.0 mL). Then the aqueous layer was extracted with ethyl acetate (3 x 5.0 mL). The combined organic layers were dried over anhydrous Na₂SO₄, filtered, and concentrated in vacuo. The resulting crude product was purified using silica gel chromatography (Combi flash *R_f*, 15% Hex-EA) to produce **Mosher's ester of 2-rac** (2 mg, 0.004 mmol, 12%) as colorless oil. ¹H NMR (600 MHz, CDCl₃): δ 7.52-7.51 (m, 2H), 7.40-7.38 (m, 2H), 7.23-7.21 (m, 1H), 5.42-5.37 (m, 1H), 5.35-5.33 (m, 2H), 3.53-3.52 (m, 1.5H), 3.45-3.44

(m, 1.5H), 1.98-1.97 (m, 4H), 1.74-1.72 (m, 1H), 1.63-1.58 (m, 2H), 1.54-1.21 (m, 22H), 0.99-0.89 (m, 3H) ppm;

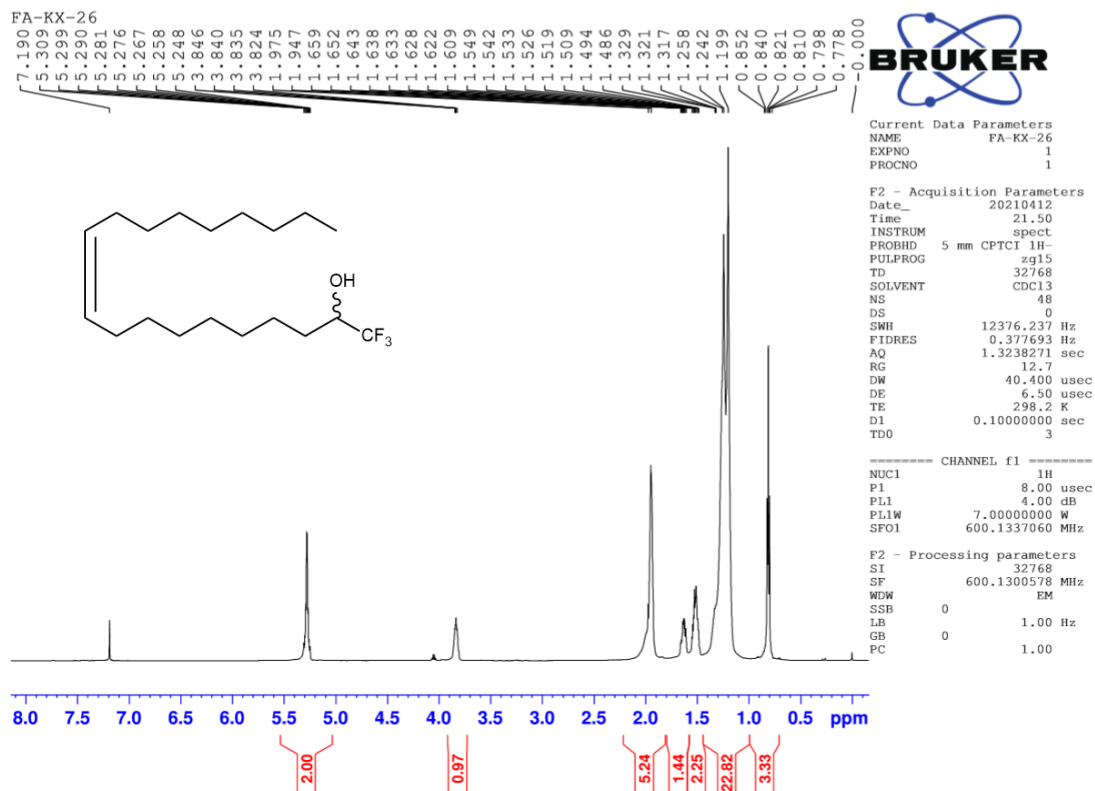
¹H-NMR Spectra of (Z)-1,1,1-trifluorononadec-10-en-2-one (1):



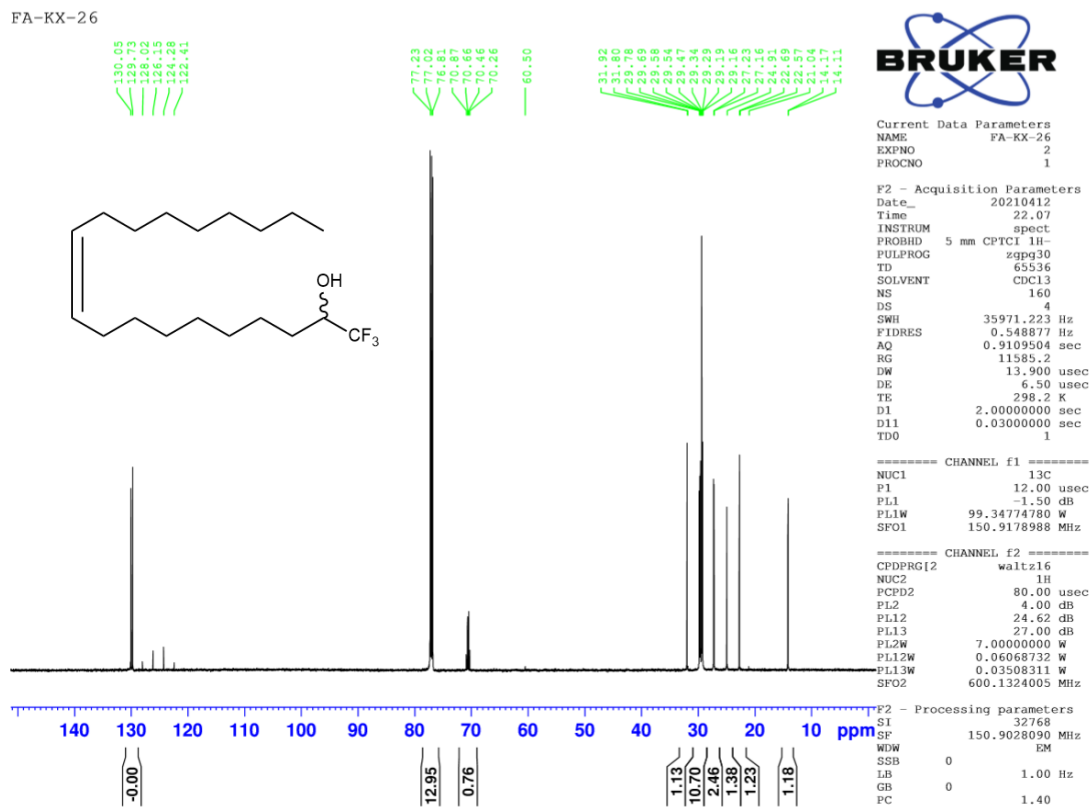
¹³C-NMR Spectra of (Z)-1,1,1-trifluorononadec-10-en-2-one (1):



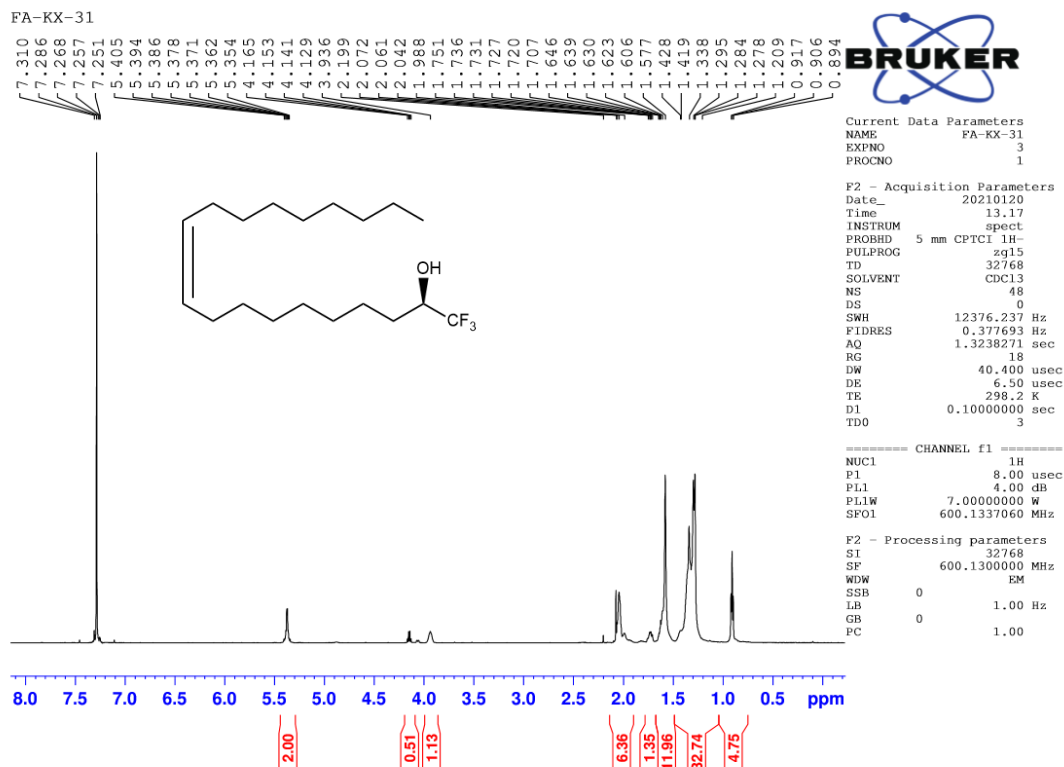
¹H-NMR Spectra of (Z)-1,1,1-trifluorononadec-10-en-2-ol (2-rac):



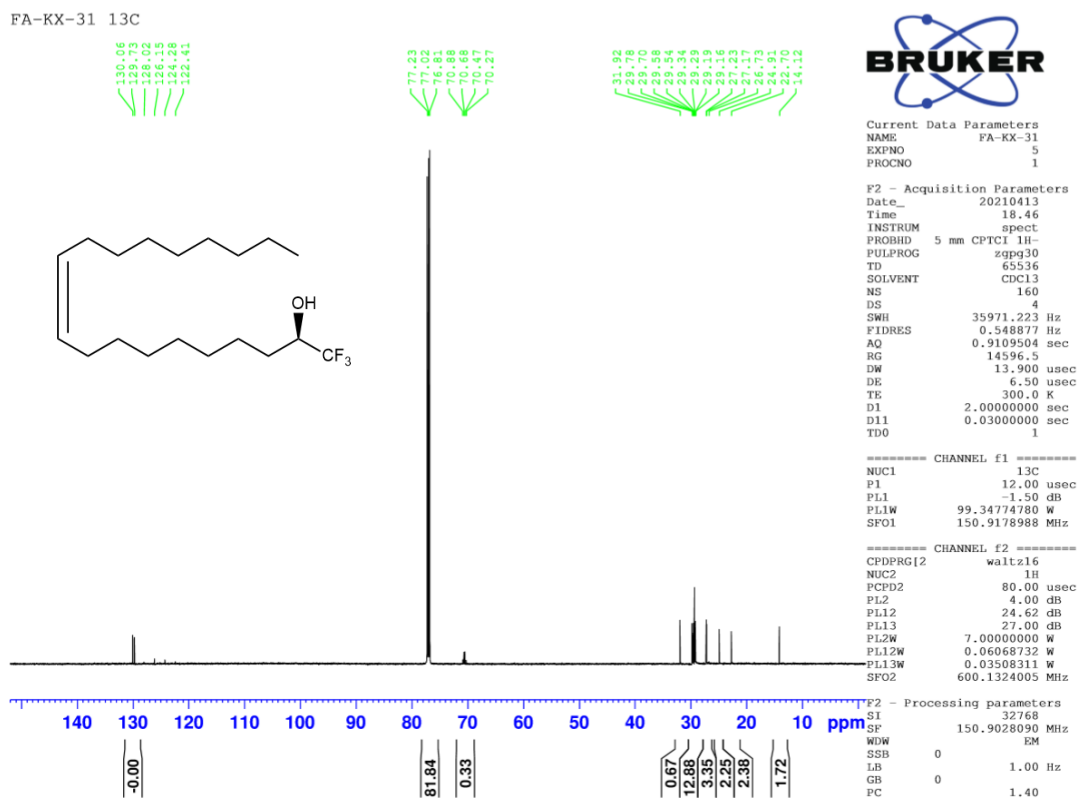
¹³C-NMR Spectra of (Z)-1,1,1-trifluorononadec-10-en-2-ol (2-rac):



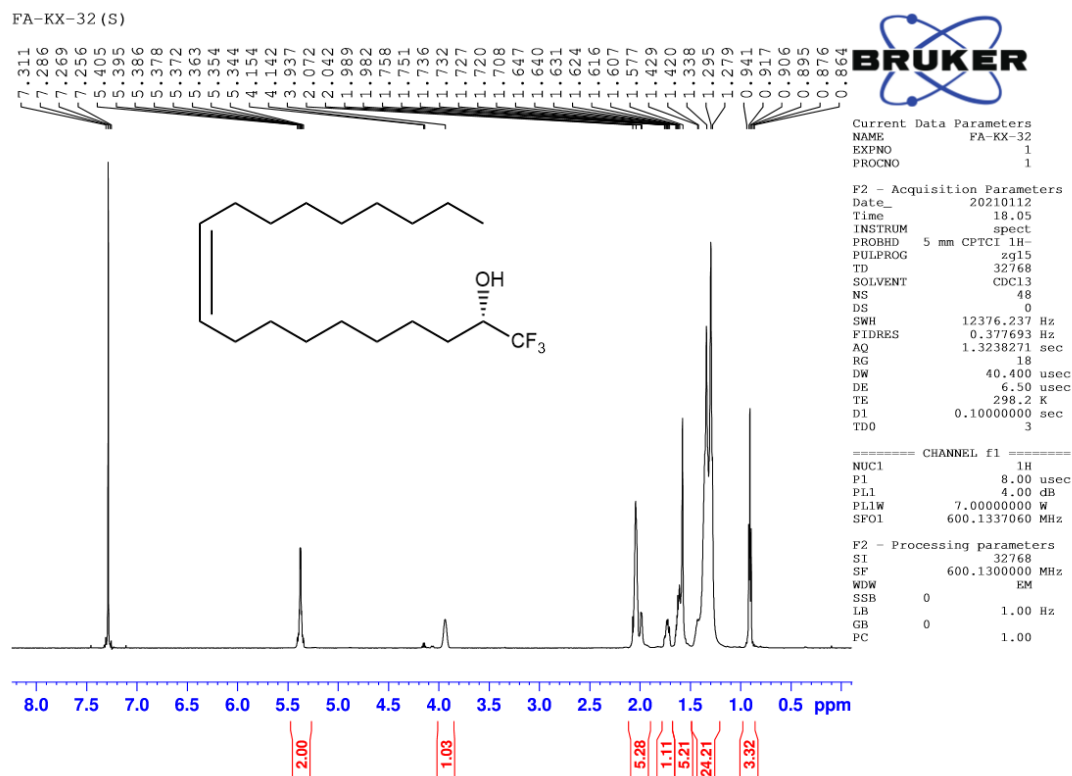
¹H-NMR Spectra of (R,Z)-1,1,1-trifluorononadec-10-en-2-ol (2-R):



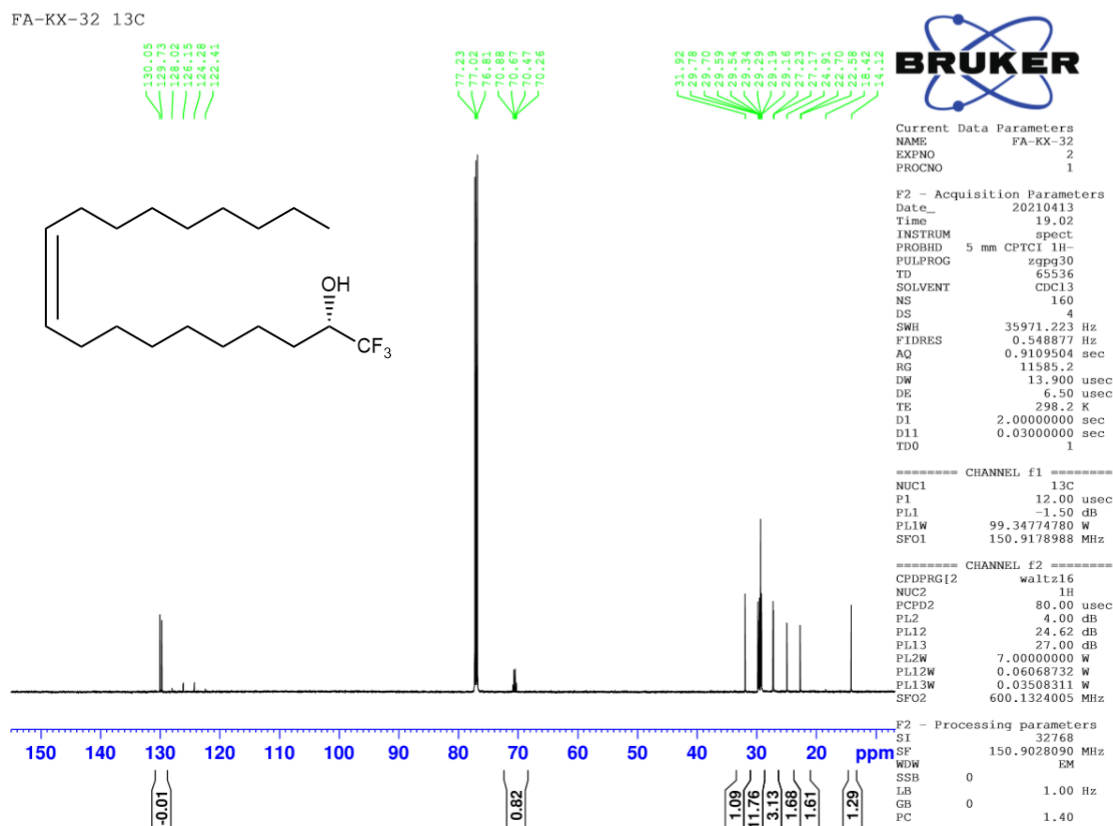
¹³C-NMR Spectra of (R,Z)-1,1,1-trifluorononadec-10-en-2-ol (2-R):



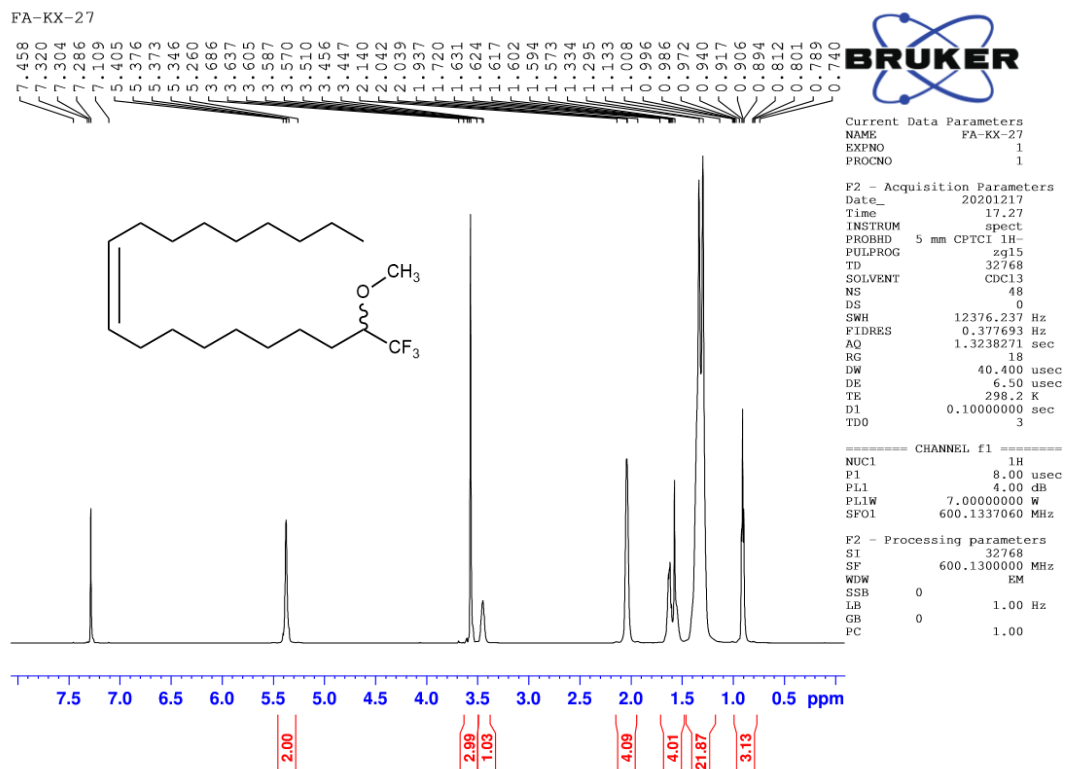
¹H-NMR Spectra of (S,Z)-1,1,1-trifluorononadec-10-en-2-ol (2-S):



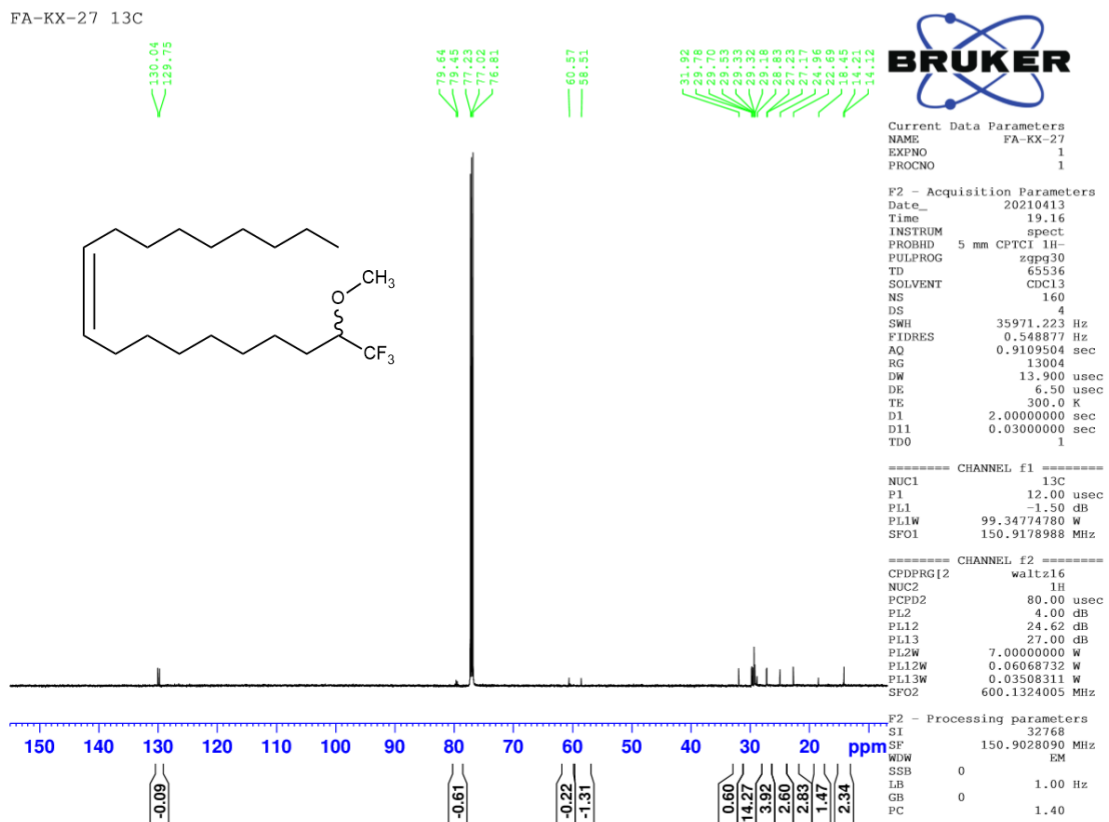
¹³C-NMR Spectra of (S,Z)-1,1,1-trifluorononadec-10-en-2-ol (2-S):



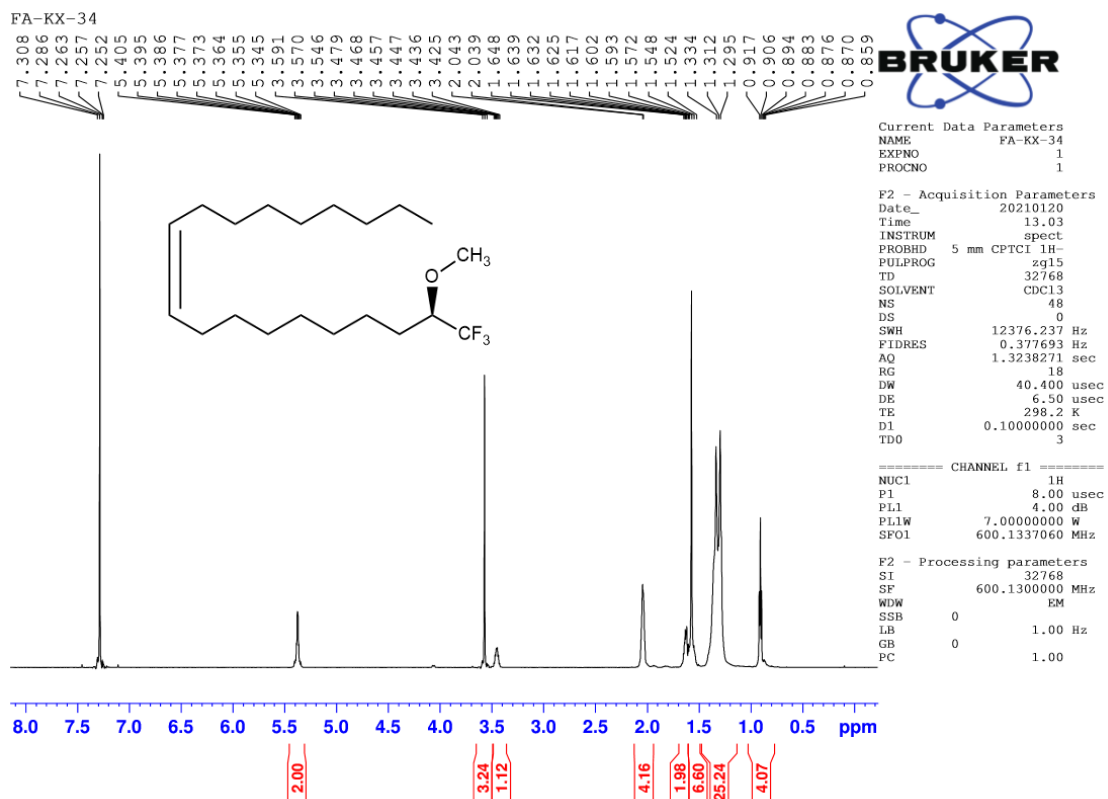
¹H-NMR Spectra of (Z)-19,19,19-trifluoro-18-methoxynonadec-9-ene (3-rac):



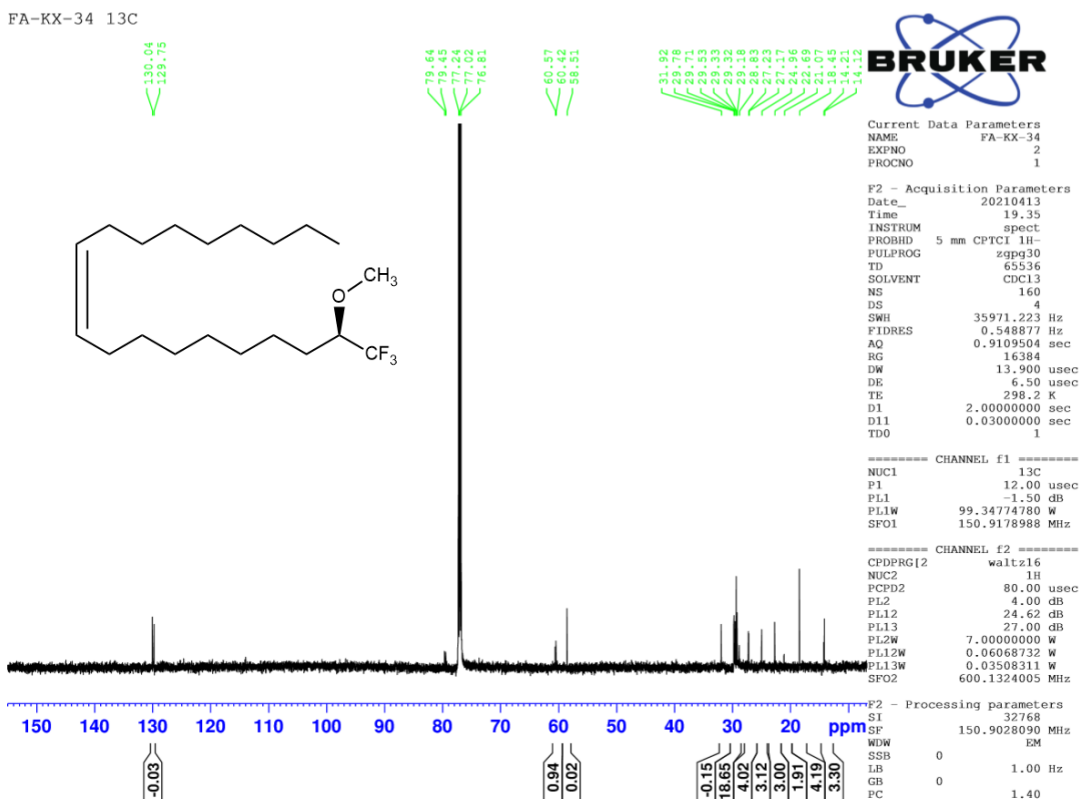
¹³C-NMR Spectra of (Z)-19,19,19-trifluoro-18-methoxynonadec-9-ene (3-rac):



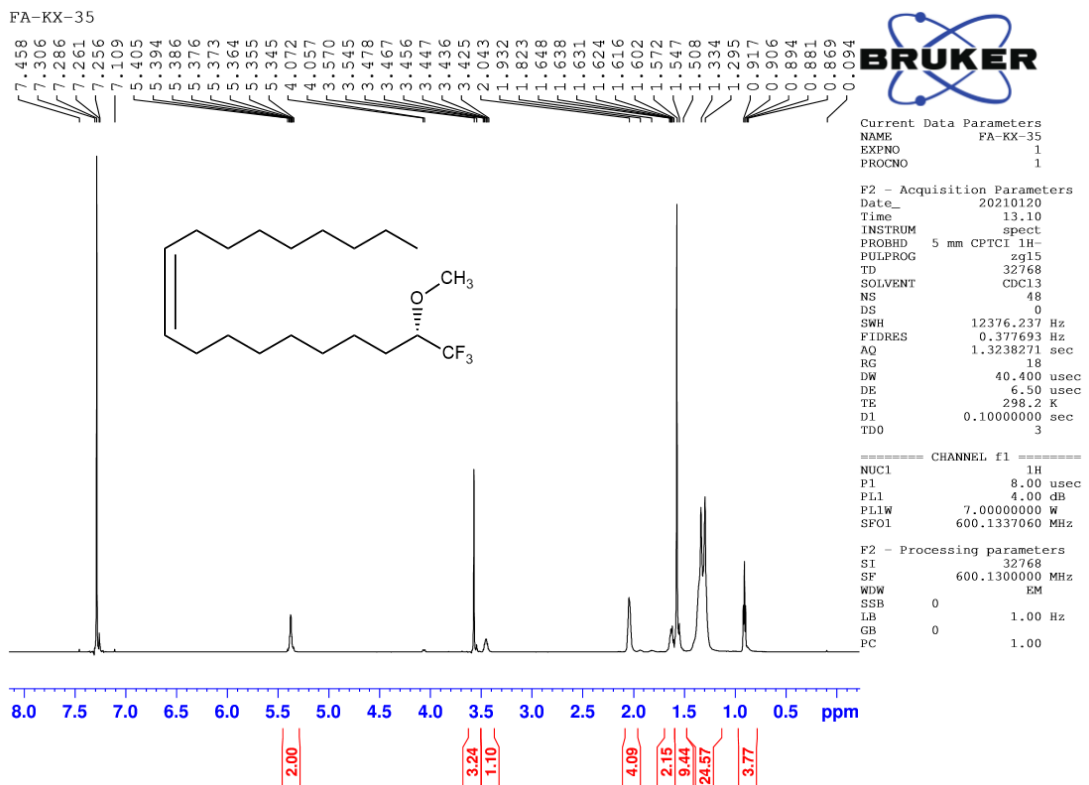
¹H-NMR Spectra of (R,Z)-19,19,19-trifluoro-18-methoxynonadec-9-ene (3-R):



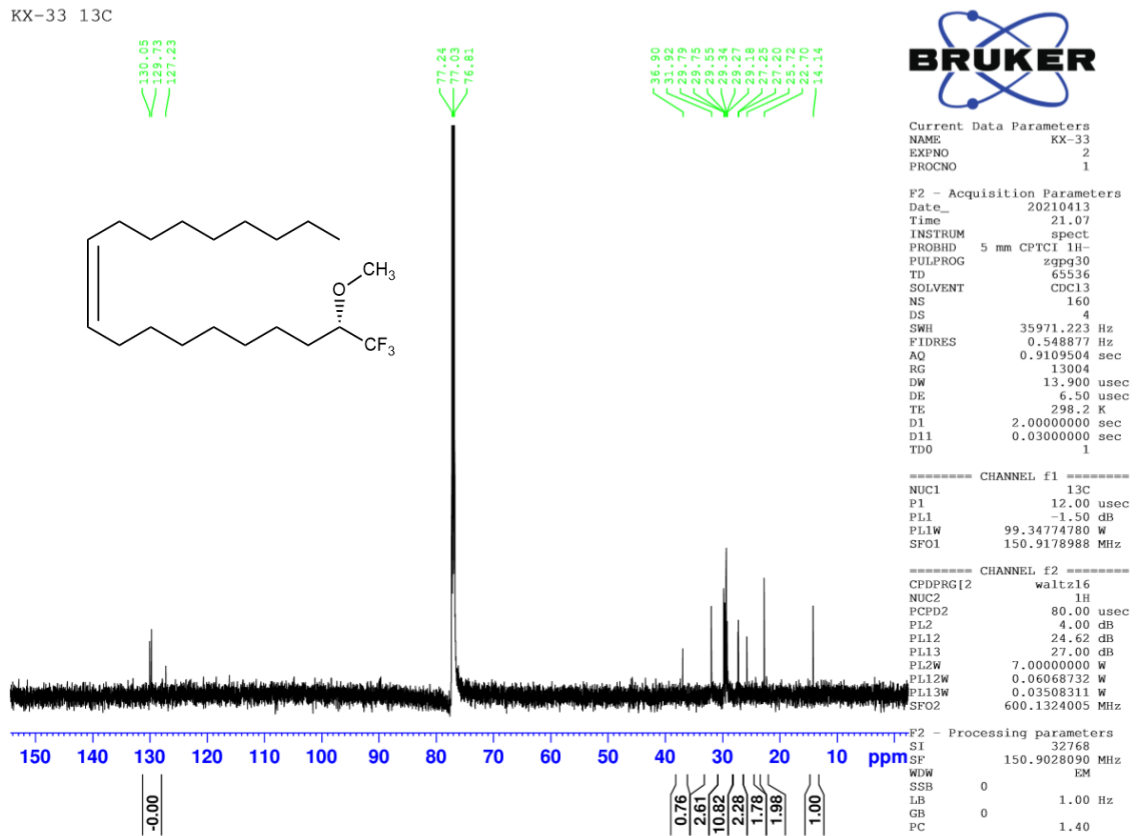
¹³C-NMR Spectra of (R,Z)-19,19,19-trifluoro-18-methoxynonadec-9-ene (3-R):



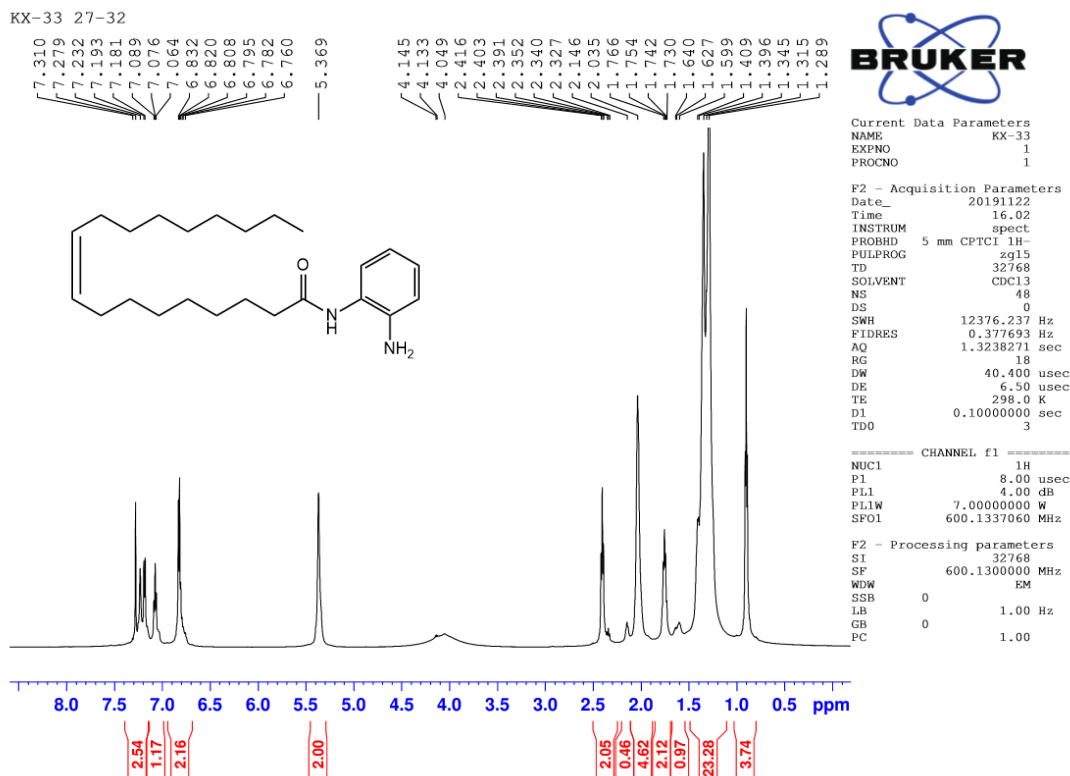
¹H-NMR Spectra of (S,Z)-19,19,19-trifluoro-18-methoxynonadec-9-ene (3-S):



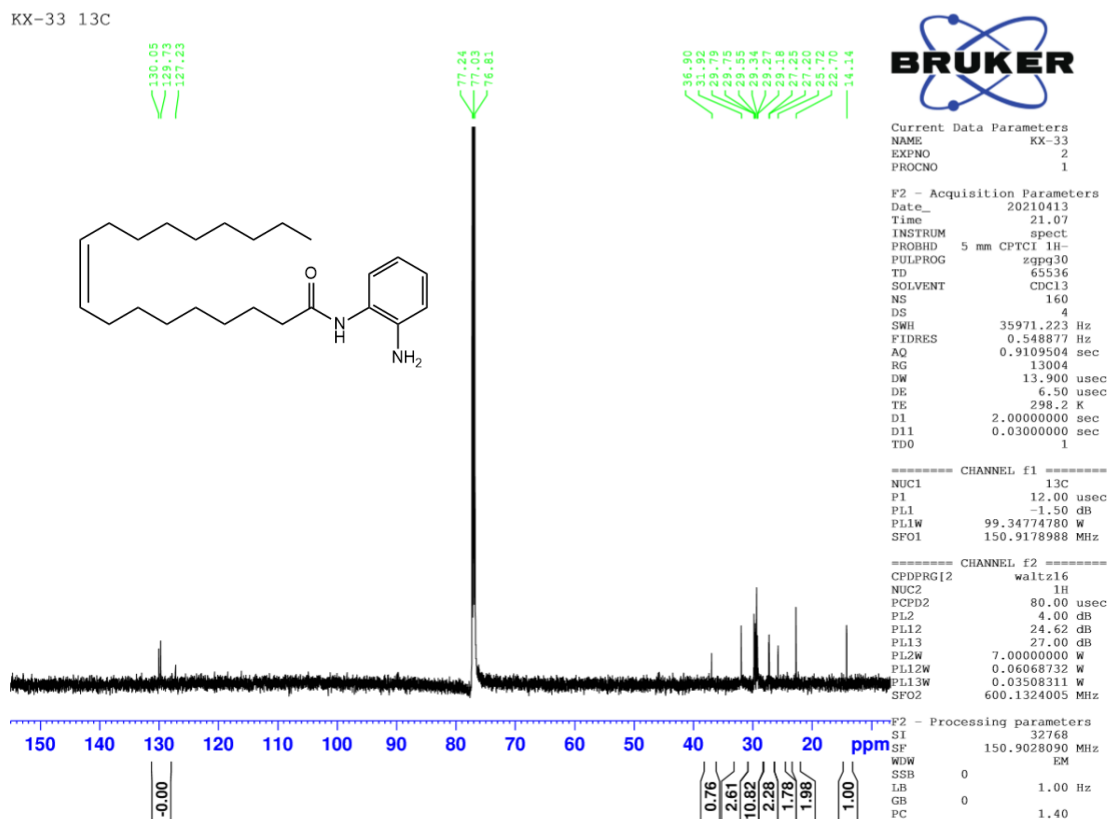
¹³C-NMR Spectra of (S,Z)-19,19,19-trifluoro-18-methoxynonadec-9-ene (3-S):



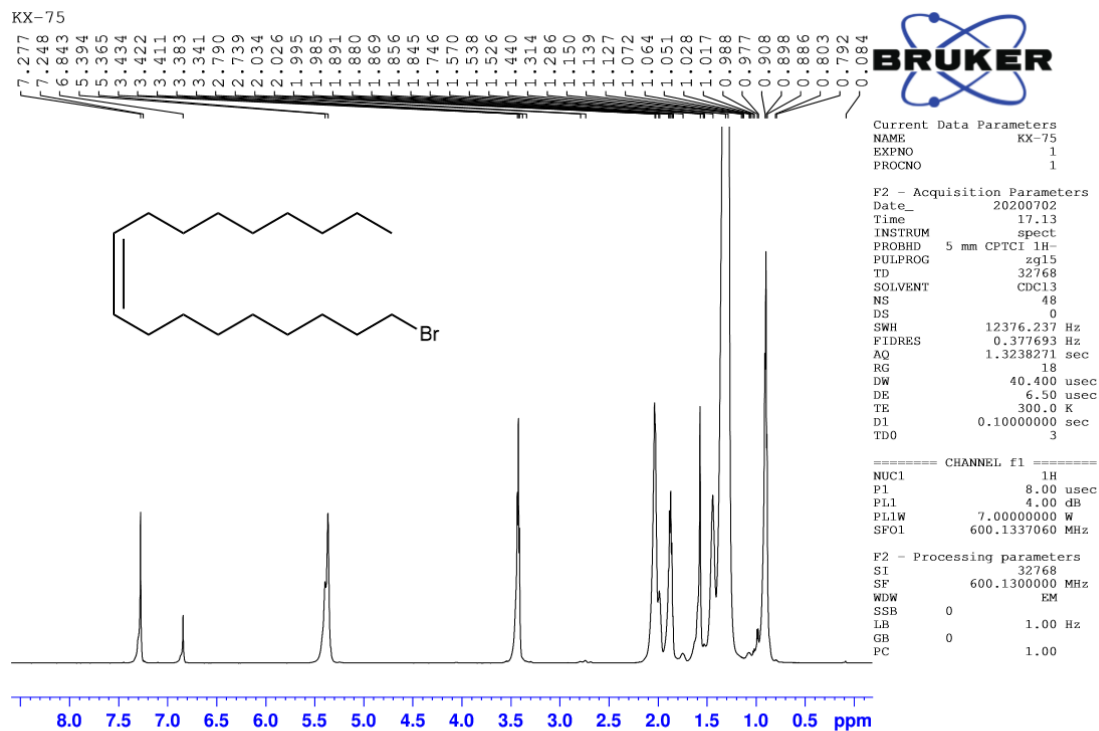
¹H-NMR Spectra of N-(2-aminophenyl)oleamide (4):



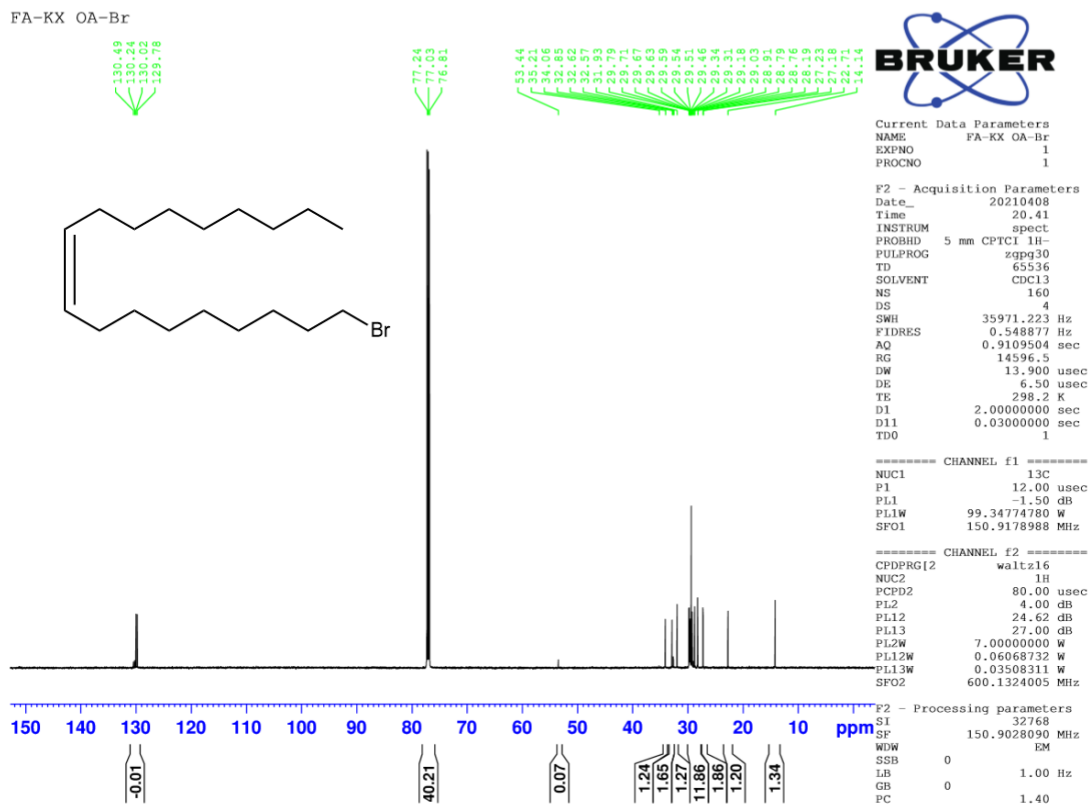
¹³C-NMR Spectra of N-(2-aminophenyl)oleamide (4):



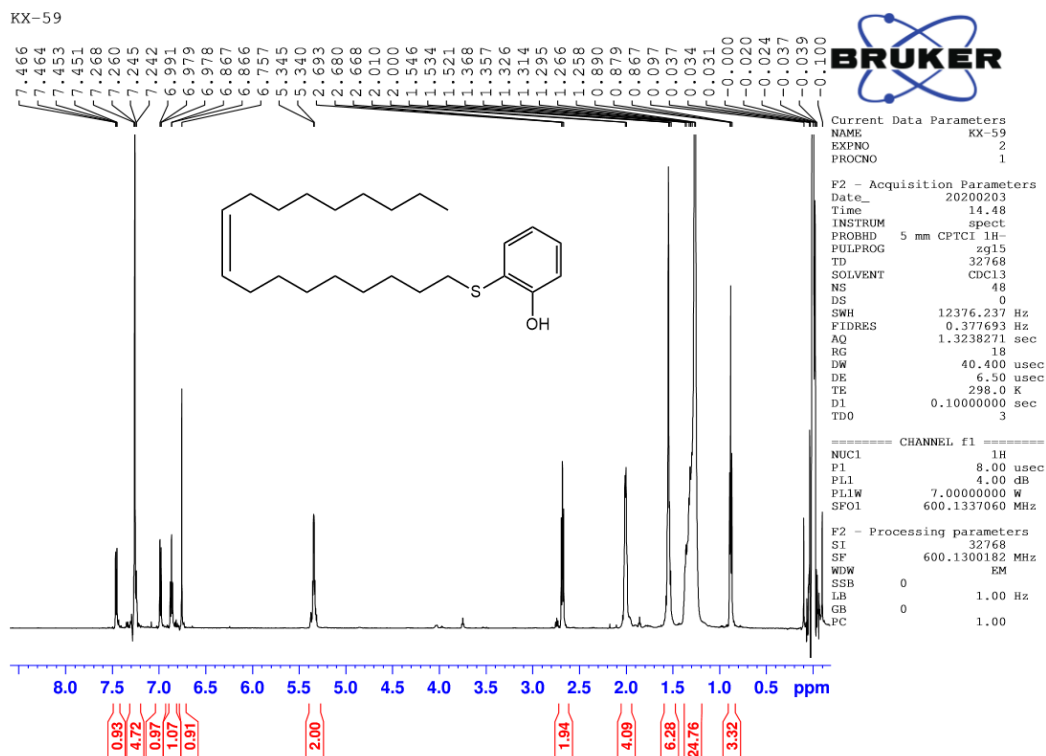
¹H-NMR Spectra of (Z)-1-bromooctadec-9-ene:



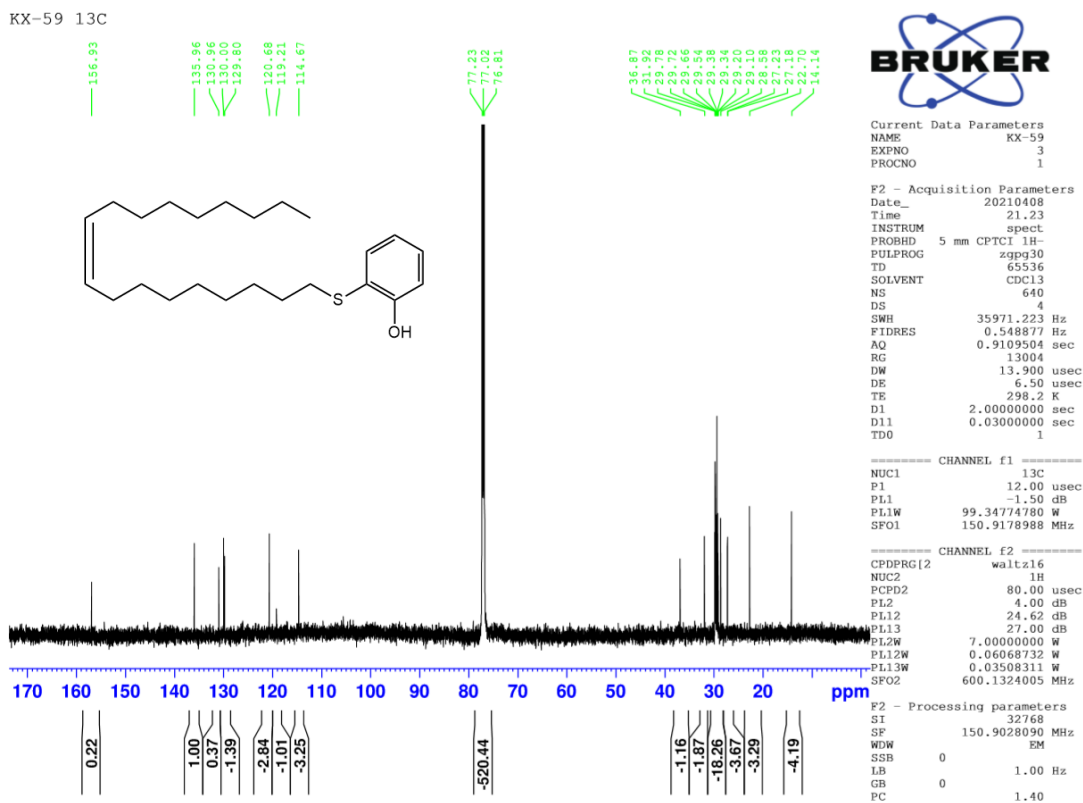
¹³C-NMR Spectra of (Z)-1-bromooctadec-9-ene:



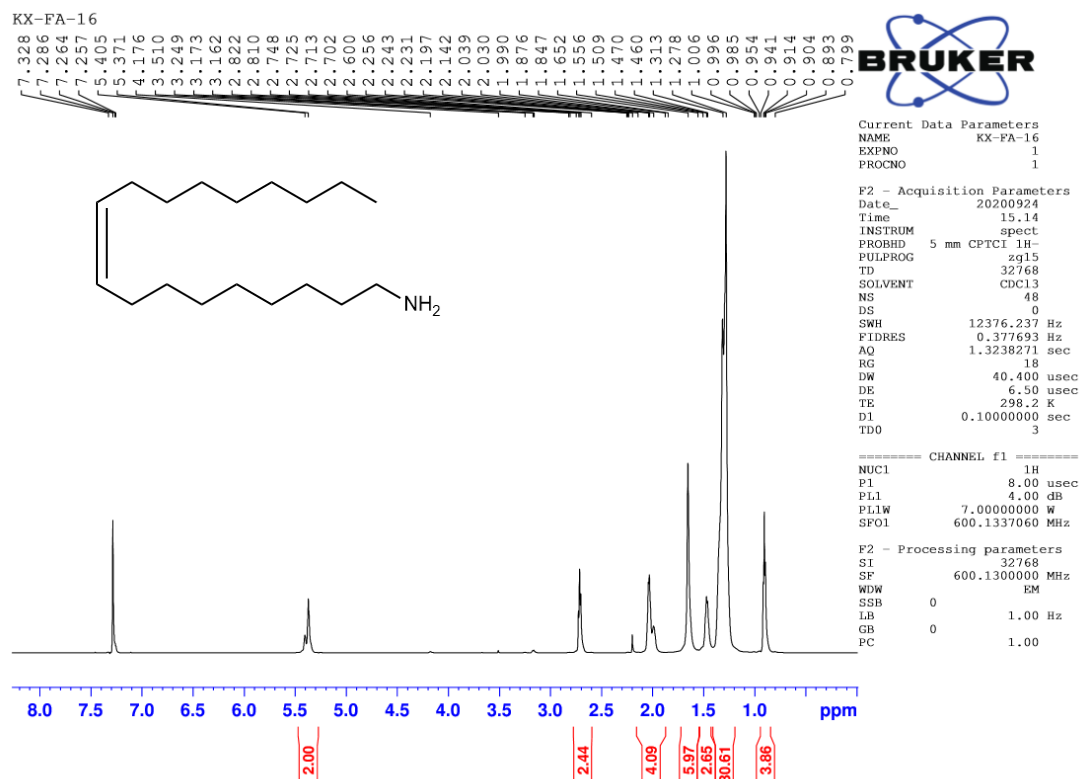
¹H-NMR Spectra of (Z)-2-(octadec-9-en-1-ylthio)phenol (5):



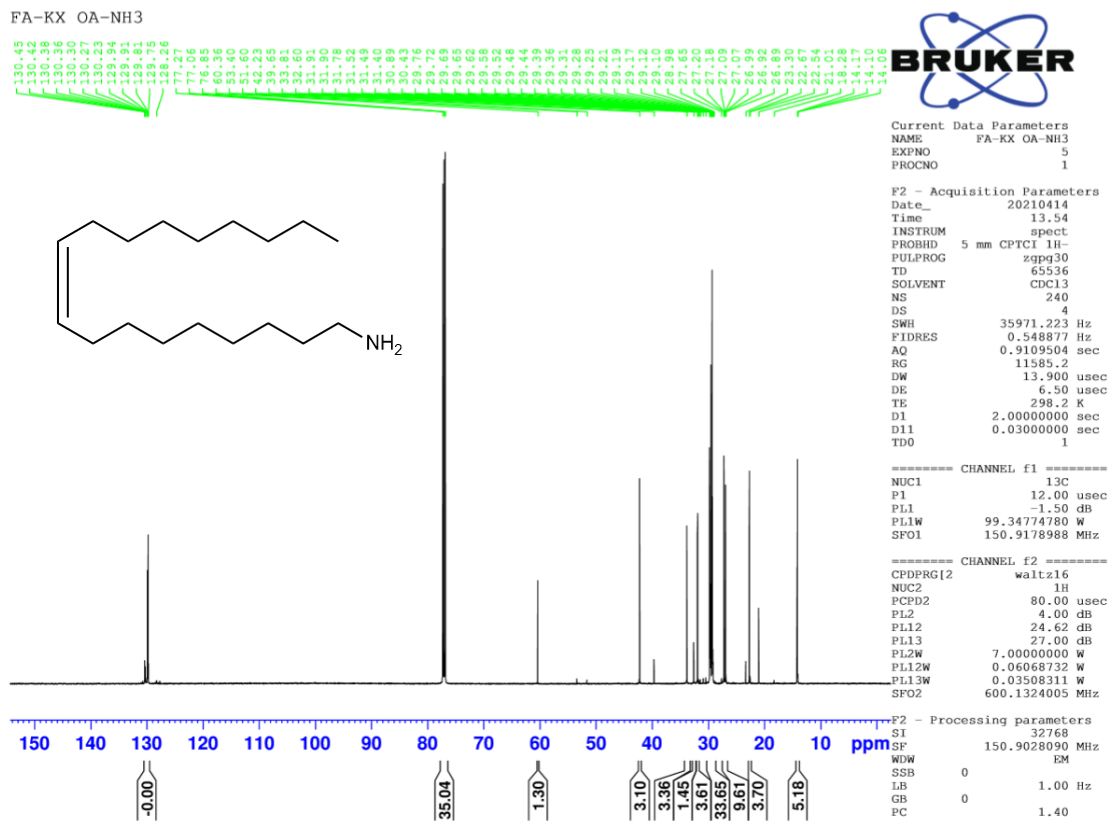
¹³C-NMR Spectra of (Z)-2-(octadec-9-en-1-ylthio)phenol (5):



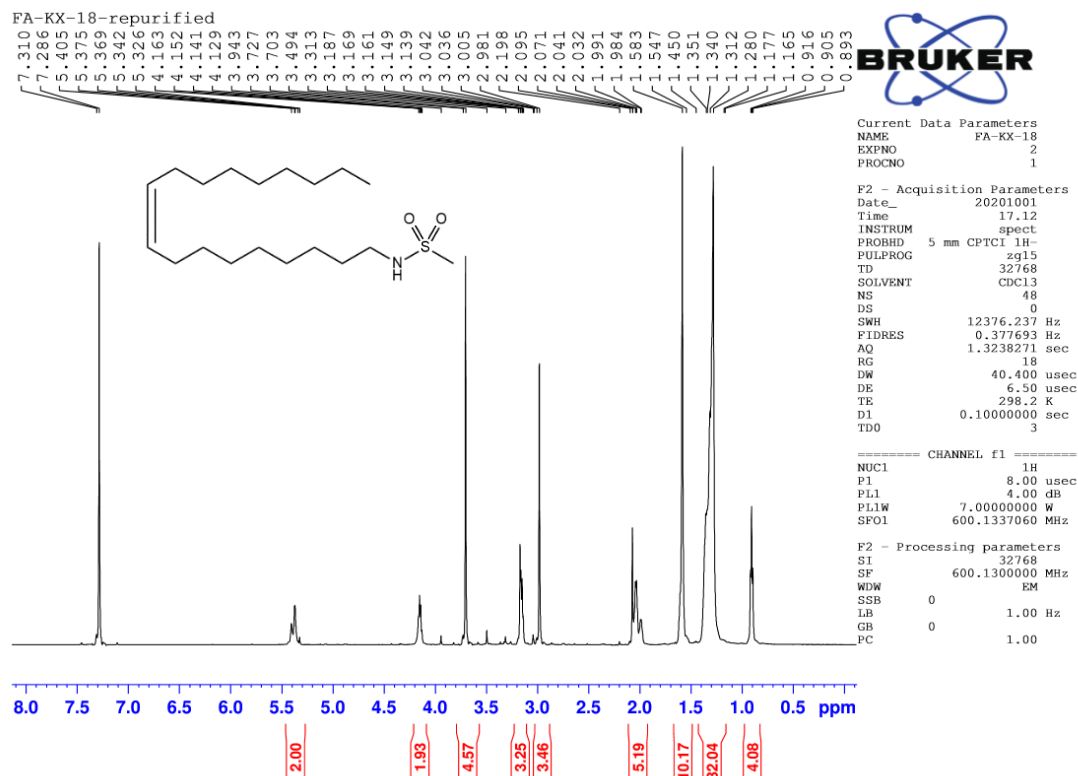
¹H-NMR Spectra of Oleylamine purified:



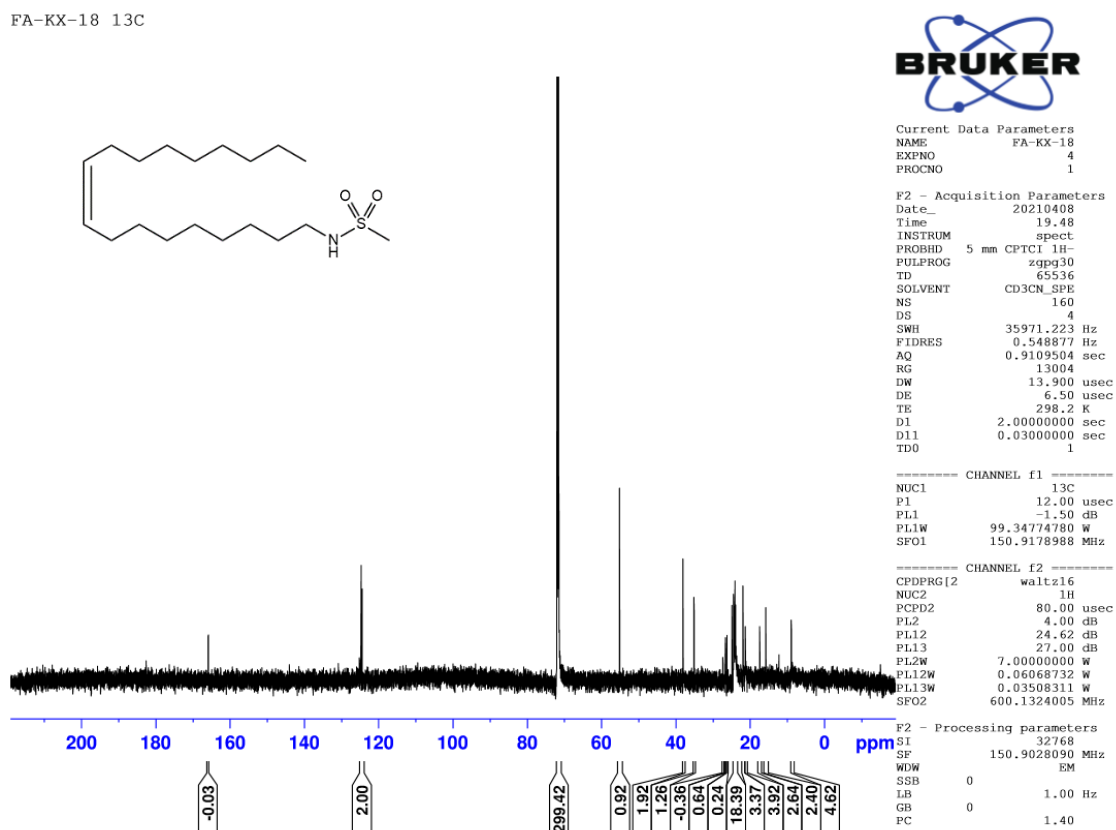
¹³C-NMR Spectra of Oleylamine purified:



¹H-NMR Spectra of (Z)-N-(octadec-9-en-1-yl)methanesulfonamide (6):

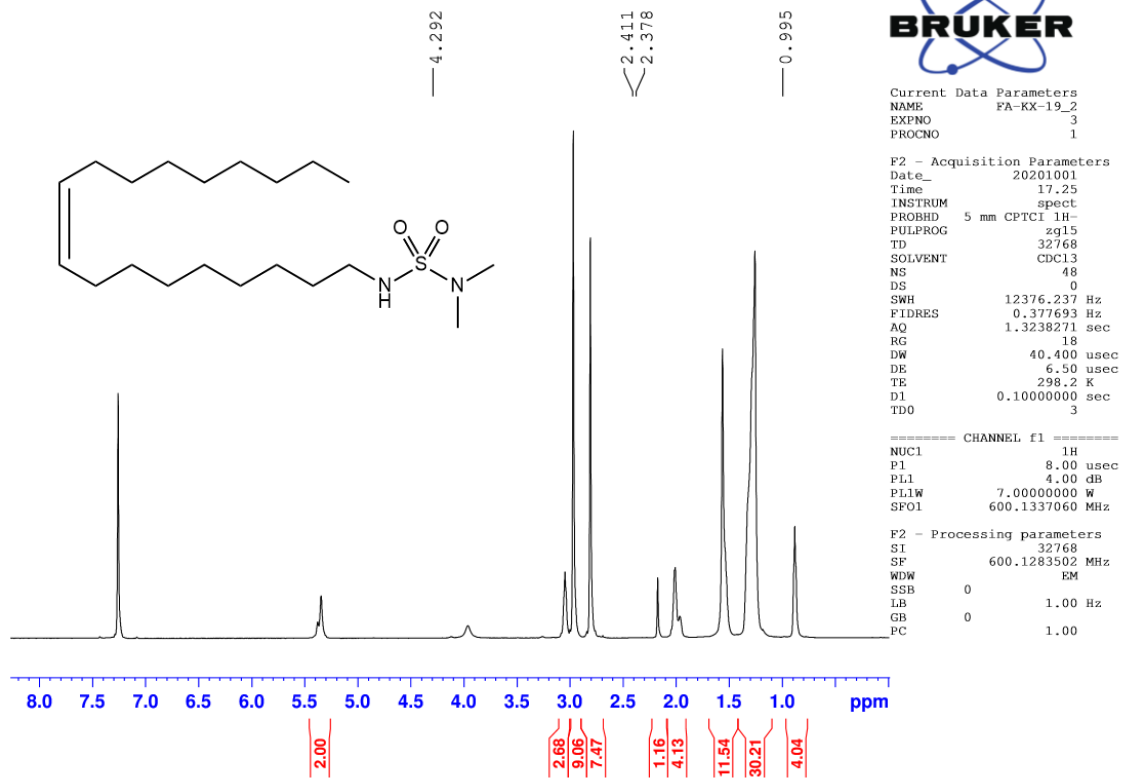


¹³C-NMR Spectra of (Z)-N-(octadec-9-en-1-yl)methanesulfonamide (6):



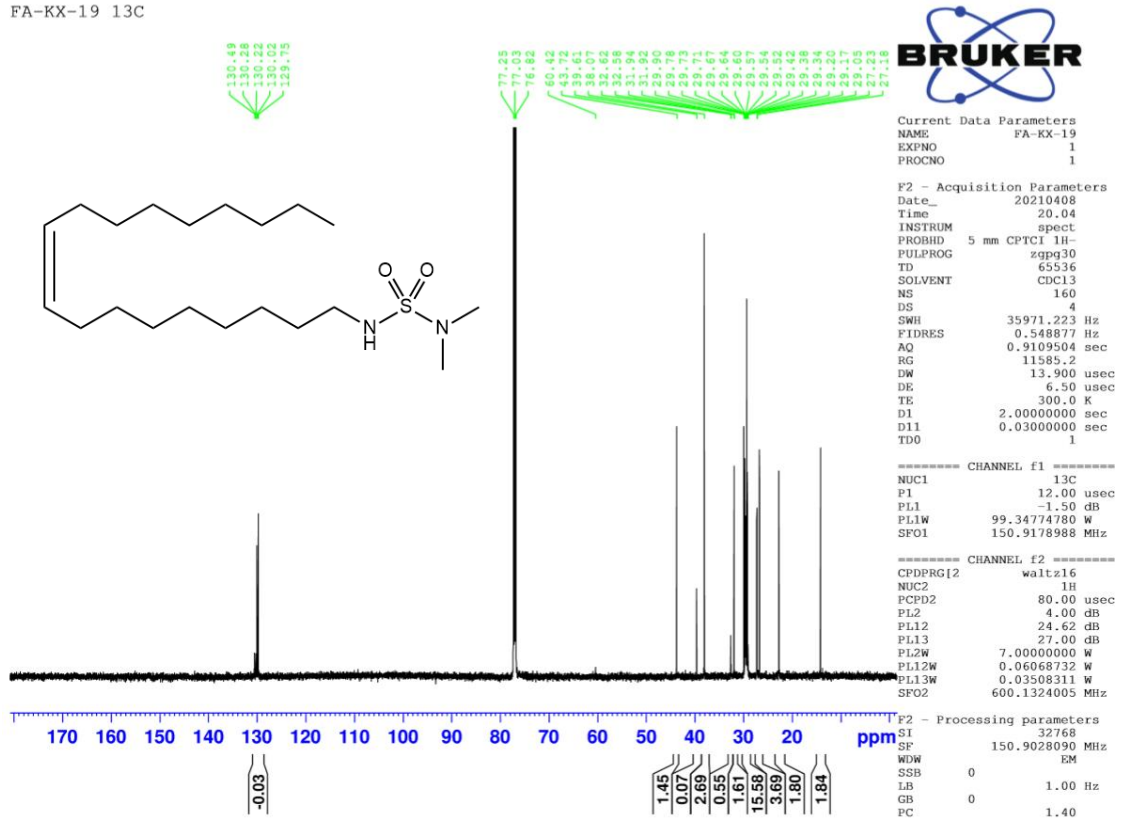
¹H-NMR Spectra of (Z)-N'-(octadec-9-en-1-yl)-N,N-dimethylsulfamide (7):

FA-KX-19-repurified

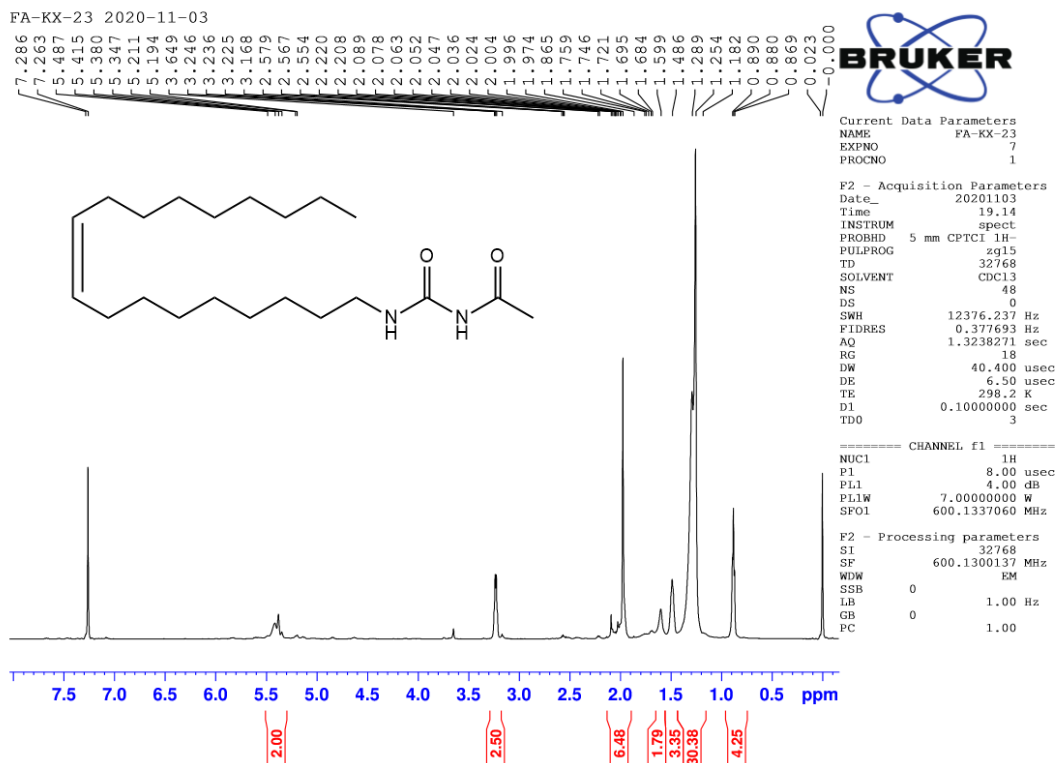


¹³C-NMR Spectra of (Z)-N'-(octadec-9-en-1-yl)-N,N-dimethylsulfamide (7):

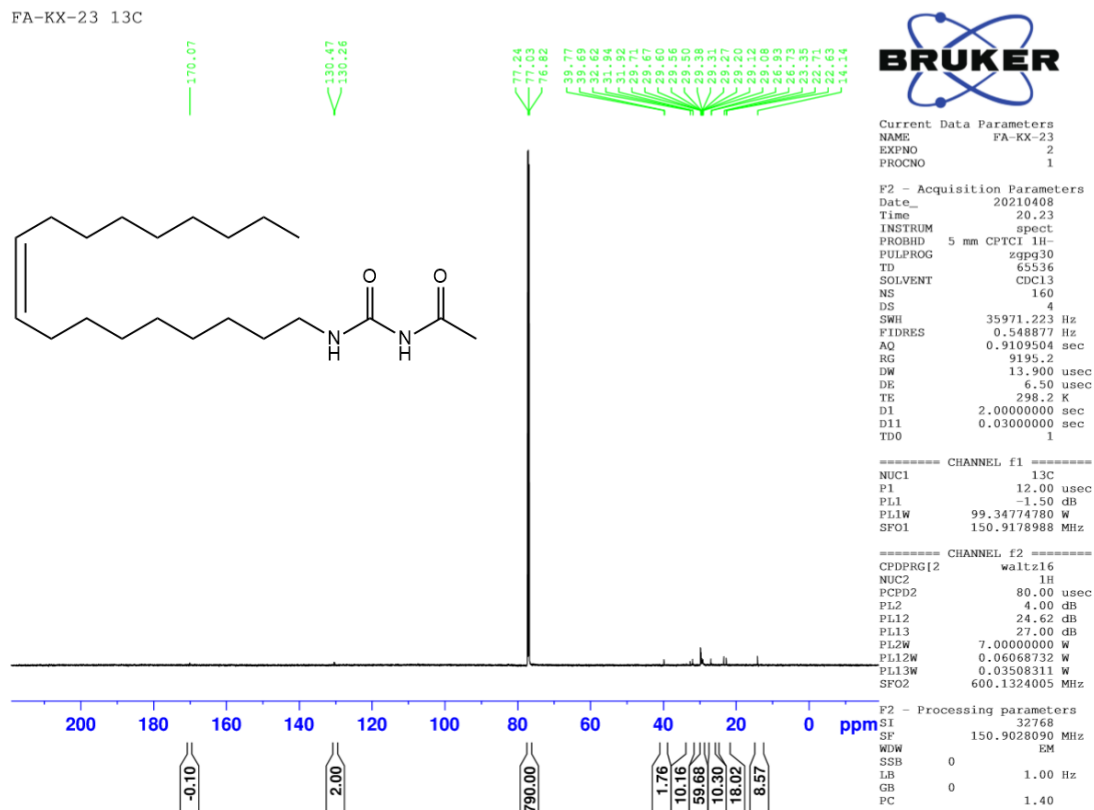
FA-KX-19 13C



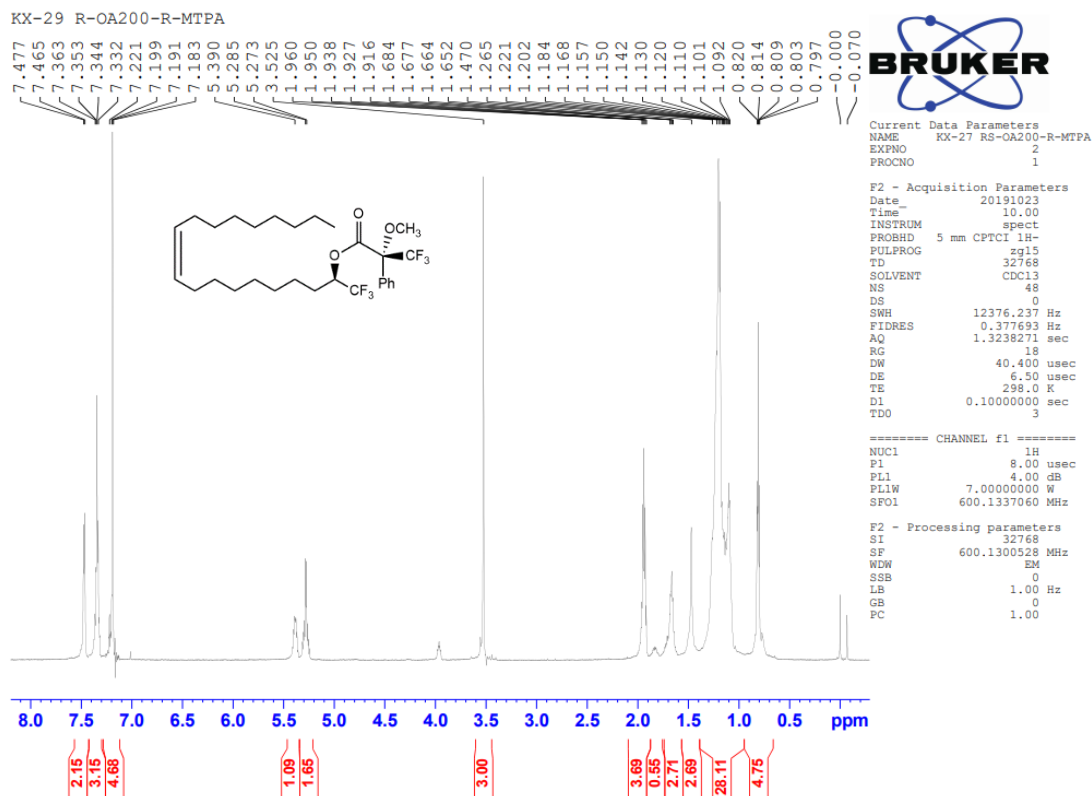
¹H-NMR Spectra of (Z)-N-(octadec-9-en-1-ylcarbamoyl)acetamide (8):



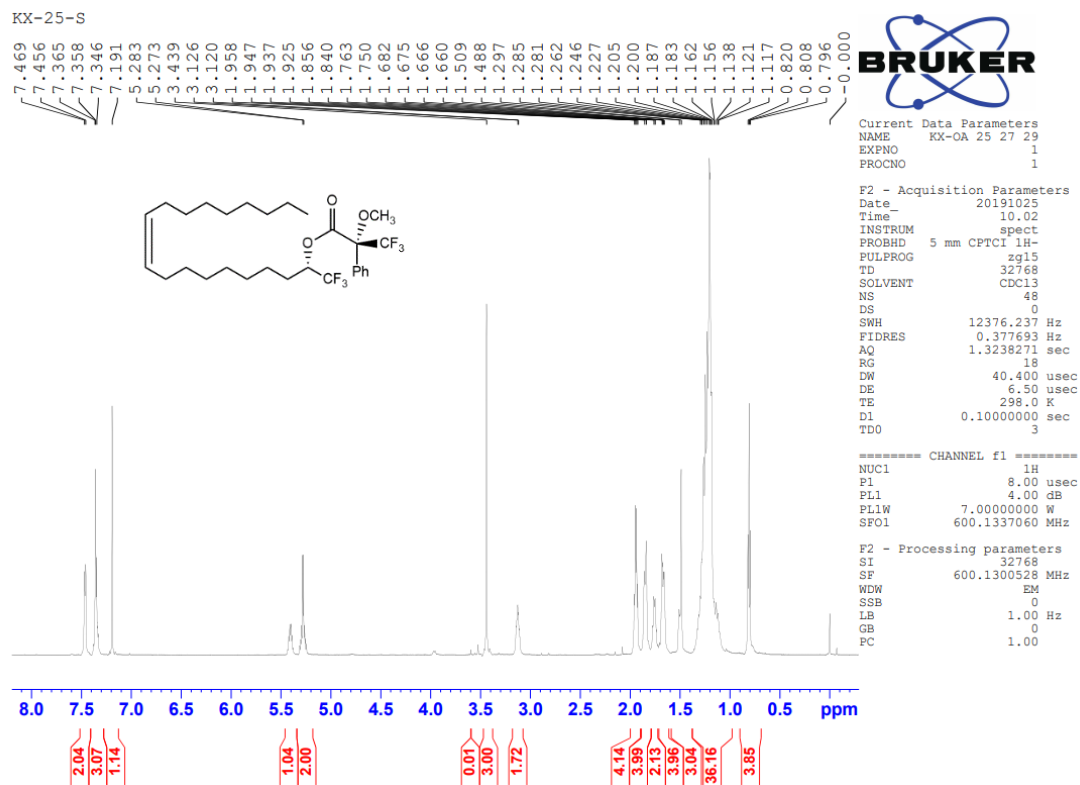
¹³C-NMR Spectra of (Z)-N-(octadec-9-en-1-ylcarbamoyl)acetamide (8):



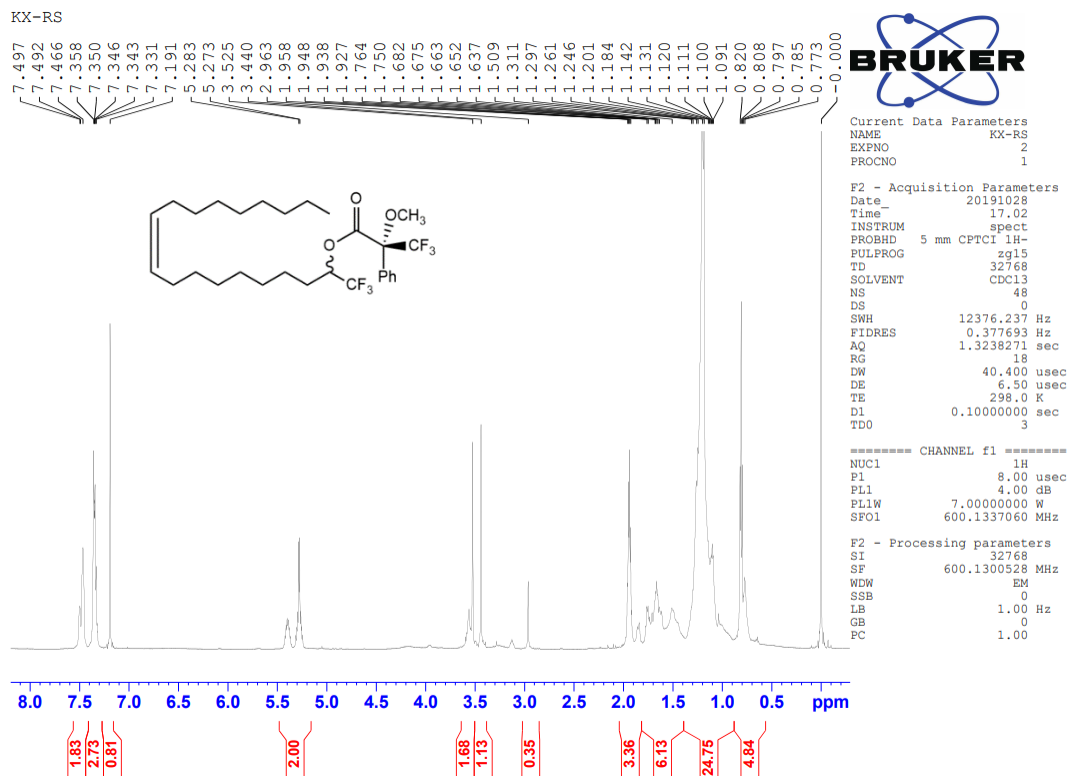
¹H-NMR Spectra of Mosher's ester of 2-R:



¹H-NMR Spectra of Mosher's ester of 2-S:



¹H-NMR Spectra of Mosher's ester of 2-rac:



REFERENCES

1. Stockwell, B.R., et al., *Ferroptosis: A Regulated Cell Death Nexus Linking Metabolism, Redox Biology, and Disease*. Cell, 2017. **171**(2): p. 273-285.
2. Marmolino, D., *Friedreich's ataxia: past, present and future*. Brain Res Rev, 2011. **67**(1-2): p. 311-30.
3. Richardson, T.E., et al., *Therapeutic strategies in Friedreich's ataxia*. Brain Res, 2013. **1514**: p. 91-7.
4. *Friedreich's Ataxia: Autosomal Recessive Disease Caused by an Intronic GAA Triplet Repeat Expansion*. 2020.
5. *HDAC Inhibitors Correct Frataxin Deficiency in a Friedreich Ataxia Mouse Model*. 2008.
6. Cotticelli, M.G., et al., *Ferroptosis as a Novel Therapeutic Target for Friedreich's Ataxia*. J Pharmacol Exp Ther, 2019. **369**(1): p. 47-54.
7. Calmels, N., et al., *The first cellular models based on frataxin missense mutations that reproduce spontaneously the defects associated with Friedreich ataxia*. PLoS One, 2009. **4**(7): p. e6379.
8. Cotticelli, M.G., et al., *Insights into the role of oxidative stress in the pathology of Friedreich ataxia using peroxidation resistant polyunsaturated fatty acids*. Redox Biol, 2013. **1**: p. 398-404.
9. Cotticelli, M.G., et al., *Identification of a Novel Oleic Acid Analog with Protective Effects in Multiple Cellular Models of Friedreich Ataxia*. ACS Chem Neurosci, 2020.
10. Cotticelli, M.G., et al., *Primary and secondary drug screening assays for Friedreich ataxia*. J Biomol Screen, 2012. **17**(3): p. 303-13.
11. Dixon, S.J., et al., *Ferroptosis: an iron-dependent form of nonapoptotic cell death*. Cell, 2012. **149**(5): p. 1060-72.
12. Yang, W.S., et al., *Peroxidation of polyunsaturated fatty acids by lipoxygenases drives ferroptosis*. Proc Natl Acad Sci U S A, 2016. **113**(34): p. E4966-75.
13. Lassalas, P., et al., *Structure Property Relationships of Carboxylic Acid Isosteres*. J Med Chem, 2016. **59**(7): p. 3183-203.
14. Kelly, C.B., M.A. Mercadante, and N.E. Leadbeater, *Trifluoromethyl ketones: properties, preparation, and application*. Chem Commun (Camb), 2013. **49**(95): p. 11133-48.
15. Patterson J E, O.I.R., Cravatt B F, et al., *Inhibition of Oleamide Hydrolase Catalyzed Hydrolysis of the*. Journal of the American Chemical Society, 1996. **118**(25): p. 5938-5945.
16. K., H.W., *The Many Roles for Fluorine in Medicinal Chemistry*. J Med Chem, 2008. **51**(15): p. 4359-4369.
17. Boivin J, E.K.L., Zard S Z., *An expedient access to trifluoromethyl ketones from carboxylic acids*. Tetrahedron letters, 1992. **33**(10): p. 1285-1288.
18. Dale J A, D.D.L., Mosher H S., *α -Methoxy- α -trifluoromethylphenylacetic acid, a versa-tile*

- reagent for the determination of enantiomeric composition of alcohols and amines. The Journal of organic chemistry, 1969. **34**(9): p. 2543-2549.
19. James A. Dale, D.L.D., and Harry S. Mosher, *α -Methoxy- α -trifluoromethylphenylacetic Acid, a Versatile Reagent for the Determination of Enantiomeric Composition of Alcohols and Amines*. J. Org. Chem., 1969. **34**(9): p. 2543–2549.
 20. Etheridge, C.J., *Sulfone-Assisted Heterocyclic Synthesis*. 1994. p. No pp.
 21. Kovalenko, S.V.S., Joel *Production of methyl fluoroalkyl ethers by reaction of chloromethane with fluoroalkoxides*. 2010: US.
 22. Saiah, E.V., George *Preparation of amino acid as modulators of sestrin-gator interaction*. 2018, Assignee Navitor Pharmaceuticals, Inc., USA.
 23. Yadav, J.S.S., Borra; Srihari, Pabbaraja, *Stereoselective Total Synthesis of the Marine Macrolide Sanctolide A*. European Journal of Organic Chemistry, 2015. **2015**(26): p. 5856-5863
 24. Gilissen, P.J.B.-A., Daniel; Rutjes, Floris P. J. T. , *Oxidation of Secondary Methyl Ethers to Ketones*. Gilissen, Pieter J.; Blanco-Ania, Daniel; Rutjes, Floris P. J. T. , 2017. **82**(13): p. 6671-6679.
 25. Esaki, H.O., Rumi; Maegawa, Tomohiro; Monguchi, Yasunari; Sajiki, Hironao *Novel Pd/C-Catalyzed Redox Reactions between Aliphatic Secondary Alcohols and Ketones under Hydrogenation Conditions: Application to H-D Exchange Reaction and the Mechanistic Study*. Journal of Organic Chemistry, 2007. **72**(6): p. 2143-2150.
 26. Moeckel, R.B., Emre; Hilt, Gerhard *Iodine(III)-Mediated Electrochemical Trifluoroethoxylactonisation: Rational Reaction Optimisation and Prediction of Mediator Activity*. Chemistry - A European Journal, 2018. **24**(59): p. 15781-15785
 27. Wickens, Z.K.M., Bill; Grubbs, Robert H.; Skaku, Kacper; Bronner, Sarah *Aldehyde-selective Wacker-type oxidation of unbiased alkenes*. Assignee California Institute of Technology, USA, Assignee California Institute of Technology, USA.
 28. Cramer, J., C.P. Sager, and B. Ernst, *Hydroxyl Groups in Synthetic and Natural-Product-Derived Therapeutics: A Perspective on a Common Functional Group*. J Med Chem, 2019. **62**(20): p. 8915-8930.
 29. *Equilibrium pKa Table (DMSO Solvent and Reference)*. Available from: https://organicchemistrydata.org/hansreich/resources/pka/pka_data/pka-compilation-reich-bordwell.pdf.
 30. Charifson, P.S. and W.P. Walters, *Acidic and basic drugs in medicinal chemistry: a perspective*. J Med Chem, 2014. **57**(23): p. 9701-17.
 31. Ballatore, C., D.M. Huryn, and A.B. Smith, 3rd, *Carboxylic acid (bio)isosteres in drug design*. ChemMedChem, 2013. **8**(3): p. 385-95.
 32. Liu, Q., et al., *Nitric oxide-sensing actuators for modulating structure in lipid-based liquid crystalline drug delivery systems*. J Colloid Interface Sci, 2017. **508**: p. 517-524.
 33. Chen, P.-J., H.-Y. Wang, and A.-Y. Peng, *A mild and efficient amide formation reaction mediated by P(OEt)₃ and iodine*. RSC Advances, 2015. **5**(114): p. 94328-94331.
 34. Hartsel, J.A.W., Dawn M.; Mutunga, James M.; Ma, Ming; Anderson, Troy D.; Wysinski, Ania; Islam, Rafique; Wong, Eric A.; Paulson, Sally L.; Li, Jianyong; Lam, Polo C. H.; Totrov, Maxim M.; Bloomquist, Jeffrey R.; Carlier, Paul R. , *Re-engineering aryl methylcarbamates to confer high selectivity for inhibition of Anopheles gambiae versus human acetylcholinesterase* Bioorganic & Medicinal Chemistry Letters, 2012. **22**(14): p. 4593-4598
 35. Koga, C.K., Michinari; Taniguchi, Tatsuo; Kishikawa, Keiki *Does Introduction of a Bent Tail*

- Stabilize Biaxiality and Lateral Switching Behavior of Smectic A Liquid Crystal Phases of Rodlike Molecules?* Journal of Physical Chemistry, 2019. **123**(19): p. 4324-4332.
36. Moore, J.E.M., Thomas M.; Sokolova, Anna V.; de Campo, Liliana; Pearson, Graeme R.; Wilkinson, Brendan L.; Tabor, Rico F. , *Worm-like micelles and vesicles formed by alkyl-oligo(ethylene glycol)-glycoside carbohydrate surfactants: The effect of precisely tuned amphiphilicity on aggregate packing.* Journal of Colloid and Interface Science, 2019. **547**: p. 275-290.
 37. De Roo, J.Z., Zimu; Wang, Jiaying; Deblock, Loren; Crosby, Alfred J.; Owen, Jonathan S.; Nonnenmann, Stephen S. , *Synthesis of Phosphonic Acid Ligands for Nanocrystal Surface Functionalization and Solution Processed Memristors.* Chemistry of Materials, 2018. **30**(21): p. 8034-8039
 38. Moore, J.E.M., Thomas M.; de Campo, Liliana; Sokolova, Anna V.; Garvey, Christopher J.; Pearson, Graeme; Wilkinson, Brendan L.; Tabor, Rico F. , *Wormlike micelle formation of novel alkyl-tri(ethylene glycol)-glucoside carbohydrate surfactants: Structure-function relationships and rheology* Journal of Colloid and Interface Science, 2018. **529**: p. 464-475.
 39. Sytniczuk, A.D., Michal; Banach, Lukasz; Urban, Mateusz; Czarnocka-Sniadala, Sylwia; Milewski, Mariusz; Kajetanowicz, Anna; Grela, Karol *At Long Last: Olefin Metathesis Macrocyclization at High Concentration.* Journal of the American Chemical Society, 2018. **140**(28): p. 8895-8901
 40. Carballo, R.M.V., Guillermo; Purino, Martin; Martin, Victor S.; Padron, Juan I. , *Broadening the Synthetic Scope of the Iron(III)-Catalyzed Aza-Prins Cyclization.* European Journal of Organic Chemistry, 2010(12): p. 2304-2313, S2304/1-S2304/42
 41. polymers, M.o.p.n.s., *Method of preparing norbornene sulfonamide polymers.* Assignee B.F. Goodrich Company, USA.
 42. Fong, C.W., Darrell; Krodkiewska, Irena; Hartley, Patrick G.; Drummond, Calum J., *New Role for Urea as a Surfactant Headgroup Promoting Self-Assembly in Water.* Chemistry of Materials, 2006. **18**(3): p. 594-597.
 43. Lassalas, P.G., Bryant; Lasfargeas, Caroline; James, Michael J.; Tran, Van; Vijayendran, Krishna G.; Brunden, Kurt R.; Kozlowski, Marisa C.; Thomas, Craig J.; Smith, Amos B.; Huryn, Donna M.; Ballatore, Carlo *Structure Property Relationships of Carboxylic Acid Isosteres.* Journal of Medicinal Chemistry, 2016. **59**(7): p. 3183-3203.
 44. Peesa, J.P., et al., *A perspective review on role of novel NSAID prodrugs in the management of acute inflammation.* Journal of Acute Disease, 2016. **5**(5): p. 364-381.
 45. *Grignard Reaction - Organic Chemistry Portal.* Available from: <https://www.organic-chemistry.org/namedreactions/grignard-reaction.shtm>.
 46. Olson, K.M.S., Courtney M.; Williams, Russell B.; O'Neil-Johnson, Mark; Huang, Zhongping; Ellis, Michael; Reilly, John E.; Eldridge, Gary R., *Novel pentadecenyl tetrazole enhances susceptibility of methicillin-resistant Staphylococcus aureus biofilms to gentamicin.* Antimicrobial Agents and Chemotherapy, 2011. **55**(8): p. 3691-3695.
 47. *Amino Protecting Groups Stability - Organic Chemistry Portal.* Available from: <https://www.organic-chemistry.org/protectivegroups/amino.shtm>.